Doctoral Dissertation

Targeting macrophages in the tumor-microenvironment to enhance their anti-tumorous functions by gene silencing using optimized siRNA-loaded lipid nanoparticles

（siRNA 搭載脂質ナノ粒子を用いた遺伝子抑制によるがん微小環境中におけるマクロファージの抗腫瘍性強化）

Nour A. K. Shobaki

The Laboratory for Molecular Design of Pharmaceutics

Biomedical and Pharmaceutical Science Course

Graduate School of Life Science, Hokkaido University

September 2019

Table of Contents

Terminology and abbreviations

2-ME	2-mercaptoethanol
ACK	ammonium-chloride-potassium
ACT	adoptive cell transfer
AF	alexa fluor
AGO	argonaute 2
ARG1	arginase 1
ASO	antisense ON
AUC	area under the curve
ApoE	apolipoprotein E
ApoE-LDLR	ApoE-low-density lipoprotein
AuNP	gold nanoparticle
BMDC	bone marrow-derived cells
BMDM	bone marrow-derived macrophages
BSA	bovine serum albumin
CA	corosolic acid
CAF	cancer-associated fibroblast
CAR T cell	chimeric antigen receptor T cell
CCL	C-C motif chemokine ligand
CCR	C-C motif chemokine receptor
CD	cluster of differentiation
CNI	Cancer National Institute
COX-2	cyclooxygenase 2
CRS	cytokine release syndrome
CSF	colony-stimulating factor
CSF1R	CSF 1 receptor
CTLA4	cytotoxic T lymphocyte antigen 4
CXCL	C-X-C motif chemokine ligand
CXCR	C-X-C chemokine receptor type
DAMP	damage-associated molecular pattern

DC	dendritic cell
DDS	drug delivery system
DLS	dynamic light scattering
DMEM	Dulbecco's modified eagle's medium
DMG-PEG 2,000	1,2-dimirystoyl-*rac*-glycero-3-methylpolyoxyethylene
DNA	deoxyribonucleic acid
DSG-PEG 2,000	1,2-distearoyl-*rac*-glycero-3-methylpolyoxyethylene
DSPC	1,2-distearoyl-*sn*-glycero-3-phosphocholine
DSPE-PEG 2,000	*N*-(carbonyl-methoxypolyethyleneglycol 2000)-1,2-distearoyl-*sn*-glycero-3-phosphoethanolamine, sodium salt
Dox	doxorubicin
EC	endothelial cell
ED_{50}	50% effective dose
EDTA	ethylenediaminetetraacetic acid
EE	encapsulation efficiency
EGF	epidermal growth factor
EMA	European Medicines Agency
EPR	enhanced permeation and retention
ERBB2	Erb-B2 receptor tyrosine kinase 2
FACS	fluorescence-activated cell sorting
FBS	fetal bovine serum
FDA	Food and Drug Administration
FGF2	fibroblast growth factor 2
FVII	coagulation factor VII
GAPDH	glyceraldehyde 3-phosphate dehydrogenase
GEM	genetically-engineered macrophages
GLUT-1	glucose transporter 1
GM-CSF	granulocyte-M-CSF
GUSB	glucuronidase beta
H_2O_2	hydrogen peroxide
HA	hyaluronic acid
HBSS	Hank's balanced salt solution

HCK	hematopoietic cell kinase
HDAC	class IIA histone deacetylase
HEPES	4-(2-hydroxyethyl)-1-piperazineethanesulfonic acid
HIF-1α	hypoxia-inducible factor 1α
HLA	human leukocyte antigen
HRG	histidine-rich glycoprotein
HSV	herpes simplex virus
IFN	interferon
IL	interleukin
IL-4Rα	IL-4 receptor α
IO	immune-oncology
IRF4	interferon regulatory factor 4
Jmjd3	Jumonji domain containing 3
LNP	lipid nanoparticle
LPS	lipopolysaccharide
M-CSF	macrophage-CSF
M2NP	M2-like TAM dual-targeting nanoparticle
M2pep	M2 macrophage binding peptide
MARCO	macrophage receptor with collagenous structure
MDSC	myeloid-derived suppressor cells
MEND	multifunctional envelope-type nanodevice
MMP	matrix metalloproteinase
MPS	mononuclear phagocyte system
MR	mannose receptor
MSV	multistage vector
MnNP	mannosylated polymer nanoparticles
MnO_2 NPs	manganese dioxide NPs
Mφ	macrophage
NE	neuroendocrine
NF-κB	nuclear factor kappa-light-chain-enhancer of activated B cells
NIH	National Institutes of Health

NSCLC	non-small cell lung cancer
ON	oligonucleotide
OA	oleanolic acid
OS-RC-2	human RCC
PAMP	pathogen-associated molecular pattern
PAP	prostatic acid phosphatase
PBMC	peripheral blood mononuclear cell
PBS (-)	phosphate-buffered saline
PCR	polymerase chain reaction
PD-1	programed cell death 1
PD-L1	PD ligand 1
PDI	polydispersity index
PEG	polyethylene glycol
PGE2	prostaglandin E2
PGK	phosphoglycerate kinase 1
PI3Kγ	phosphoinositide 3-kinase γ
PLGA	poly (lactic-co-glycolic acid)
POPE	1-palmitoyl-2-oleoyl-*sn*-glycero-3-phosphoethanolamine
RAW 264.7	murine macrophage cell line
RBC	red blood cell
RCC	renal cell carcinoma
RES	reticuloendothelial system
RISC	RNA-induced silencing complex
RNA	ribonucleic acid
RNAi	RNA interference
ROI	region of interest
ROS	reactive oxygen species
RT	reverse transcription
SAR	structure-activity relationship
SD	standard deviation
SDS	sodium dodecyl sulfate

SEER	The Surveillance, Epidemiology, and End Results
SIRPα	signal regulatory protein α
SR-B1	scavenger receptor B type 1
SOCS1	suppressor of cytokine signaling
STAT	signal transducer and activator of transcription
TAM	tumor-associated macrophage
TCR	T cell receptor
TEM	transmission electron microscopy
TGF-β	transforming growth factor β
TLR	toll-like receptor
TME	tumor-microenvironment
TNF-α	tumor necrosis factor α
Th	T-helper
Treg	regulatory T cells
Trk	tropomyosin receptor kinase
US	United States
UV	ultraviolet
VEGF	vascular endothelial growth factor
Vis	visible
cDNA	complementary DNA
cKit	receptor tyrosine kinase
chol	cholesterol
dsRNA	double-stranded RNA
hATTR	hereditary transthyretin (TTR)-mediated amyloidosis
iNOS	inducible nitric oxide synthase
mAb	monoclonal antibody
mRNA	messenger RNA
mTORC2	mechanistic target of rapamycin complex 2
miRNA	microRNA
pKa	acid dissociation constant
qPCR	Quantitative PCR

qRT-PCR	quantitative real-time PCR
rmM-CSF	recombinant mouse M-CSF
siRNA	short interfering RNA
t-BuOH	*tert*-butanol

Other abbreviations:

CO_2; carbon dioxide
$CaCl_2$; calcium chloride
IU; international unit
K; kilo
L; liter
M; molar
N_2; nitrogen
O_2; oxygen
U; unit
W; watt
e.g.; for example
g; gram
g; gravitational constant
h; hour
i.e.; that is
i.v.; intravenously
kV; kilovolt
kg; kilogram
mL; milliliter
mM; millimolar
mV; millivolt
mg; milligram
min; minute
mm^3; cubic millimeter
mol; mole
msec; millisecond
nM; nanomolar
nm; nanometer
nt; nucleotide
r.t.; room temperature
rpm; round per minute
s.c.; subcutaneously
sec; second
v; volume
wk; week
wt; weight
^oC; Celsius
μL; microliter
μg; microgram

Chapter 1: General introduction

1.1. Cancer; its environment and therapeutic targets

As defined by the Cancer National Institute (CNI), cancer is the name given to a collection of related diseases, and in all types of cancer, some of the body's cells begin to divide without stopping and spread into surrounding tissues [1]. In 2018, there were around 18.1 million new cases and 9.6 million cancer-related deaths worldwide [2]. The number of new cancer cases per year is expected to rise to 23.6 million by 2030 [3]. This fact makes cancer a huge burden and one of the major global challenges. However, due to the rise of overall healthcare expenditures [4] and the intensive worldwide research efforts, the cancer status seems to have been improved, and the most recent SEER Cancer Statistics Review, released in April 2019, shows that the overall cancer death rate in the United States (US) is in decline since the early 1990s [3, 5]. Furthermore, the global age-standardized cancer death rate has declined by 17% from 1990 to 2016 [6]. This decline of death rate could be attributed to the improved understating of cancer in terms of etiology and pathology, which enabled scientists across the globe to seek for alternatives to conventional treatments (*i.e.* surgery, chemotherapy, and radiotherapy) and to develop new therapeutic modalities, such as immunotherapy, which revolutionized cancer treatment in the last decade and applied for the treatment of various malignancies, including melanoma, hematologic malignancies, non-small cell lung cancer (NSCLC), cervical cancer, Merkel cell carcinoma, hepatocellular carcinoma, prostate cancer, kidney cancer, bladder cancer, head and neck cancer, using variety of recent US Food and Drug Administration (FDA)-approved drugs (**Table 1-1**) [7, 8].

Table 1-1: Selected US FDA-approved cancer immunotherapies

Therapy	**Type**	**Approved cancers**	**Year of first approval**
Checkpoint inhibitors			
Ipilimumab	CTLA4 mAb	Melanoma[a]	2011
Pembrolizumab	PD-1 mAb	Melanoma[a], non-small-cell lung cancer, Hodgkin lymphoma, advanced gastric cancer, microsatellite instability-high cancer, head and neck	2014

		cancer and advanced urothelial bladder cancer	
Nivolumab	PD-1 mAb	Melanoma[a], bladder cancer, classical Hodgkin lymphoma, colorectal cancer, hepatocellular cancer, non-small-cell lung cancer, kidney cancer, squamous cell carcinoma of the head and neck and urothelial cancer	2014
Atezolizumab	PD-L1 mAb	Urothelial cancer[a] and non-small-cell lung cancer	2016
Avelumab	PD-L1 mAb	Merkel cell carcinoma[a] and urothelial cancer	2017
Durvalumab	PD-L1 mAb	Urothelial cancer[a] and non-small-cell lung cancer	2017
Cytokines for lymphocyte promotion			
Intron A	Recombinant IFNα2b	Hairy cell leukaemia[a], melanoma, follicular lymphoma and AIDS-related Kaposi sarcoma	1986
Roferon-A	Recombinant IFNα2a	Hairy cell leukaemia[a], chronic myelogenous leukaemia and AIDS-related Kaposi sarcoma	1986
Aldesleukin	Recombinant IL-2	Melanoma[a] and kidney cancer	1992
Imiquimod	Stimulates TNF, IL-12 and IFNγ production[b]	Basal cell carcinoma	2004
Engineered T cell therapies			
Tisagenlecleucel	CD19-specific CAR T cells	B cell acute lymphocytic leukaemia[a] and non-Hodgkin lymphoma	2017
Axicabtagene ciloleucel	CD19-specific CAR T cells	Large B cell lymphoma[a]	2017
Vaccines			
Sipuleucel-T	Autologous PBMCs activated with recombinant human PAP–GM-CSF	Prostate cancer[a]	2010

Bacillus Calmette–Guérin	Strain of *Mycobacterium tuberculosis* variant *bovis*	Bladder cancer	1990
Oncolytic viruses			
Talimogene laherparepvec	Genetically modified HSV type 1 designed to replicate within tumours and produce GM-CSF	Melanoma[a]	2015
Bispecific antibodies			
Blinatumomab	CD19 and CD3 bispecific antibody	B cell acute lymphocytic leukaemia[a]	2014

CAR, chimeric antigen receptor; CTLA4, cytotoxic T lymphocyte antigen 4; CD, cluster of differentiation; FDA, Food and Drug Administration; GM-CSF, granulocyte macrophage-colony stimulating factor; HSV, herpes simplex virus; IFN, interferon; IL, interleukin; PAP, prostatic acid phosphatase; PBMC, peripheral blood mononuclear cell; PD-1, programmed cell death 1; PD-L1, PD ligand 1; US, United States; mAb, monoclonal antibody. [a]First indication to be approved. [b]Increases production of cytokines when topically applied. The table is adapted from reference [8].

1.1.1. Immune-oncology and immunotherapy

Immune-oncology (IO) is a new and growing field of cancer research that studies the tumor-microenvironment (TME) aiming to harness the power of the immune system to fight cancer in a strategy referred to as immunotherapy. The rationale behind this approach is the fact that the tumor is not merely a mass of homogenous cancerous cells but rather is a collection of heterogenous cell populations that include cancer-associated fibroblasts (CAFs) [9, 10], immune and inflammatory cells [11-13], neuroendocrine (NE) cells [14-16], adipose tissues [17-19], and the blood and lymphatic vessels [20-24]. These cellular and other non-cellular components, such as the extracellular matrix proteins, build the TME niche in which they interact and communicate collectively to determine the fate of cancer to be eradication or in most cases, progression (**Fig. 1-1**) [25, 26].

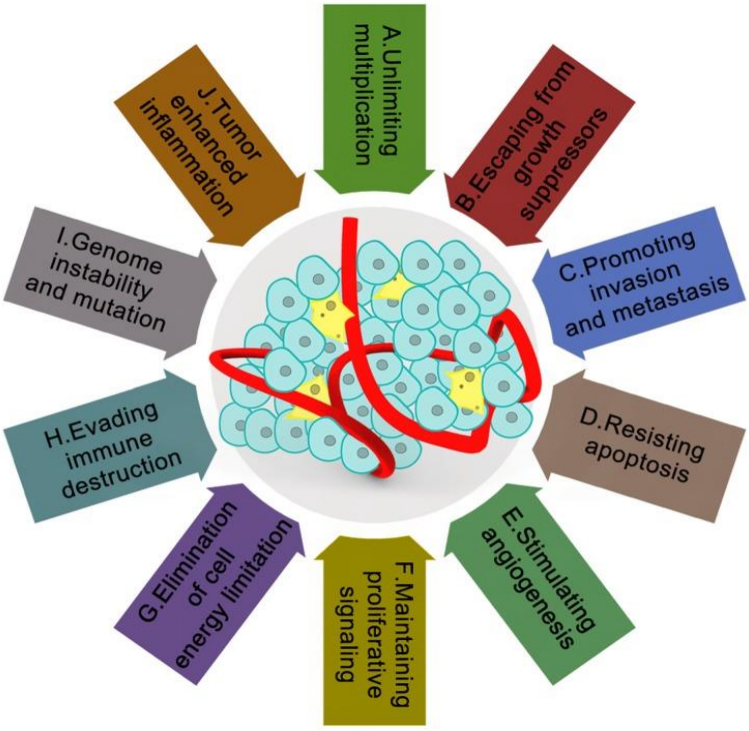

Fig. 1-1: The TME and characteristics of cancer. It is currently widely recognized that tumor microenvironments are wildly influenced by the ten main characteristics of cancer: A. unlimited multiplication; B. escaping from growth suppressors; C. promoting invasion and metastasis; D. resisting apoptosis; E. stimulating angiogenesis; F. maintaining proliferative signaling; G. elimination of cell energy limitation; H. evading immune destruction; I. genome instability and mutation; J. tumor-enhanced inflammation. Lower cure rate and poor prognosis of cancer patients are closely related to these ten characteristics of cancer. These ten characteristics make cancer more mysterious within the complex tumor microenvironments. The figure is adapted from reference [26]. TME, tumor-microenvironment.

In specific, immune cells play crucial roles in the TME at different tumor stages and they are ideal targets for cancer therapy. The pioneers of this field are Dr. William B. Coley, who attempted to treat inoperable sarcoma using bacterial toxins in the 1890s [27], Paul Ehrlich, and Burnet and Thomas who introduced and enriched the concept of immunosurveillance, respectively [28, 29], and Schreiber *et al*, who introduced the concept of immune-editing and described the three sequential phases of the interaction between tumor cells and immune system, *i.e.* elimination, equilibrium, and escape [11, 30]. The main current immunotherapeutic approaches fall into the following categories: checkpoint inhibitors (*e.g.* programmed cell death 1 (PD-1), PD ligand 1 (PD-L1), cytotoxic T lymphocyte antigen 4 (CTLA4) checkpoint blockade) [31, 32], cytokines (*e.g.* interferons (IFNs), interleukins (ILs), granulocyte-macrophage-colony stimulating factor (GM-CSF)) [33], adoptive cell transfer (ACT) of engineered T cells; chimeric antigen receptor T cells (CAR T cells) and T cell receptor (TCR) T cells [34, 35], agonistic antibodies against co-stimulatory receptors on the surface of T cells (*e.g.* antibodies targeting 4-1BB [36, 37] and OX-

40 [38]), and cancer vaccines (*e.g.* tumor cell lysate, dendritic cells (DCs), nucleic acids (such as messenger ribonucleic acid (mRNA)), and neo-antigens) [39-44]. Despite clinical success of these immunotherapeutic approaches (especially checkpoint inhibitors and CAR T cells [32, 45, 46]), they still have some challenges and limitations, such as systemic side effects and toxicity [47-50], resistance [51, 52], and difficult application for the treatment of solid tumors due to the complexity of their TME as well as the difficulty in selecting suitable target antigens that are specific for tumor cells-but not normal cells- to minimize off-target toxicity [53-56]. And even if suitable antigens of solid tumors were identified and targeted, CAR T cells have poor accumulation to tumor tissues [57], limited survival within the host body [58, 59], and they are susceptible for suppression in the TME [60]. In this study, another immune cell population in the TME, *i.e.* macrophages (Mφ), was explored and manipulated aiming to overcome challenges of CAR T cell therapy, contribute in improving current immunotherapeutic modalities and/or providing a safer and more promising therapeutic alternative, especially for the treatment of solid tumors.

1.1.2. Tumor-associated macrophages (TAMs)

Phagocytes, which are an essential part of the innate immune system, were first described by the Russian zoologist Élie Metchnikoff in 1882, who later won a Nobel prize in Physiology or Medicine for that discovery in 1908 [61]. Mononuclear phagocyte system (MPS) is a term that includes myeloid immune cells (monocytes, Mφ, and DCs) [62]. Mφ, or "big eaters" as their name means in Greek [63, 64], are cells with around 21 micrometers in diameter [65] that play significant roles in the innate immune system and are main components of the MPS. Mφ have two types regarding their source or origin; monocyte-derived Mφ and tissue-resident Mφ. The first type is derived from bone-marrow monocytes and is recruited at the time of inflammation and pathogen challenge, it is also involved in homeostasis and tissue remodeling. The second type is acquired from birth in the yolk sac, these Mφ reside in tissues and undergo self-renewal during the human's life, during which they play significant roles in the development, homeostasis, and during mild inflammation or injury which occur in their tissue of origin (**Fig. 1-2**) [66-68].

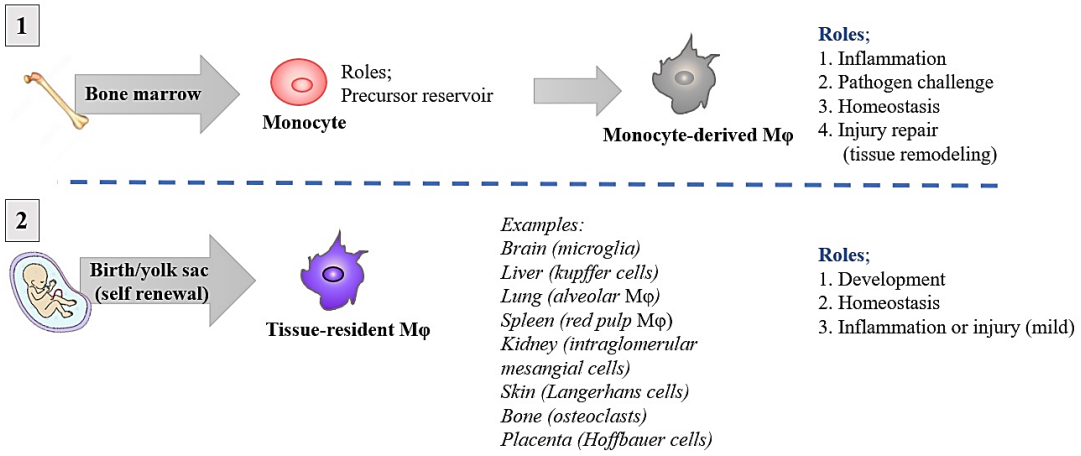

Fig. 1-2: Origins of Mφ. The two main sources of Mφ in the human body and their distinct roles in the innate immune system. Mφ, macrophage.

Mφ play significant roles in the physiology and the pathology of the human body, but not all Mφ play with the same roles, and they are known for their "plasticity" [69, 70] or "divided loyalty" [71] or for being a "double-edged sword" [72, 73], since they are skewed (or polarized) into different phenotypes under different circumstances and under the influence of various cytokines and triggers (**Fig. 1-3, 1-4**). For instance; both monocyte-derived and tissue-resident Mφ are polarized into a killing phenotype once they recognize pathogen-associated molecular patterns (PAMPs) and are triggered by specific stimuli such as bacterial infection, lipopolysaccharide (LPS), or IFNγ. This phenotype is known as M1, or IFNγ-induced or classically activated Mφ and is mainly involved in pathogenic removal, pro-inflammatory and anti-tumorous functions [69, 74-77]. In the other hand, Mφ are skewed (or polarized) into a healing phenotype once they recognize damage-associated molecular patterns (DAMPs) and are triggered by other stimuli such as IL-4, IL-10, IL-13, macrophage-colony stimulating factor (M-CSF), glucocorticoids, or parasite infection. This phenotype is known as M2, or IL-4-induced or alternatively activated Mφ and is mainly involved in tissue repair and growth, anti-inflammatory and pro-tumorous functions [69, 74-77] (**Fig. 1-3, 1-4**). The M1 and M2 nomenclature was basically introduced to describe the two different effects of Mφ on T-helper (Th) response -M1 activates Th1 while M2 activates Th2- [78], and despite the fact that this nomenclature is an oversimplification of the complexity of Mφ polarization and functions in the *in vivo* environment, and the fact that M2 Mφ can be further divided into subsets; M2a, M2b, M2c, and M2d [79-81], the nomenclature was used in this study

to describe and distinguish the two main extremes of Mφ to facilitate an easier data interpretation and sharing.

The TME is highly infiltrated with Mφ, referred to as tumor-associated macrophages (TAMs), and as a result of the cell-cell interaction between tumor cells and TAMs, the later acquire M2 phenotype and support tumor progression through the following pro-tumorous functions: activation of tumor proliferation and survival, enhancement of angiogenesis, neovascularization, and metastasis, and suppression of the immunity (**Fig. 1-3, 1-5**) [76, 82-88]. TAMs are also involved in mediating resistance to some anti-cancer therapeutic modalities such as chemotherapy [89, 90], immunotherapy [91], and anti-angiogenic therapy [92]. Therefore, TAMs are ideal targets of therapeutic interventions aiming to reprogram their phenotype from M2 to M1 or alter their function from pro-tumorous to anti-tumorous to realize novel immunotherapy for cancer.

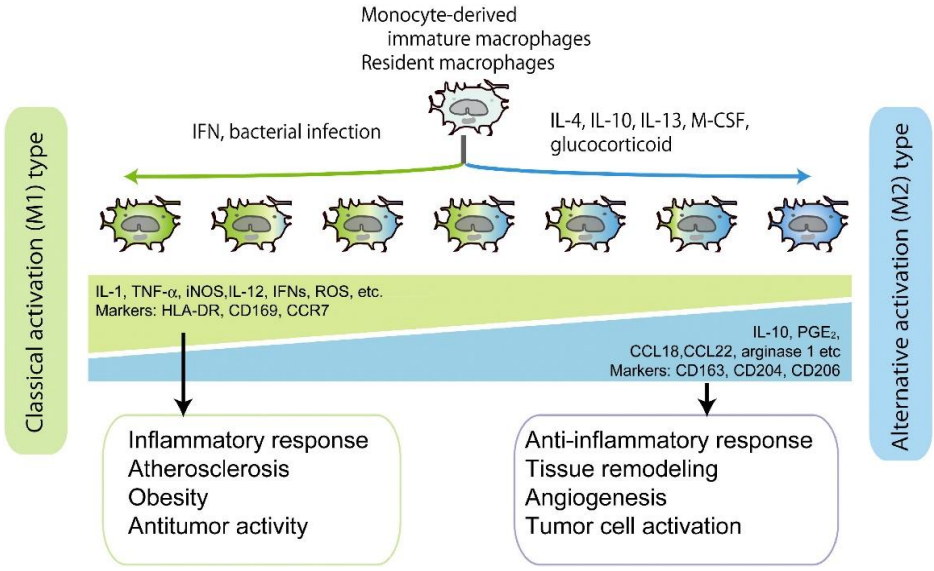

Fig. 1-3: Heterogeneity and polarization of Mφ. TAMs derived from circulating monocytes and resident Mφ differentiate into several phenotypes due to the cytokine balance or to other factors including hypoxic conditions in the TME. TAMs show M2-like functions and phenotype, and contribute to tumor progression. CCR, C-C motif chemokine receptor; CCL, C-C motif chemokine ligand; CD, cluster of differentiation; HLA, human leukocyte antigen; IFN, interferon; IL, interleukin; M-CSF, macrophage-colony stimulating factor; Mφ, macrophage; PGE2, prostaglandin E2; ROS, reactive oxygen species; TAMs, tumor-associated macrophages; TNF-α, tumor necrosis factor α; iNOS, inducible nitric oxide synthase. The figure is adapted from reference [76].

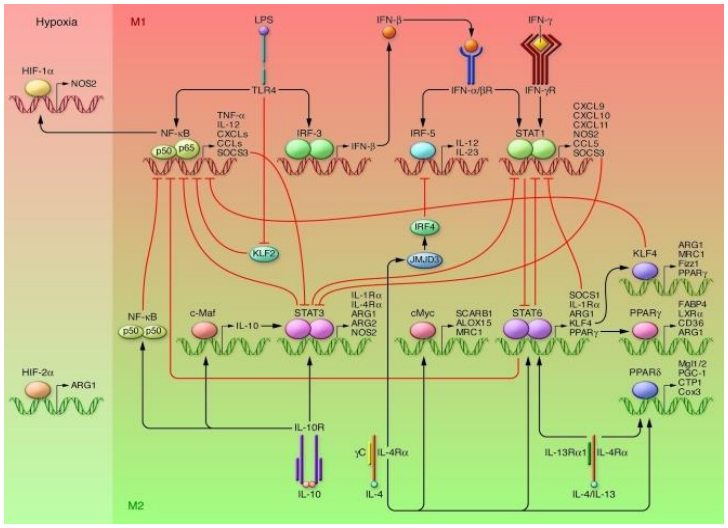

Fig. 1-4: Mechanisms of Mφ polarization. The major pathways of Mφ polarization are outlined. The crosstalk between the M1-M2 Mφ-polarizing pathways is also indicated. The balance between activation of STAT1 and STAT3/STAT6 finely regulated Mφ polarization and activity. A predominance of NF-κB and STAT1 activation promotes M1 Mφ polarization, resulting in cytotoxic and inflammatory functions. In contrast, a predominance of STAT3 and STAT6 activation results in M2 Mφ polarization, associated with immune suppression and tumor progression. Mφ, macrophage; NF-κB, nuclear factor kappa-light-chain-enhancer of activated B cells; STAT, signal transducer and activator of transcription. The figure is adapted from reference [69].

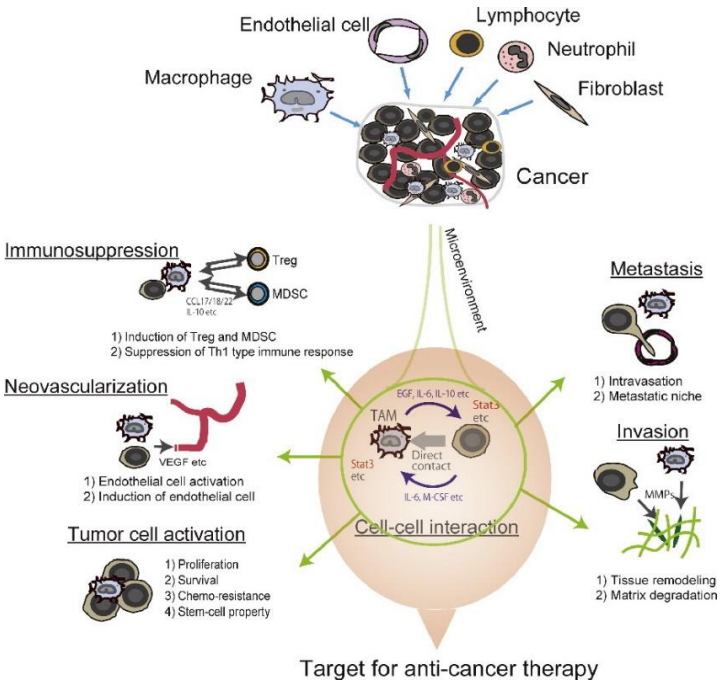

Fig. 1-5: Functions of TAMs. There have been many suggested aspects of the protumor functions of Mφ. STAT3 is one of the transcription factors that are activated by cell–cell interaction. Activated M2 TAMs and cancer cells by direct cell–cell contact are key players in the protumor microenvironment. EGF, epidermal growth factor; IL, interleukin; M-CSF, macrophage-colony stimulating factor; MDSC; myeloid-derived suppressor cells; MMPs, matrix metalloproteinases; Mφ, macrophage; TAMs, tumor-associated macrophages; Treg, regulatory T cell; STAT3, signal transducer and activator of transcription 3; VEGF, vascular endothelial growth factor. The figure is adapted from reference [76].

1.2. Targeting TAMs for cancer therapy

1.2.1. Main strategies for targeting TAMs

As a result of realizing the significant role that Mφ play in the TME, scientists across the globe have been trying to deliver various therapeutic agents to TAMs aiming to inhibit their infiltration to the TME, kill them or re-educate them to fight the tumor. Some of these studies have successfully reached clinical trials as described in **Table 1-2**, which summarizes National Institutes of Health (NIH) clinical trials of Mφ inhibition [88].

Currently, there are three main strategies for targeting TAMs to obtain anti-tumor therapeutic response [88, 93]:

I. Killing or depleting Mφ

There have been approaches to kill or deplete TAMs by delivering toxic drugs such as trabectedin [94-96], bisphosphonates (*e.g.* clodronate, zoledronate, alendronate [97-99]) or doxorubicin (Dox) [100, 101] using nanotechnological approaches such as PEGylated liposomes "liposomes shielded with polyethylene glycol (PEG)-lipids" [102] or poly (lactic-co-glycolic acid) (PLGA)-nanoparticles [100]. To target TAMs, these systems were decorated with various ligands, peptides, or molecules such as folate [103, 104], Ly-P1 [102], RNA aptamers with affinity for IL-4 receptor α (IL-4Rα) [105], and mostly commonly mannose [99, 100], to target mannose receptor (MR), which is also known as cluster of differentiation 206 (CD206) and highly expressed in TAMs, especially those with M2 phenotype [106]. These strategies still have some challenges to be addressed. For instance, the systems decorated with folate failed to induce anti-tumor response in murine tumor models [103, 104], and systems decorated with RNA aptamers against IL-4Rα or mannose lack the selectivity for TAMs since their target receptors (IL-4Rα and CD206) are also expressed by other immune cells, endothelial cells (ECs), or Mφ of the MPS in other organs such as liver, lungs, and spleen [107], and this requires special interventions to minimize their systemic toxicity.

II. Inhibition of macrophage's recruitment

Targeting chemokines, signaling pathways, or receptors responsible for TAMs recruitment; *e.g.* C-C motif chemokine ligand 2 (CCL2) [108, 109], C-X-C motif chemokine ligand 12 (CXCL12)/C-X-C chemokine receptor type 4 (CXCR4) axis [110, 111], CSF 1 receptor (CSF1R) [112, 113], CD11b [114]. For instance, antibodies are used to neutralize CCL2 [115], C-C motif

chemokine receptor 2 (CCR2) [116, 117], or CSF1R [118]. The anti-CCL2 antibody carlumab (CNTO 888) did not induce enough clinical response [119, 120]. Whereas, anti-CCR2 and anti-CSF1R antibodies are undergoing clinal trials [116, 117, 121-126] (**Table 1-2**). Other research studies are attempting to silence CCR2 using short interfering RNA (siRNA) siRNA-loaded lipid nanoparticles (LNPs) instead of using antibodies [127], and despite the promising results of targeting CSF1R using antibodies, targeting them using nanoparticles has not yet been developed. It is noteworthy to mention that killing or inhibiting TAM's recruitment might not be the best solution to treat and modify the TME since TAMs with M1 phenotype and anti-tumorous functions might add an extra advantage and provide a better therapeutic outcome. Furthermore, although using antibodies is sufficient to target and neutralize surface proteins expressed on TAMs, targeting and inhibiting internal genes or proteins require an alternative strategy; *e.g.* using siRNA-loaded LNPs for gene silencing.

III. Altering macrophage's phenotype and function

Reprogramming and re-educating Mφ to fight cancer. For instance, suppressing TAMs which have M2 phenotype and pro-tumorous functions by inhibiting certain genes or targets such as Jumonji domain containing 3 (Jmjd3) [128], signal transducer and activator of transcription 6 (STAT6) [129], STAT3 [130, 131], Dicer [132], superoxide (O(2-)) [133], IL4Rα [134], cyclooxygenase 2 (COX-2) [135], phosphoinositide 3-kinase γ (PI3Kγ) [136], CSF1R [113], macrophage receptor with collagenous structure (MARCO) [137], hematopoietic cell kinase (HCK) [138], nuclear factor kappa-light-chain-enhancer of activated B cells (NF-κB) [139], and class IIA histone deacetylase (HDAC) [140], or stimulating TAMs which have M1 phenotype and anti-tumorous functions through the administration of IFNα [141], CD40 agonists [142], histidine-rich glycoprotein (HRG) [143], and toll-like receptors (TLRs) [144]. Another interesting approach is the indirect activation of TAMs to enhance their phagocytic activity of tumor cells by inhibiting the "don't eat me signal" of CD47-signal regulatory protein α (SIRPα) immune checkpoint using antibodies against CD47 protein expressed on tumor cells [145, 146]. However, the major challenge of this approach is how to avoid systemic toxicity on normal cells, especially, red blood cells (RBCs), which also express CD47 protein [147, 148].

Table 1-2: Selected NIH clinical trials of Mφ inhibition

Target	Phase	Trial Number	Tumor type	Drug name/ pharmcocompany	Effect	Reference
CSF1/CSF1R	I/II	NCT01346358	Advanced solid tumors	IMC-CS4/Eli Lilly Inc.	CSF1R-blocking antibody	[123]
		NCT01444404	Advanced solid tumors	AMG 820/Merck	CSF1R-blocking antibody	[124]
		NCT01804530	Pancreatic cancer	PLX7486/Plexxikon Inc.	Kinase inhibitor of CSF1R and Trk	[125]
		NCT01004861	Advanced solid tumors	PLX3397/Plexxikon Inc.	Kinase inhibitor of CSF1R and cKit	[126]
CCL2/CCR2	II	NCT01015560	Bone metastasis	MLN1202/Millennium Pharmaceuticals Inc.	Anti-CCR2 antibody	[116]
		NCT01413022	Locally advanced pancreatic cancer	PF-04136309/Pfizer Inc/.	CCR2 antagonist	[117]
IL-6R	I/II	NCT01637532	Ovarian cancer	Tocilizumab and Peg-Intron/Genentech	IL-6R monoclonal antibody	[149]
DNA repair mechanisms	III	NCT01692678	Liposarcoma and leimyosarcoma	YONDELIS (Trabectedin)/ PharmaMar	DNA backbone cleavage and cell apoptosis	[94]

	II	NCT01772979	Ovarian cancer	YONDELIS	DNA backbone cleavage and cell apoptosis	[95]
	I	NCT01426633	Liposarcoma and leimyosarcoma	YONDELIS	DNA backbone cleavage and cell apoptosis	[96]
CD40	I/II	NCT01433172	Lung cancer	(GM.CD40L) vaccine in combination with CCL21	Boosts the immune system	[150]
	I/II	NCT01103635	Metastatic melanoma	Tremelimumab and CP-870, CP-893/ AstraZeneca	CD40 agonist mAb	[151]
STAT3	I	NCT01839604	Metastatic hepatocellular carcinoma	AZD9150/ AstraZeneca	Antisense oligonucle-otide inhibitor of STAT3	[152]

CCL2, C-C motif chemokine ligand 2; CCL21, C-C motif chemokine ligand 21; CCR2, C-C motif chemokine receptor type 2; CD, cluster of differentiation; CSF1, colony stimulating factor 1; CSF1R, colony stimulating factor 1 receptor, IL-6R, interleukin 6 receptor; Mφ, macrophage; NIH, National Institute of Health; STAT3, signal transducer and activator of transcription 3; Trk, tropomyosin receptor kinase; cKit, receptor tyrosine kinase; mAb, monoclonal antibody. The table adapted from reference [88].

1.2.2. Reprogramming TAMs from M2 to M1 through gene silencing

Despite the encouraging results of the three strategies of targeting TAMs, the third approach is the most appealing since keeping Mφ in the TME while educating them to have anti-tumorous functions could be more beneficial and powerful than depleting them or blocking their infiltration altogether, and due to the plasticity of Mφ polarization and the fact that M1 and M2 Mφ have distinct differences at their genetic level (**Table 1-3**), TAMs could be reprogramed from one phenotype into another by performing genetic manipulation; such as silencing of certain genes

responsible for M2 polarization. The purpose of this study is to reprogram TAMs from M2 to M1 phenotype. In other words, reverse the pro-tumorous functions and enhance the anti-tumorous functions of Mφ aiming to realize novel Mφ-based cancer immunotherapy (**Fig. 1-6**). This could be achieved through gene silencing of specific targets that are specific and highly expressed in M2 Mφ using siRNA, which is a short sequence of nucleotides that after entering the cell can cleave target mRNA and silence any desirable gene.

Table 1- 3: Key differences between M1 and M2 Mφ at the genetic level

Comparison parameter	M1	M2
Signal transduction molecules	TSC2, SOCS3 Notch	mTOR, SHIP1, SOCS1, PDL-1, CD163, CD204, CD206, CD301, IRAK-M, Ron, TRAF-2, Rock2
Soluble mediators (cytokines, growth factors)	IL-12, TNF-α, Gas6, CXCL9, CXCL10, CXCL11	IL-1, IL-4, IL-6, IL-10, L-33, IL-34, TGF-β, CSF-1, Ym1, Fizz1, SDF-1, WNT5A, WNT7B, BMP6, CCL1, CCL2, CCL17, CCL18, CCL22, CCL24, CXCL8, CXCL12
Transcription factors	NF-κB p65/p50, STAT1	NF-κB p50/p50, STAT3, STAT6, PPARγ, RORC1/RORγ, HIF-1, HIF-2, IRF4
miRNAs	miR-155, miR-33	miR-146a, miRNA let 7b, miR-223

The table is adapted from reference [153]. Mφ, macrophage; miRNA, microRNA.

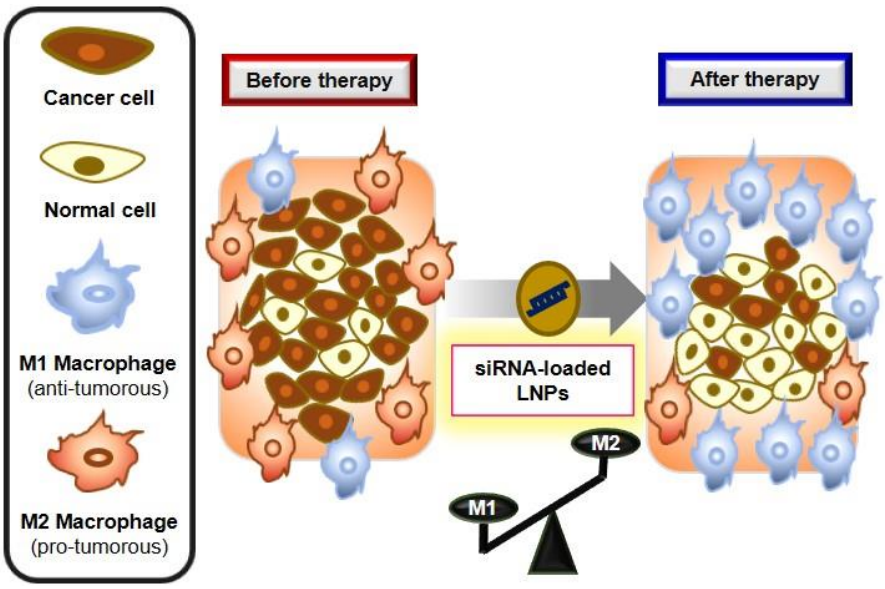

Fig. 1-6: The purpose of this study. Targeting TAMs in the TME to reprogram their phenotype and enhance their anti-tumorous functions by gene silencing using siRNA to realize novel Mφ-based cancer immunotherapy. Mφ, macrophage; TAMs, tumor-associated macrophages; TME, tumor-microenvironment; siRNA, short interfering RNA.

1.3. Gene silencing and delivery of siRNA

With the rapid growth of human genome data and the progress in understating the genetic causes and alterations in various diseases, gene therapy using oligonucleotides (ONs), which are short, single- or double-stranded deoxyribonucleic acid (DNA) or RNA molecules consisting of strands of 10-50 nucleotides (nt) [154], has become more promising alternative for conventional therapeutic of small molecular drugs and proteins since gene therapy can fix the root of illnesses. Therapeutic ONs include antisense ONs (ASO) [155], siRNA [156], and aptamers [157]. ASO and siRNA are used to modulate the expression of genes and proteins, while aptamers act as antibodies to bind and inhibit proteins.

Gene therapy using siRNA, which is a short sequence of double-stranded RNA (dsRNA) molecules (20-25 base pairs) that can cleave target mRNA and silence any desirable gene [158], is a novel strategy to cure many genetic-related diseases including cancer. In 1998, Fire and Mello *et al.* discovered RNA interference (RNAi) in C. elegans in 1998 [159] to win later on a Nobel Prize in Physiology or Medicine for this valuable discovery. Elbashir and Tuschl *et al.* reported in 2001 that synthetic siRNAs could induce RNAi in mammalian cells [158]. After the entry of dsRNA into cells and reaching the cytoplasm, it binds to an enzyme called Dicer, which breaks it into smaller

siRNA fragments. One strand (guide or passenger) of these fragments is loaded into RNA-induced silencing complex (RISC) [160-163]. The strand bound by RISC then links the protein complex to mRNA by Watson-Crick base-pairing in a sequence-specific manner. The argonaute 2 (AGO2) component of RISC has an endonuclease activity that cleaves the target mRNA and the resulting cleaved mRNA fragments are then further destroyed by cellular exonucleases. As a result, no protein is synthesized, and the target gene is silenced [160-163] (**Fig. 1-7**). The siRNA-based therapeutics have unlimited possible applications to treat a variety of diseases in which the expression of certain proteins is undesirable. However, systemic delivery of siRNAs can be challenging due to their high molecular weight and hydrophilic and anionic status, which hinder their entry into cells [164]. Furthermore, naked siRNAs are unstable in the *in vivo* environment and they are rapidly degraded by serum nucleases and eliminated through kidneys [165]. Therefore, the development of delivery systems to load and deliver siRNA into specific body tissues and organs is crucial to realize this type of therapy.

Drug delivery systems (DDS) are engineered technologies, methods, systems, approaches, or formulations (*e.g.* nanotechnologies) for packaging, transporting and delivering pharmaceutical compounds or therapeutic agents into specific body tissues and organs for medical and theranostic purposes [166, 167]. The field of nanomedicine aims to harness nanotechnology, which is defined as the "intentional design, characterization, production, and applications of materials, structures, devices, and systems by controlling their size and shape in the nanoscale range (1 to 100 nm) [168, 169]" for the diagnosis and treatment of medical diseases at the molecular level [169]. Examples of these nanotechnologies are liposomes [170], LNPs [171], dendrimers [172], carbon nanotubes [173], nanogels [174], polymeric particles and micelles [175, 176], and metal particles [177, 178], which can be used to deliver various therapeutic cargos such as small molecular drugs, chemotherapeutic reagents, proteins, and nucleic acids (*e.g.* siRNAs).

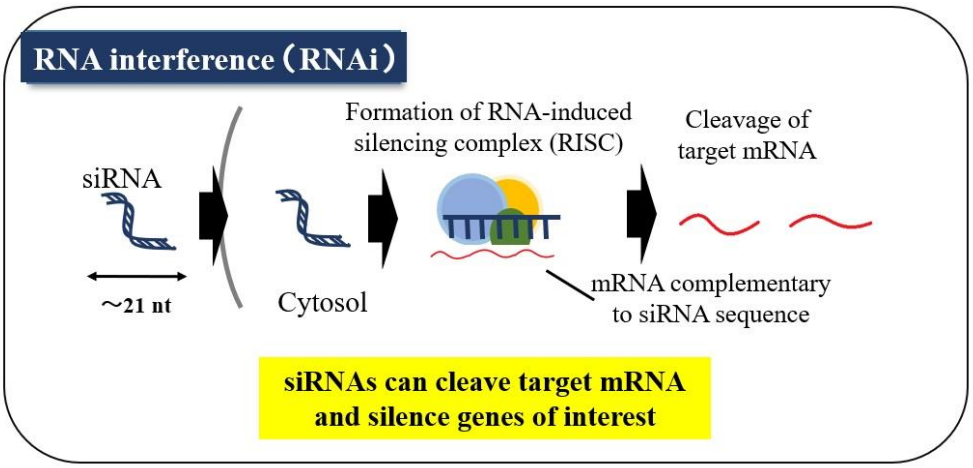

Fig. 1-7: The mechanism of action of siRNA. mRNA, messenger RNA; nt, nucleotide; siRNA, short interfering RNA.

There are few reported attempts to target TAMs using siRNA-loaded vectors aiming to deplete or block the infiltration of TAMs or to reprogram TAMs and modify their function. As for studies aiming to block the infiltration of TAMs; Leuschner *et al.* developed LNPs loaded with siRNA against CCR2 in Ly6C^{high} monocytes (TAMs precursors) aiming to inhibit the infiltration of TAMs to the TME and they succeeded in obtaining an anti-tumor therapeutic response in xenograft tumor models [127]. In addition, Ban *et al.* reported on developing bone marrow-targeted porous silicon-based multistage vector (MSV) nanoparticles decorated with thioapatamer for E-selectin and loaded with siRNA against CCL5 to inhibit the autocrine CCL5/CCR5 axis. The treatment abrogated the generation of granulocytic myeloid-derived suppressor cells and TAMs, enhanced the anti-tumor immunity and resulted in an anti-tumor therapeutic response, especially in combination with the CCR5 inhibitor Maraviroc® [179]. In another study, Qian *et al.* developed "M2-like TAM dual-targeting nanoparticles (M2NPs), whose structure and function were controlled by α-peptide (a scavenger receptor B type 1 (SR-B1) targeting peptide) linked with M2pep (an M2 macrophage binding peptide)", and they succeeded in using this siRNA-loaded formulation to achieve specific targeting of TAMs as well as obtaining anti-tumor response in melanoma models by silencing CSF1R in TAMs aiming to deplete them from the TME [180]. As for studies aiming to keep TAMs while re-educating them and modify their functions, Ortega *et al.* succeeded in developing mannosylated polymer nanoparticles (MnNP) loaded with siRNA against IκBα to restore the NF-κB pathway and re-polarize TAMs into the classical M1 phenotype. So far, their methodology has been limited to the *in vitro* studies and not yet applied for *in vivo* applications

[181, 182]. Furthermore, as stated earlier, systems decorated with mannose lack the selectivity for TAMs since their target receptors (CD206) are also expressed on other cells such as ECs or Mφ of the MPS in other organs such as liver, lungs, and spleen [107], and this could result in systemic toxicity. In another study, Conda *et al.* developed PEGylated gold nanoparticles (AuNPs) conjugated to TAMs-targeting peptides (M2pep) and loaded with siRNA against vascular endothelial growth factor (VEGF) which are expressed by M2 Mφ. The formulation was used successfully to induce an anti-tumor therapeutic response in murine lung cancer orthotopic murine model, however, it was not specific for TAMs and induced silencing in tumor cells as well [183]. Kortylewski *et al.* developed ON TLR9 agonist-STAT3 siRNA conjugates and succeeded in using it to improve the immunity of the TME by inducing silencing of STAT3, but this silencing was not limited to Mφ and induced silencing in other immune cells such as DCs and B cells [184]. Furthermore, there were other few attempts to reprogram Mφ from M2 phenotype to M1 phenotype using siRNAs against certain genes such a STAT6 or STAT3 [185, 186]. However, the study aims to silence STAT6 was limited to *in vitro* experiments [185, 186], and in the study aiming to silence STAT3 in TAMs in glioma-bearing animals, a commercially-available transfection reagent was used to transfect siRNA into tumor locally and no systemic delivery system for siRNA was developed [186].

Due to lack of enough studies in this research area, we aimed to contribute in realizing Mφ-based therapeutics by investigating the potentiality of reprograming TAMs from M2 phenotype to M1 phenotype to enhance their anti-tumorous functions through developing and using siRNA-loaded LNPs. To achieve this goal, the LNP should obtain the following requirements:

- Well tolerability by cells
- High stability in the blood circulation
- High accumulation in tumor tissues
- High and selective uptake by TAMs
- Strong gene silencing in TAMs

The following chapters explain the process of optimizing Mφ-targeted and siRNA-loaded LNP formulation which was used successfully to obtain strong gene silencing activity in Mφ, *in vitro* and *in vivo*, and an anti-tumor therapeutic response by targeting TAMs, reversing their pro-tumorous functions, and increasing their M1 phenotype proportion in tumor-bearing mice.

Chapter 2: Optimization of siRNA-loaded and Mφ-targeted LNPs

2.1. Introduction and background

Since the major challenge of siRNA-based therapeutics is their delivery, we focus on developing DDS to load and deliver siRNA to various tissues, *in vitro* and *in vivo*. In specific, we have developed LNPs, which are referred to as multifunctional envelope-type nanodevice (MEND) in some publications [187-189]. The LNPs mimic an envelope type virus based on a novel packaging strategy and are composed mainly of novel pH-sensitive cationic lipids synthesized in our laboratory, in addition to cholesterol (chol); to stabilize the LNP formulation, and PEG-lipids such as 1,2-dimirystoyl-*rac*-glycero-3-methylpolyoxyethylene (DMG-PEG 2,000); which serve as a shield to prevent the LNP's undesirable interaction with blood components and improve its stability and pharmacokinetics (**Fig. 2-1**). The LNPs are typically prepared using an alcohol dilution method which results in >90% encapsulation efficiency (EE) of siRNA, homogenous size distribution (polydispersity index (PDI): 0.0 ~ 0.2), and neutral surface charge (ζ-potential: -5.0 ~ +5.0 mV). The pH-sensitive cationic lipids improved the LNP's efficiency and activity by overcoming what is referred to as "PEG dilemma". PEG dilemma is the conflicting issue regarding PEG modification of the carrier, in which adding PEG results in the enhancement of the carrier's pharmacokinetics but deteriorates its intracellular trafficking [190]. However, after the systemic administration of the LNP composed of pH-sensitive cationic lipids, the LNP has a neutral charge in the blood stream where pH is around 7.40 and this prevents its interaction with serum components and increases the stability of the formulation. However, when the LNP enters an acidic environment with a lower pH values such as the endosome, it becomes cationic, interacts with the anionic endosomal membrane, fuses and escapes efficiently to deliver siRNA into the cytosol for effective gene silencing [187, 188] (**Fig. 2-2**). The LNPs were successfully used to target hepatocytes, especially using a novel and a pH-sensitive cationic lipid referred to as CL4H6 lipid, which has an acid dissociation constant (pKa) value of 6.30 and a chemical structure shown in **Fig. 2-3**. A previously conducted structure-activity relationship (SAR) study enabled the selection of an adequate combination of a hydrophilic head group and hydrophobic tails and permitted the LNP composed of CL4H6 lipid (CL4H6-LNP) to be developed [191]. The CL4H6-LNP demonstrated robust silencing efficiency of coagulation factor VII (FVII) gene at the protein level in hepatocytes (50% effective dose (ED_{50}): 0.0025 mg/kg), which is a higher efficiency than that of previous lipid generations developed in our

laboratory (*i.e.* YSK05 and YSK13 lipids [187, 188, 192]) and that of DLin-MC3-DMA (ED_{50} :0.005 mg/kg) [193], a lipid ingredient of Onpattro (Patisiran), a drug that has been recently approved by the FDA and European Medicines Agency (EMA) for the treatment of polyneuropathy of hereditary transthyretin (TTR)-mediated amyloidosis (hATTR) [194] (**Fig. 2-3**). The *in vivo* experiments also showed that the CL4H6-LNP demonstrated efficient endosomal escape of siRNA, biodegradability, and well-tolerability [191]. The aim of this study was to use the CL4H6-LNP and to optimize its composition and physical characteristics to target another cell population; which is TAMs.

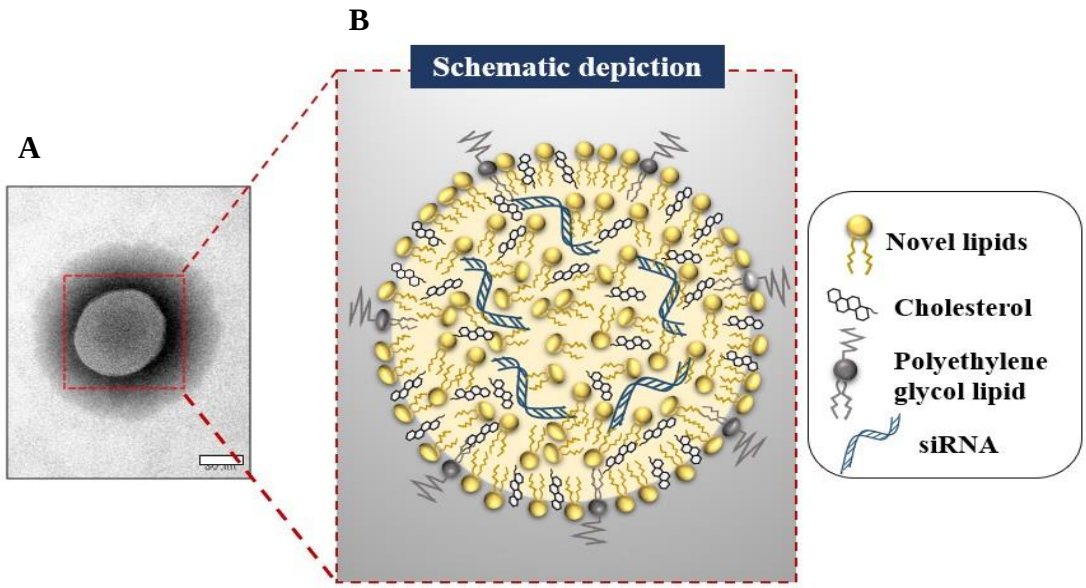

Fig. 2-1: The siRNA-loaded LNPs used in this study. TEM photo of one of the LNP formulations synthesized in our laboratory taken by JEM-1400Plus; JEOL. Scale bar: 50 nm (**A**), and a schematic depiction of the possible nanostructure of those LNPs (**B**). LNP, lipid nanoparticle; TEM, transmission electron microscopy; siRNA, short interfering RNA.

2.2. Results and discussion

2.2.1. Preparation and characterization of siRNA-loaded LNPs

The siRNA-loaded LNPs used in this study are composed of CL4H6 lipid, chol, and PEG-lipids, and they are prepared using an alcohol dilution procedure, in which siRNA in an aqueous solution is mixed with lipids dissolved in alcohol (*i.e. tert*-butanol (*t*-BuOH)) under the presence of an acidic buffer; to facilitate the precipitation and formation of the LNPs by electrostatic interactions

between the negatively-charged siRNA and the positively-charged lipids. Then, ultrafiltration and purification are carried to remove alcohol, adjust pH, and concentrate the LNPs. Finally, the physical characteristics of the LNPs are measured by dynamic light scattering (DLS) for size, PDI, and ζ-potential, and by RiboGreen assay for EE% of siRNA (**Fig. 2-4**) (see material and methods section for more details). The resulted LNPs have typically >90% EE of siRNA, homogenous size distribution (PDI: 0.0 ~ 0.2), and neutral surface charge (ζ-potential: -5.0 ~ +5.0 mV). An example of those physical characteristics is shown in (**Table 2-1**).

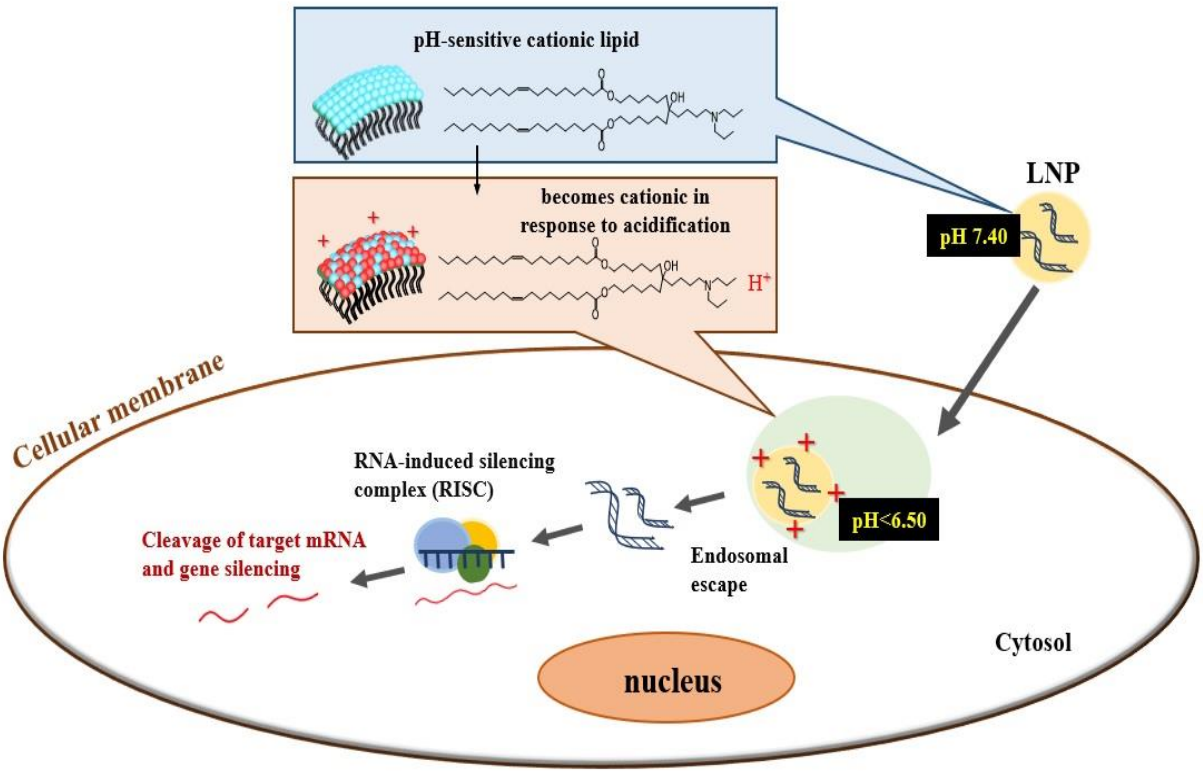

Fig. 2-2: Schematic illustration of the mechanism of siRNA delivery using LNPs. The pH-sensitive cationic lipid represented here is CL4H6. LNP; lipid nanoparticle, siRNA; short interfering RNA.

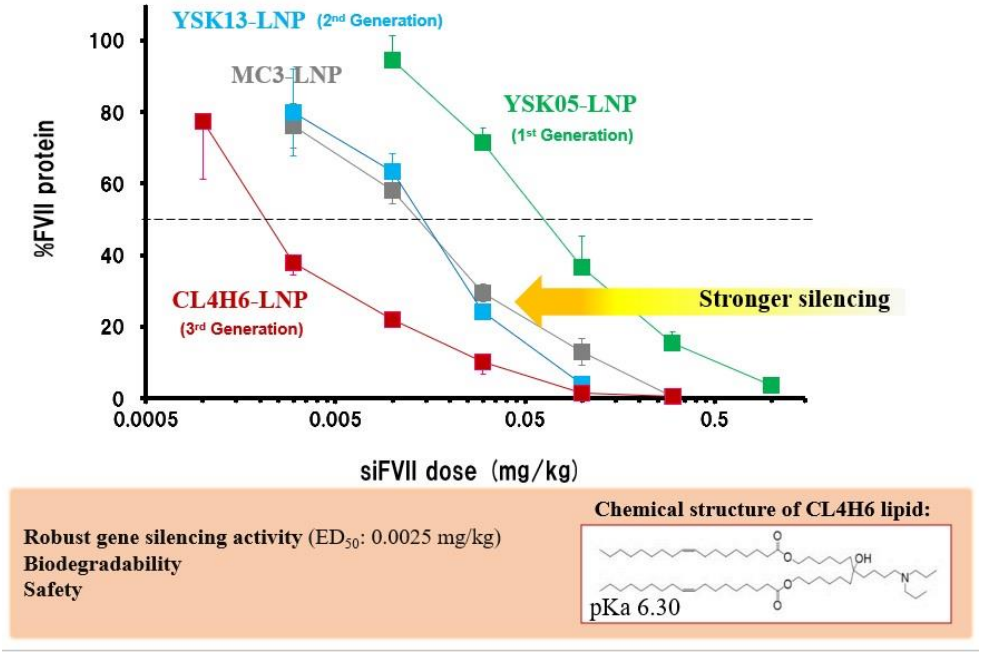

Fig. 2-3: Gene silencing of CL4H6-LNPs in hepatocytes. The silencing efficiency of CL4H6-LNPs compared to other lipids measured at the protein level of FVII in hepatocytes after 24 h of i.v. administration. Means ± SD (n=3) [191]. ED_{50}, 50% effective dose; FVII, coagulation factor VII; LNP, lipid nanoparticle; SD, standard deviation; i.v., intravenous; pKa, acid dissociation constant.

2.2.2. Optimizing the CL4H6-LNP to target TAMs

As stated in the previous chapter, in order to use the LNP formulation to target TAMs, it should meet the following criteria:

- Well tolerability by cells
- High stability in the blood circulation
- High accumulation in tumor tissues
- High and selective uptake by TAMs
- Strong gene silencing in TAMs

The optimized CL4H6-LNP formulation which met the previous criteria has the following composition: CL4H6:chol:DSG-PEG 2,000 (60/40/1 mol% of total lipids), (DSG-PEG 2,000 is 1,2-distearoyl-*rac*-glycero-3-methylpolyoxyethylene). This formulation was optimized after manipulating the following three variables regarding the LNP's composition; *i.e.* lipid ratio, PEG-lipid structure, and PEG-lipid amount.

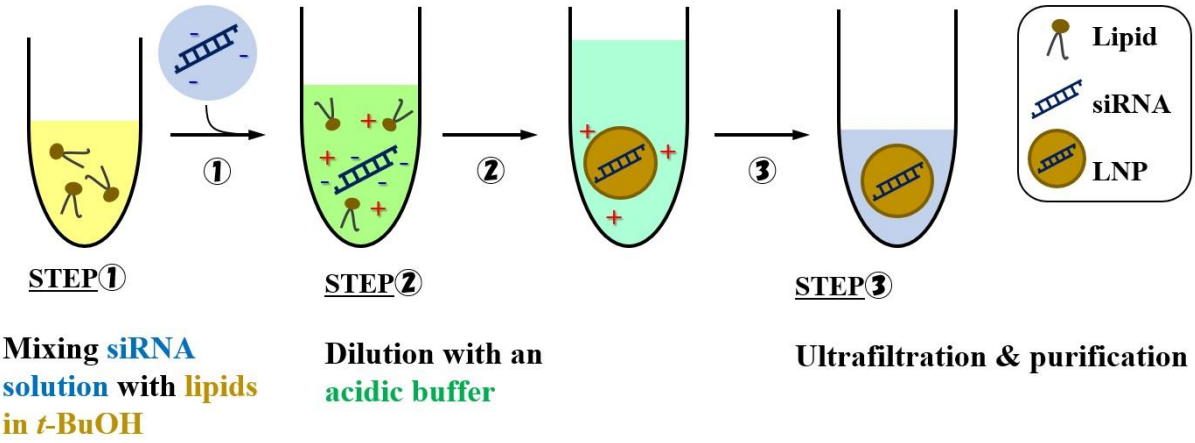

Fig. 2-4: Preparation method of the siRNA-loaded LNPs using an alcohol dilution method. LNP, lipid nanoparticle; siRNA, short interfering RNA; *t*-BuOH, *tert*-butanol.

Table 2-1: Typical physical characteristics of CL4H6-LNPs

Size (nm)	Number mean (nm)	PDI	ζ-potential (mV)	EE (%)
122.47 ± 2.58	94.09 ± 3.10	0.07 ± 0.01	0.21 ± 0.63	92.50 ± 1.25

LNP composition: CL4H6:chol:DSG-PEG 2,000 (60/40/1 mol% of total lipids). Means ± SD (n=3). DSG-PEG 2,000, 1,2-distearoyl-*rac*-glycero-3-methylpolyoxyethylene; EE, encapsulation efficiency; LNP, lipid nanoparticle; PDI, polydispersity index; SD, standard deviation; chol, cholesterol.

- ***First variable: lipid ratio***

The LNP's lipid ratio was fixed at CL4H6:chol (60/40 mol% of total lipids) for the following reasons: first; this lipid ratio was optimized previously to obtain robust silencing in hepatocytes, *in vivo* [191]. Second; this ratio resulted in LNPs with robust silencing activity in Mφ, *in vitro* and *in vivo*. During the screening process, we tried to manipulate the lipid ratio and evaluate its influence on the LNP's efficiency *in vitro*, in murine macrophage cell line (RAW 264.7 cells) or bone marrow-derived macrophages (BMDM), and *in vivo*, in TAMs. The lipid ratio compositions which resulted in LNPs with strong activity in Mφ, *in vitro*, are composed of CL4H6:chol (60/40 or 70/30 mol% of total lipids). Furthermore, another formulation composed of the helper phospholipid: 1-palmitoyl-2-oleoyl-*sn*-glycero-3-phosphoethanolamine (POPE) and composed of the following ratio: CL4H6/chol/POPE (50/25/25 mol% of total lipids) resulted in high uptake and silencing (**Table 2-2**). However, the activity of these formulations was varied in the *in vivo* environment,

and despite the comparable activity in vitro, they induced different activity in TAMs. The formulation containing CL4H6:chol (60/40 mol% of total lipids) was selected because it induced robust silencing activity both *in vitro* and *in vivo* (**Table 2-2**). A possible explanation is that this optimized lipid ratio maximized the stability of the LNP, which resulted in efficient uptake and activity. Data are presented and discussed in more details in **Chapter 3**.

Table 2-2: The influence of the lipid ratio on the LNP's activity

LNP's composition	**Activity *in vitro (mRNA level)* (BMDM or RAW 264.7 cells)**	**Activity *in vivo (protein level)* (TAMs) †**
CL4H6:chol:PEG-lipid (**60/40**/2 mol%)	(**82%** gene silencing at 30 nM siRNA (n=1))	
CL4H6:chol:PEG-lipid (**60/40**/1 mol%)	(**86%** gene silencing at 30 nM siRNA (n=3)) (BMDM)	(**72%** gene silencing at 2 doses of 2 mg siRNA/kg (n=4))
CL4H6:chol:PEG-lipid (**70/30**/2 mol%)	(**81**% gene silencing at 30 nM siRNA (n=1)) (BMDM)	(**66%** gene silencing at 2 doses of 2 mg siRNA/kg (n=2))
CL4H6:chol:POPE:PEG-lipid (**50/25/25**/2 mol%)	(**70%** gene silencing at 30 nM siRNA (n=1)) (RAW 264.7 cells)	(**26%** gene silencing at 2 doses of 2 mg siRNA/kg (n=2))

† In the s.c.-administrated human RCC (OS-RC-2) xenograft model in BALB/c Ajcl-nu/nu mice.

Model targeted gene in all experiments is CD45 (using siCD45).

BMDM, bone marrow-derived macrophages; CD, cluster of differentiation; LNP, lipid nanoparticle; PEG, polyethylene glycol; POPE, 1-palmitoyl-2-oleoyl-*sn*-glycero-3-phosphoethanolamine; RAW 264.7, murine macrophage cell line; RCC, renal cell carcinoma; TAMs, tumor-associated macrophages; chol, cholesterol; mRNA, messenger RNA; s.c., subcutaneous; siRNA, short interfering RNA.

- ***Second variable: PEG-lipid structure***

The second variable that was manipulated is PEG-lipid structure. PEG-lipids are molecules distributed on the surface of the LNP (**Fig. 2-1**) and could influence the size of the LNP as well its interaction with blood components and hence its stability and behavior in the *in vivo* environment. The PEG-lipid's molecular structure was altered from DMG-PEG 2,000, which has a short scaffold

(alkyl chain (C-14)) that results in rapid dissociation of the PEG shield and distribution to hepatocytes [191], into DSG-PEG 2,000, which has a longer scaffold (alkyl chain (C-18)) that results in slower dissociation of the PEG shield, extends the LNP's blood circulation, and shifts its accumulation from hepatocytes into tumor tissues [195]. Data are presented and discussed in more details in **Chapter 3**.

- ***Third variable: PEG-lipid amount***

The third variable that was manipulated is the PEG-lipid amount. In a previous study [196] and during the screening process of this study, we noticed that manipulating the PEG-lipid amount influenced the particle's mean diameter, and as a result of changing the size, it determined the LNP's stability in the blood and its pharmacokinetics. For instance, the LNP composed of 1 mol% of PEG-lipid resulted in LNPs with 90 to 100 nm size, which was found to be an optimized size to maximize the stability and the integrity of the LNP, minimize siRNA leakage from the formulation in the blood stream, and improve its pharmacokinetics. Data are presented and discussed in more details in **Chapter 3**.

2.3. Conclusion

As a result of the above findings, the LNP formulation with the following composition: CL4H6:chol:DSG-PEG 2,000 (60:40:1 mol% of total lipids) and a mean diameter of 90 to 100 nm was selected to proceed in subsequent experiments to target Mφ and to obtain an anti-tumor therapeutic response. Data are represented in **chapters 3 and 4**.

Chapter 3: Targeting TAMs using the optimized siRNA-loaded LNPs

3.1. Introduction

As mentioned in previous chapters, the aim of this study is to target TAMs in the TME to manipulate their function through gene silencing using siRNA-loaded LNPs to realize novel and Mφ-based cancer immunotherapy. As mentioned in **Chapter 2**, an optimized LNP formulation, referred to as CL4H6-LNP and composed of: CL4H6:chol:DSG-PEG 2,000 (60/40/1 mol% of total lipids), was optimized and selected to target Mφ, *in vitro* and *in vivo*. This chapter presents and discusses the experiments related to the optimization process and confirmed the efficiency of this formulation to target Mφ, *in vitro* (in BMDM) -with high efficiency and tolerability by cells-, to obtain high stability in the blood, and to obtain high and selective uptake and strong silencing efficiency in TAMs in tumor-bearing mice. The experiments will be presented in a sequential manner from *in vitro* to *in vivo*.

3.2. Results and discussion

3.2.1. Gene silencing in BMDM

After optimizing the protocol of BMDM isolation from ICR mice and confirming their phenotype and surface markers ($CD45^+$, $CD11b^+$, $F4/80^+$, $Ly6G^-$) using flow cytometry (**Fig. 3-1A**), and their morphology using microscopy (**Fig. 3-1B)** (see material and method section for more details), they were selected as the *in vitro* model of Mφ to evaluate the efficiency of the CL4H6-LNP and fix its lipid composition (CL4H6:chol molar ratio) before proceeding in the *in vivo* experiments (see **Table 2-2** for more details). The BMDM were transfected with the optimized siRNA-loaded CL4H6-LNPs with the following composition: CL4H6:chol:DMG-PEG 2,000 (60:40:1 mol% of total lipids), and the efficiency of those LNPs was compared to that of the commercially available Invitrogen™ Lipofectamine™ RNAiMAX transfection reagent. After 24 h of transfection, the CL4H6-LNPs induced stronger gene silencing than RNAiMAX in BMDM of the model target gene (CD45) at the mRNA level, measured by quantitative real-time polymerase chain reaction (qRT-PCR) at 3 and 10 nM siRNA concentration (**Fig. 3-2A**). It also induced less cellular toxicity than RNAiMAX as observed by microscopy (**Fig. 3-2B**).

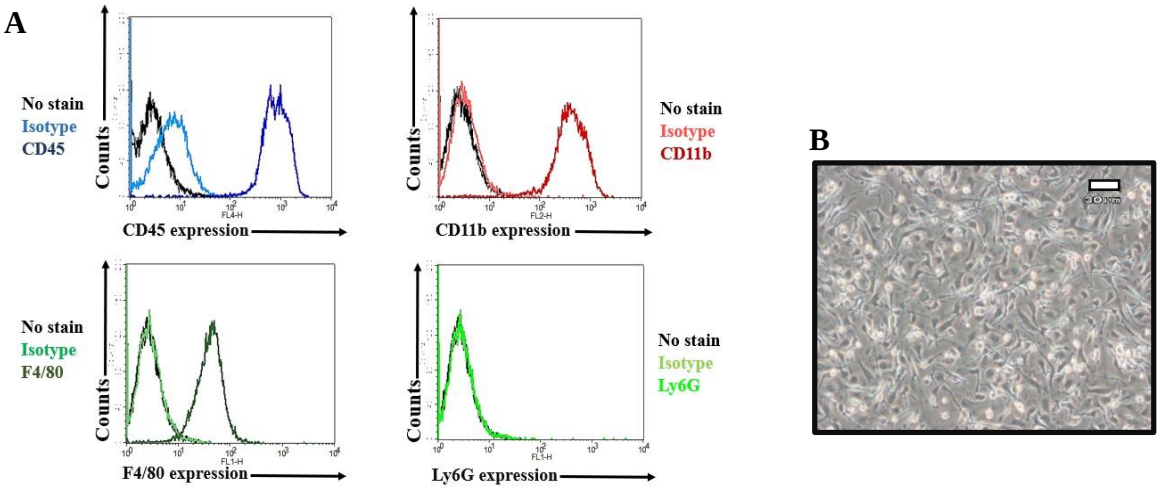

Fig. 3-1: Confirming the quality of isolated BMDM. BMDC were isolated from ICR mice, and after *ex vivo* culture for one week in a medium supplemented with M-CSF, cells were collected, and their phenotype and surface markers of Mφ were confirmed using flow cytometry (**A**), and their morphology was observed using microscopy (**B**). The image was taken by Olympus (IX70) microscope. Scale bar: 30 µm. BMDC, bone marrow-derived cells; BMDM, bone marrow-derived macrophages; CD, cluster of differentiation; M-CSF, macrophage-colony stimulating factor; Mφ, macrophage.

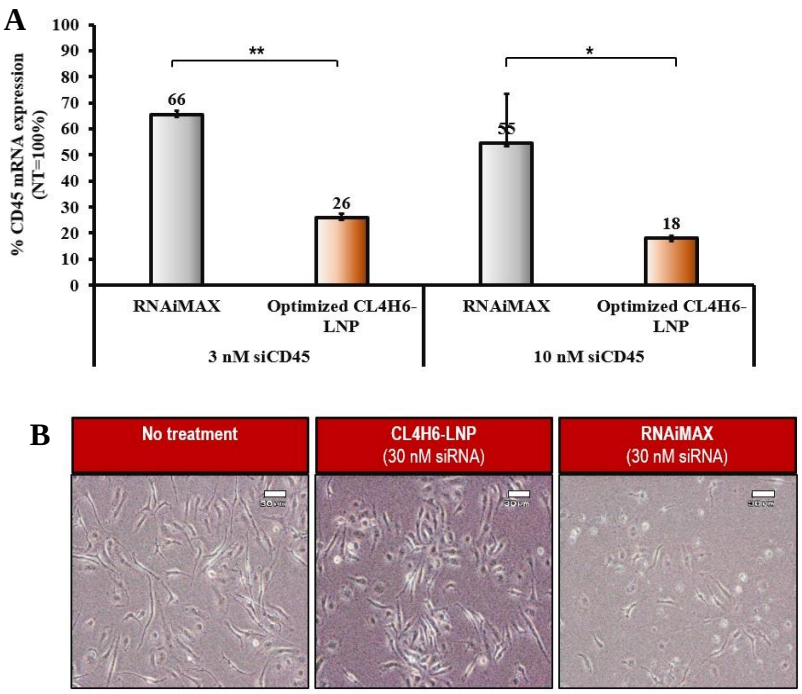

Fig. 3-2: Gene silencing in BMDM. Percentage of target gene expression at mRNA level, measured by qRT-PCR (**A**), and cellular morphology of BMDM (**B**) after transfection with either CL4H6-LNPs or RNAiMAX for 24 h. The optimized LNP composition: CL4H6:chol:DMG-PEG 2,000 (60/40/1 mol% of total lipids). * $P < 0.05$, ** $P < 0.01$ (Two-tailed unpaired student's t-test). Means ± SD (n=3). Images were taken by Olympus (IX70) microscope, brightness and contrast were enhanced at the same level (40%) in all photos by Microsoft software. Scale bar: 30 µm. BMDM, bone marrow-derived macrophages; CD, cluster of differentiation; DMG-PEG 2,000, 1,2-dimirystoyl-*rac*-glycero-3-methylpolyoxyethylene; LNP, lipid nanoparticle; SD, standard deviation; chol, cholesterol; mRNA, messenger RNA; siRNA, short interfering RNA.

It is noteworthy to mention that the CL4H6-LNP's superior efficiency than RNAiMAX could be attributed to the chemical structure, shape, and pKa value of CL4H6 lipid, which could have maximized the LNP's cellular uptake and facilitated an efficient endosomal escape of siRNA into the cytosol [191]. Furthermore, due to the biodegradability and the neutral surface charge of CL4H6-LNPs (pKa 6.30), they were more tolerable and less damaging to cells compared to RNAiMAX, which has a high cationic surface charge.

3.2.2. Pharmacokinetics and blood stability

After fixing the following lipid composition of the LNP (CL4H6:chol (60/40 mol% of total lipids)), which demonstrated strong gene silencing in Mφ, *in vitro*, PEG-lipid's structure was altered and its amount was manipulated for screening, *in vivo*. As mentioned in previous chapters, PEG-lipids are molecules distributed on the surface of the LNP (**Fig. 2-1**) and could influence the size of the LNP as well its interaction with blood components and hence its stability and behavior in the *in vivo* environment. The PEG-lipid's molecular structure was altered from DMG-PEG 2,000, which has a short scaffold and used to target hepatocytes [191], into DSG-PEG 2,000, which has a longer scaffold and this extends the LNP's blood circulation and shifts its accumulation from hepatocytes into tumor tissues (see **Section 3.2.4.** for more details). Manipulating the amount of DSG-PEG 2,000 in the LNP (1 to 3 mol% of total lipids) was significant and it influenced the mean diameter of the LNP (**Table 3-1**) and determined its pharmacokinetics. After injecting the LNPs, which have various PEG-lipid amounts and mean diameters, intravenously (i.v.) to ICR mice and measuring the fluorescence of both siRNA and lipid in the blood circulation at different time points, we found that although the PEG-lipid amount did not influence the blood circulation of both lipid and siRNA (**Fig. 3-3A, B**), it influenced the stability of the LNP since the LNP formulation which was modified with DSG-PEG 2,000 at 1 mol% of total lipids resulted in a formulation with a mean diameter of 90 to 100 nm, and obtained the highest siRNA/lipid ratio (area under the curve $(AUC)_{siRNA}$/area under the curve $(AUC)_{lipid}$) (**Table 3-1**). This higher siRNA/lipid ratio could be interpreted as minimal siRNA leakage and high LNP's integrity and stability in the blood circulation (**Fig. 3-3C**). Although PEG-lipid amount did not influence the blood circulation hence the LNPs with various PEG-lipid's amounts (1 to 3 mol%) had nearly similar circulation time of both siRNA and lipids (**Fig. 3-3A, B**), decreasing PEG-lipid amount up to 1 mol% resulted in LNPs with relatively larger size which could have increased the LNP's stability, minimized its absorption

to serum proteins, and decreased siRNA leakage. This coincides with our previous report regarding the effect of the LNP's size and its stability and silencing activity [196]. The size of 90 to 100 nm was optimum to target TAMs for two possible reasons. First, this size resulted in a higher stability and integrity of the LNP in the blood circulation compared to LNPs with smaller sizes (**Fig. 3-3C**). Second, this size is a medium and a balanced size, not very large (*e.g.* 150-200 nm) which could hinder the LNP's ability to accumulate in tumor tissues, and not very small (*e.g.* ≤50 nm) which could help the LNP to penetrate deeply in tumor tissues and be taken up by tumor cells to a high extent [197-200]. Those findings are part of the screening process that enabled the selection of the optimized LNP formulation with the following composition: CL4H6:chol:DSG-PEG 2,000 (60/40/1 mol% of total lipids) and a mean diameter of 90 to 100 nm to proceed in subsequent experiments to target TAMs and to obtain an anti-tumor therapeutic response.

Table 3-1: Relationship between PEG-lipid's amount and siRNA/lipid ratio

PEG-lipid's amount in the LNP (mol%)	**Mean diameter (nm)**	**siRNA/lipid ratio (AUC_{siRNA}/AUC_{lipid})**
1	89.26	0.91 ± 0.04 *
2	58.47	0.80 ± 0.18
3	51.58	0.60 ± 0.04

* P < 0.05 (1 mol% against 3 mol%) (Non-repeated ANOVA followed by SNK test). Means ± SD (n=3). AUC, area under the curve; LNP, lipid nanoparticle; PEG, polyethylene glycol; siRNA, short interfering RNA.

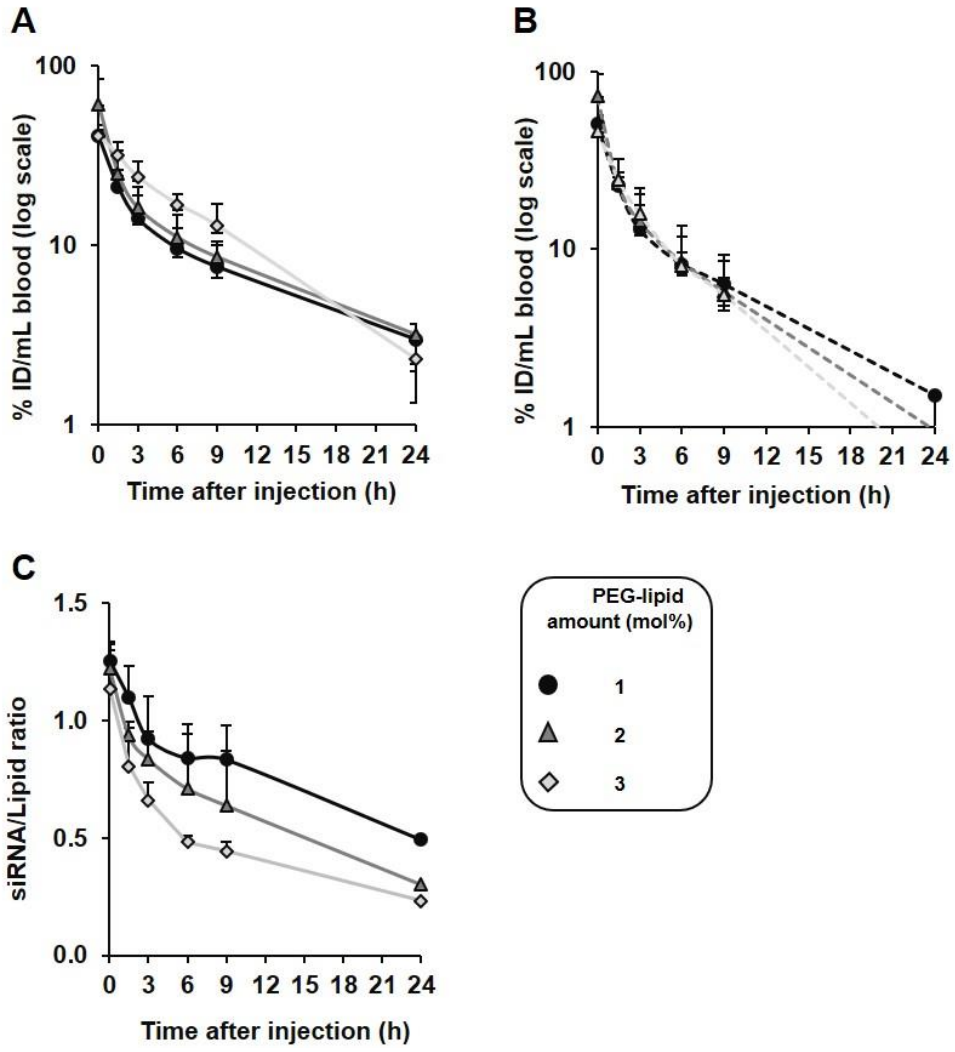

Fig. 3-3: The influence of PEG-lipid's amount on the pharmacokinetics of the CL4H6-LNPs. (**A**) The blood circulation of lipids. (**B**) The blood circulation of siRNAs (**C**) siRNA/lipid ratio. Mice were injected with DiI-labeled LNPs composed of CL4H6:chol (60/40 mol% of total lipids) with different amounts of DSG-PEG 2,000 (1 to 3 mol% of total lipids) i.v. at a dose of 1 mg AF-647-conjugated siRNA/kg. DiI excitation/emission wavelength 549/565 nm, AF-647 excitation/emission wavelength 649/679 nm. AF, alexa fluor; AUC, area under the curve; DSG-PEG 2,000, 1,2-distearoyl-*rac*-glycero-3-methylpolyoxyethylene; ID, injected dose; LNP, lipid nanoparticle; PEG, polyethylene glycol; SD, standard deviation; chol, cholesterol; i.v., intravenously; siRNA, short interfering RNA.

3.2.3. Selection of a tumor model for *in vivo* experiments

The tumor model that was selected for the *in vivo* experiments, in which TAMs will be targeted using the optimized siRNA-loaded CL4H6-LNPs and their function will be manipulated by gene silencing to obtain an anti-tumor therapeutic response, is the subcutaneous (s.c.) human renal cell carcinoma (RCC) (OS-RC-2) xenograft model in BALB/c Ajcl-nu/nu mice [201-203]. There are

two main reasons for selecting this model. First, since this mouse strain is immune-deficient, lacks the presence of T cells while has Mφ as the main population among leukocytes, this could enable us to study and manipulate Mφ exclusively while excluding the possibility of any negative or positive influence of T cells on the final therapeutic outcomes. In other words, this model could allow us to study the role and the influence of Mφ on the TME such as its contribution in tumor cell activation, angiogenesis, metastasis, and invasion while excluding the immune function and the interaction with other immune cells, especially T cells. Second, due to the possibility that a small proportion of the LNP will be taken up and induce gene silencing activity in tumor cells, using this model could enable us to exclude the influence of the unintended gene silencing in tumor cells on the final therapeutic response, by using murine species-specific siRNAs to silence the murine Mφ and not human tumor cells. As a result, this model could finally enable us to prove our concept regarding Mφ-based cancer immunotherapy.

3.2.4. Observation and quantification of the LNP's biodistribution

As explained previously in **Chapter 2**, The PEG-lipid's molecular structure was altered from DMG-PEG 2,000, which has a short scaffold (alkyl chain (C-14)) and was used to target hepatocytes [191], into DSG-PEG 2,000, which has a longer scaffold (alkyl chain (C-18)) aiming to slow the PEG shield dissociation from the LNP, extend its circulation time, and increase its accumulation in tumor tissues [195]. To prove this assumption, OS-RC-2-bearing mice were injected i.v. with DiD-labeled CL4H6-LNPs composed of CL4H6:chol:PEG-lipid (DMG-PEG 2,000 or DSG-PEG 2,000) (60/40/1 mol% of total lipids) at a dose of 1 mg siRNA/kg, and after 24 h of administration, body organs (liver, lungs, spleen, kidneys, and tumor) were collected and the biodistribution of the LNP was observed by *in vivo* imaging. In addition, the biodistribution was quantified using ImageJ software. As shown in **Fig. 3-4**, despite the comparable biodistribution in body organs, modifying the LNPs with DSG-PEG 2,000 enhanced their accumulation in tumor tissues compared to those modified with DMG-PEG 2,000 by 1.74-fold. The modification also slightly decreased the LNP's distribution to the liver while slightly increased its distribution in the spleen and elimination though kidneys. This could be possibly explained as a result of the difference between the fate of LNPs with both types of PEG-lipids. The DMG-PEG 2,000 has a shorter scaffold which results in rapid dissociation of the shield and absorption of the LNP by serum proteins, especially apolipoprotein E (ApoE), and distribution mainly to the liver through

apolipoprotein E-low-density lipoprotein (ApoE-LDLR) pathway [195, 204]. In the other hand, the DSG-PEG 2,000 has a longer scaffold which results in slower dissociation of the shield, longer circulation of the LNP in the blood stream, and a higher chance for to accumulate in the tumor possibly through the enhanced permeation and retention (EPR) effect [205-207]. Furthermore, the slight decrease of the LNP's distribution to the liver is compensated by the slight increase of its distribution to the spleen, and since the LNP is not rapidly metabolized in the liver, its elimination through kidneys is higher than that of DMG-PEG 2,000. Those results indicate that we succeeded in increasing the accumulation of the CL4H6-LNP in tumor tissues.

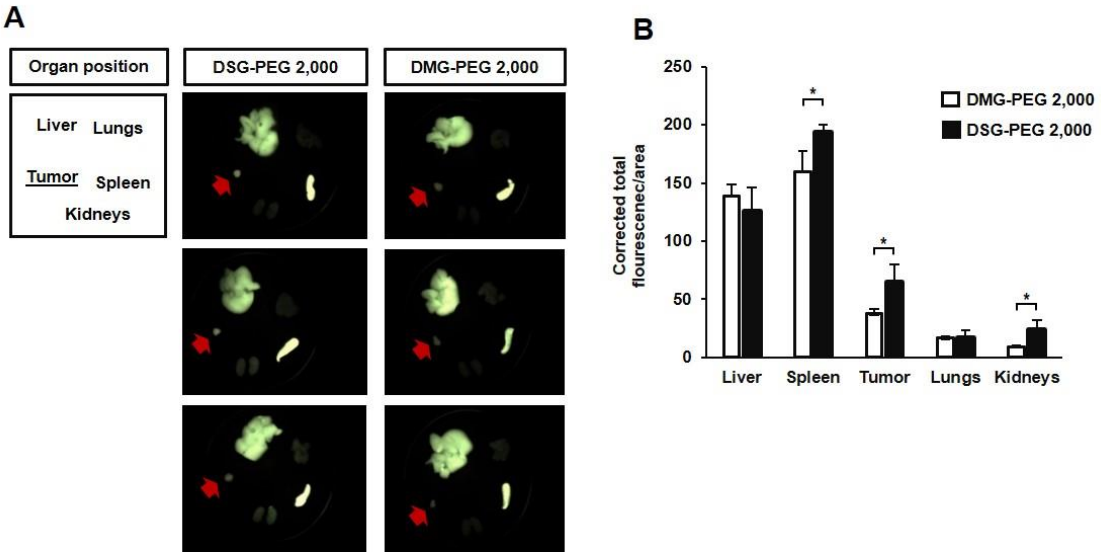

Fig. 3-4: Biodistribution of the CL4H6-LNP and the influence of PEG-lipid's structure on tumor accumulation. OS-RC-2-bearing mice were injected with DiD-labeled CL4H6-LNPs (CL4H6:chol 60/40 mol%) modified with 1 mol% DMG-PEG 2,000 or DSG-PEG 2,000 i.v. at a dose of 1 mg siRNA/kg, and after 24 h, organs were collected and biodistribution was observed using *in vivo* imaging (**A**), and quantified using ImageJ software (**B**). The red arrows indicate tumor tissues. * $P < 0.05$ (Two-tailed unpaired student's t-test). Means ± SD (n=3). DMG-PEG 2,000, 1,2-dimirystoyl-*rac*-glycero-3-methylpolyoxyethylene; DSG-PEG 2,000, 1,2-distearoyl-*rac*-glycero-3-methylpolyoxyethylene; LNP, lipid nanoparticle; PBS (-), phosphate buffered saline; PEG, polyethylene glycol; SD, standard deviation; chol, cholesterol; i.v., intravenously; siRNA, short interfering RNA.

3.2.5. The uptake of the LNPs by TAMs

Next, we evaluated the uptake of the optimized CL4H6-LNPs in tumor tissues and compared its uptake in various cell populations. In this experiment, the OS-RC-2-bearing mice were injected i.v. with DiD-labeled CL4H6-LNPs composed of CL4H6:chol:DSG-PEG 2,000 (60/40/1 mol% of total lipids) at a dose of 1 mg siRNA/kg, and after 24 h of administration, tumor tissues were collected,

single cell suspension was prepared, and the uptake was measured using multi-color flow cytometry. The CL4H6-LNP was highly taken up by leukocytes ($CD45^+$ cells), and in specific, by TAMs ($CD45^+$, $CD11b^+$, $F4/80^+$ cells). The uptake by leukocytes and TAMs was higher than that by non-leukocytes ($CD45^-$ cells), which could include tumor cells and ECs, by 6.89- and 8.67-folds, respectively. Among leukocytes, the uptake was selectively higher in TAMs compared to neutrophils ($CD45^+$, $CD11b^+$, $F4/80^-$ cells) or leukocytes other than TAMs or neutrophils ($CD45^+$, $CD11b^-$ cells) which could include DCs (**Fig. 3-5**). These results indicate that despite not attaching Mφ-targeted ligands to the LNP, the LNP was highly and selectively taken up by TAMs, and this could be attributed to two main reasons. First, adding DSG-PEG 2,000 enhanced the tumor accumulation of the LNP, probably by EPR effect as discussed in the previous section. Second, the physical characteristics of the LNP, such as neutral charge and 90 to 100 nm size, enabled it to be naturally recognized and taken up by TAMs, which are in this tumor model are the main population among leukocytes. Whereas the relatively large size of the LNP diminished its deep accumulation in tumor tissues and uptake by tumor cells.

We also compared the LNP's uptake at two time points, 2 and 24 h after the i.v. administration, to track the time-dependent uptake and distribution to tumor tissues. Unexpectedly, we found that the uptake of the LNP, both in TAMs as well as in non-leukocytes, is time-dependent and it increased over time (**Fig. 3-6**). There are two possible explanations for this phenomenon. First, the LNP was taken up by leukocytes in the spleen and then those leukocytes (Mφ in specific) carrying the LNP migrated to tumor tissues allowing us to detect the LNP with a higher extent after 24 h. Second, the LNP accumulated in tumor tissues but not all LNPs were taken up at the same time due to the normal distribution of their PEG-lipid shield. Although the LNPs have the same amount of PEG-lipid (1 mol%), some LNPs have a smaller density of PEG-lipid and after the rapid dissociation of PEG-lipid, they were taken up by cells. Whereas, LNPs which have a larger density of PEG-lipid had slower dissociation of PEG-lipid and were taken up by cells later. Although the two explanations are possible, the second explanation is more likely because after calculating the time-dependent uptake ratio (uptake at 24 h/uptake at 2 h), the ratio was almost same, 3.42 and 3.77 for the two populations TAMs and non-leukocytes, respectively. Suggesting that the LNPs were not carried in the migrated Mφ, but they were directly accumulated in tumor tissues and their uptake increased over time due to the gradual dissociation of their PEG-lipid shield.

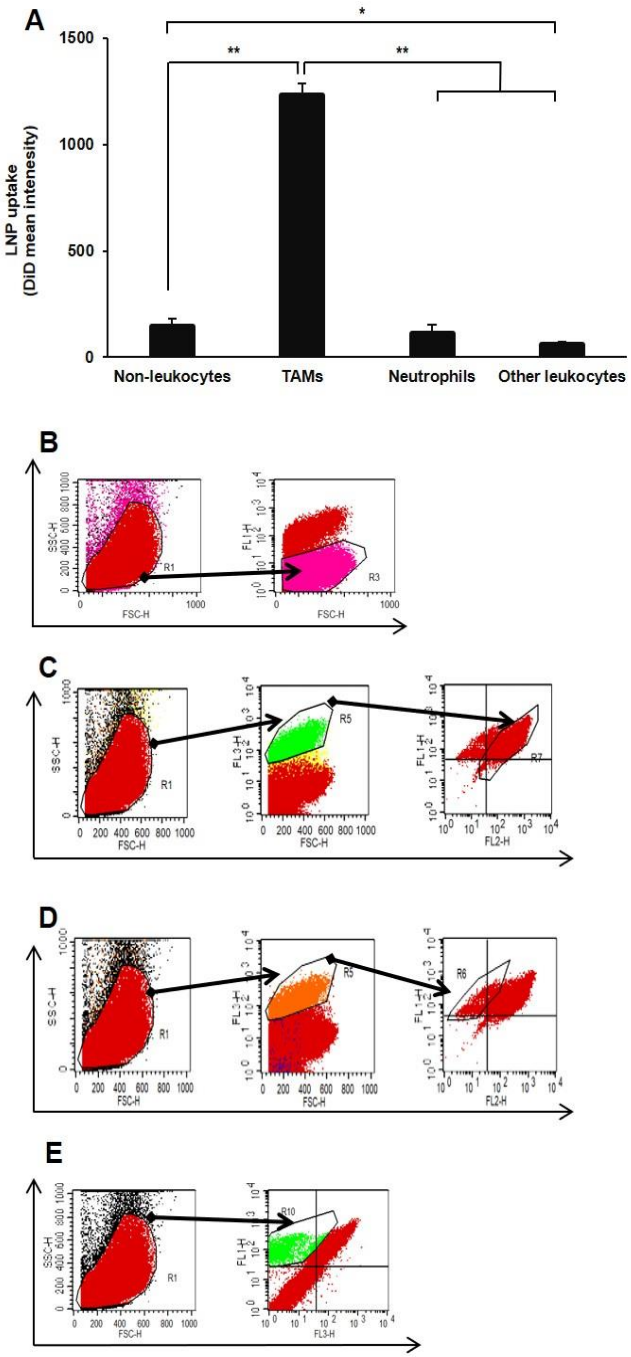

Fig. 3-5: The uptake of CL4H6-LNPs. (**A**) The uptake of the CL4H6-LNPs by various tumor populations in the TME. *****P < 0.05, ** P < 0.01 (Non-repeated ANOVA followed by SNK test). Means ± SD (n=3). (**B-E**) Gating strategy of tumor populations for measuring the uptake of CL4H6-LNPs. The fluorescence of DiD (uptake of CL4H6-LNPs) was measured using multi-color flow cytometry. The following criteria were used to define and gate different cell populations in the TME; (**B**) non-leukocytes, which could include tumor cells and ECs (FITC-CD45$^-$ cells), (**C**) TAMs (FITC-CD45$^+$, PerCP-CD11b$^+$, PE-F4/80$^+$ cells), (**D**) neutrophils (FITC-CD45$^+$, PerCP-CD11b$^+$, PE-F4/80$^-$ cells), (**E**) leukocytes other than TAMs or neutrophils, which could include DCs (FITC-CD45$^+$, PerCP-CD11b$^-$ cells). Channels used: FITC, FL1-H; PE, FL2-H; PerCP, FL3-H; DiD, FL4-H. DCs, dendritic cells; ECs, endothelial cells; SD, standard deviation; LNPs, lipid nanoparticles; TAMs, tumor-associated macrophages; TME, tumor-microenvironment.

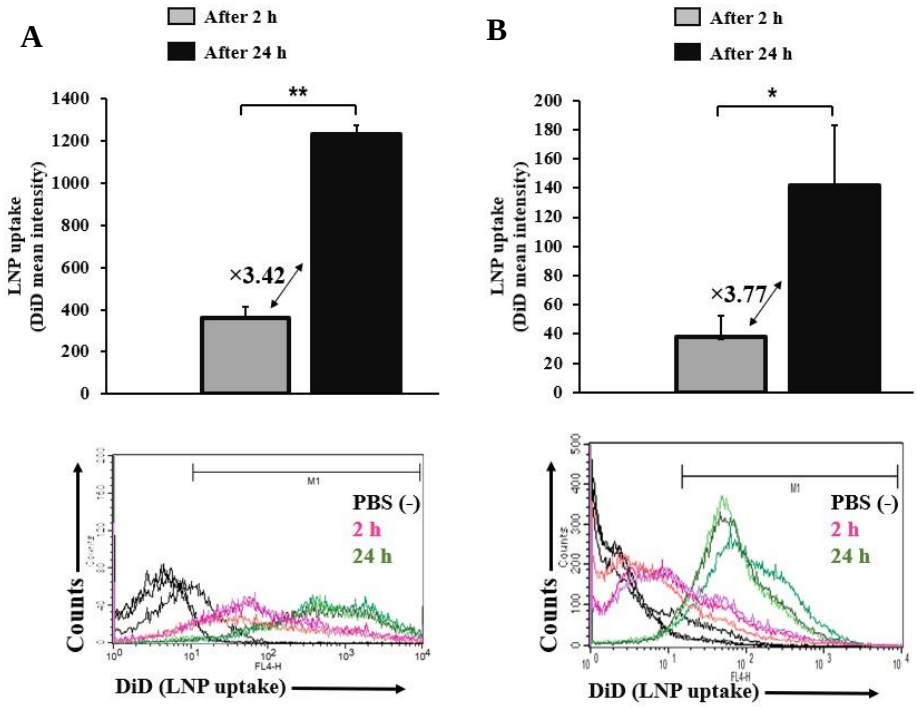

Fig. 3-6: Time-dependent uptake of CL4H6-LNPs in the TME. OS-RC-2-bearing mice were injected with DiD-labeled CL4H6-LNPs (CL4H6:chol:DSG-PEG 2,000 60/40/1 mol%) i.v. at a dose of 1 mg siRNA/kg, and after two time points, 2 and 24 h, tumor tissue was collected and uptake was analyzed using multi-color flow cytometry in TAMs ($CD45^+$, $CD11b^+$, $F4/80^+$ cells) (**A**) and in non-leukocytes ($CD45^-$ cells) (**B**). * $P < 0.05$, ** $P < 0.01$ (Two-tailed unpaired student's t-test). Means ± SD (n=3). CD, cluster of differentiation; DSG-PEG 2,000, 1,2-distearoyl-*rac*-glycero-3-methylpolyoxyethylene; LNP, lipid nanoparticle; PBS (-), phosphate buffered saline; SD, standard deviation; TAMs, tumor-associated macrophages; TME, tumor-microenvironment; chol, cholesterol; i.v., intravenously; siRNA, short interfering RNA.

3.2.6. Gene silencing in TAMs

The optimized CL4H6-LNPs (CL4H6:chol:DSG-PEG 2,000 (60/40/1 mol% of total lipids)) were then used to target TAMs in OS-RC-2-bearing mice. After the i.v. administration of the LNPs at two doses of 2 mg siRNA/kg, they induced ~70% gene silencing of the model target gene (CD45) at the protein level, measured by multi-color flow cytometry, and the activity was significant to that of siRNA-free empty CL4H6-LNPs which were used as a negative control (**Fig. 3-7**). As mentioned earlier in section 3.2.1., the CL4H6-LNP's strong silencing efficiency could be attributed to the chemical structure, shape, and pKa value of CL4H6 lipid, which could have maximized the LNP's cellular uptake and facilitated an efficient endosomal escape of siRNA into the cytosol. As discussed in more details in reference [191], the SAR study enabled the identification of the pH-sensitive cationic CL4H6 lipid which resulted in robust silencing activity, biodegradability, and safety, due to three main merits related to their chemical structure (**Fig. 2-3**).

First, the optimized pKa value, which is affected by the chemical structure of the hydrophilic head group. The CL4H6 lipid's pKa value of 6.30 improved the pH-sensitivity of the LNP by enhancing the stability of the LNP in the blood stream through minimizing the non-specific interactions with plasma proteins and avoiding rapid clearance by reticuloendothelial system (RES), while facilitated an efficient endosomal escape via membrane fusion in the endosomal compartment (**Fig. 2-2**). Second, the bulky hydrophobic tail enabled an efficient phase transition from a lamellar to an inverted hexagonal (nonbilayer) phase triggered by the formation of "cone-shaped" ion pairs between protonated pH-sensitive cationic lipids in the LNP and anionic lipids in the endosomal membrane followed by membrane fusion-mediated endosomal escape. Third, the biodegradable functional group (*i.e.* an ester bond) resulted in minimal lipid toxicity, high biocompatibility, tolerability, and safety. Although these merits were studied previously regarding the LNP's activity in hepatocytes, they can be applied to explain the activity of CL4H6-LNPs in TAMs.

3.3. Conclusion

The optimized siRNA-loaded CL4H6-LNPs which has the following composition: CL4H6:chol:DSG-PEG 2,000 (60/40/1 mol% of total lipids) and 90 to 100 nm mean diameter was successfully used to target Mφ, *in vitro*, in BMDM, and *in vivo*, in TAMs of the s.c.-administered human RCC (OS-RC-2) xenograft model in BALB/c Ajcl-nu/nu mice. This model was selected to enable us study Mφ exclusively, since they are the main population among leukocytes in this immune-deficient mouse strain. The LNP fulfilled all the necessary requirements regarding Mφ targeting (**Fig. 3-8**):

- Well tolerability by cells
  (due to the CL4H6 lipid's biodegradability and neutral charge)
- High stability in the blood circulation
  (due to optimum PEG-lipid amount and particle size)
- High accumulation in tumor tissues
  (due to the choice of PEG-lipid structure)
- High and selective uptake by TAMs
  (possible due to optimum particle size and surface charge)
- Strong gene silencing in TAMs
  (due to optimum chemical structure of the CL4H6 lipid)

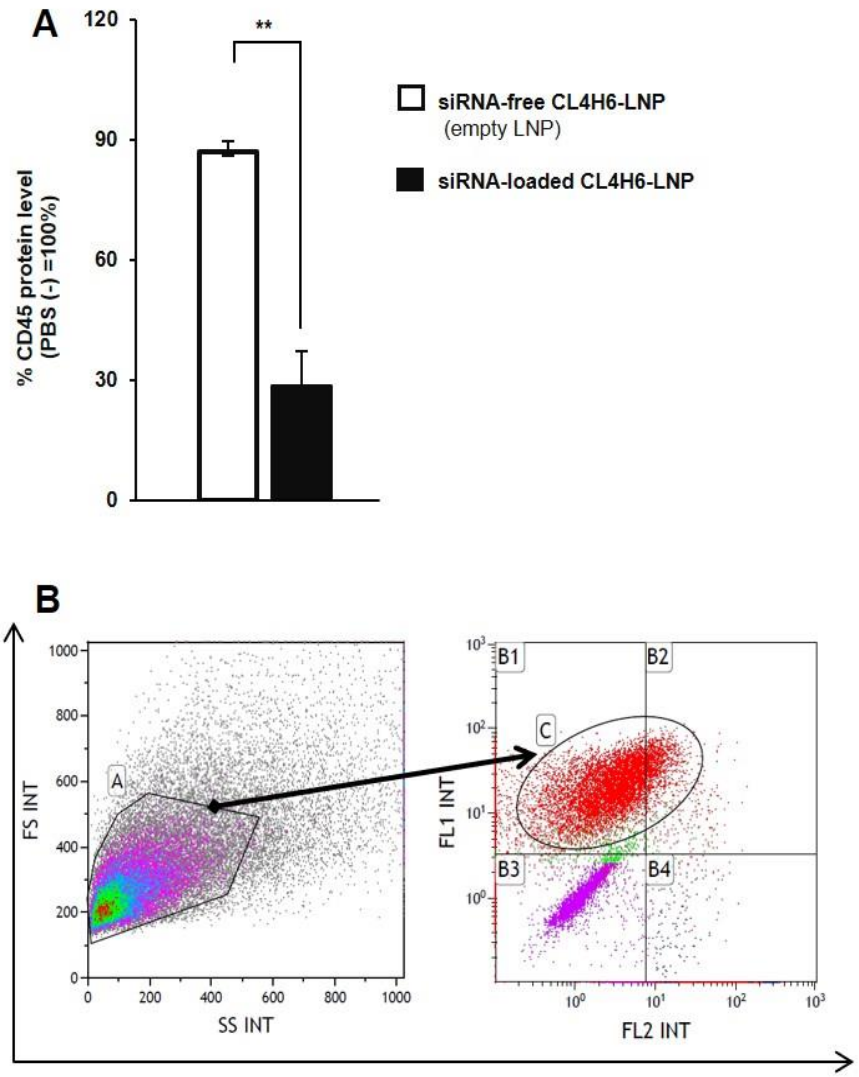

Fig. 3-7: Gene silencing of the CL4H6-LNPs in TAMs. (**A**) Gene silencing of the siRNA-loaded CL4H6-LNPs in TAMs. Percentage of target gene expression at the protein level, measured by multi-color flow cytometry. OS-RC-2-bearing mice were injected with the optimized CL4H6-LNPs (CL4H6:chol:DSG-PEG 2,000 60/40/1 mol%) i.v. at two doses of 2 mg siRNA/kg against CD45 as a model target gene. ** $P < 0.01$ (Non-repeated ANOVA followed by SNK test). Means ± SD (n=4). (**B**) Gating strategy of TAMs for measuring gene silencing of CL4H6-LNPs. The fluorescence of APC (CD45 target protein expression) was measured using multi-color flow cytometry. TAMs were defined as FITC-F4/80^{+}, PE-HLA-A,B,C^{-} cells. Channels used: FITC, FL1-H; PE, FL2-H, APC, FL6-H. CD, cluster of differentiation; DSG-PEG 2,000, 1,2-distearoyl-*rac*-glycero-3-methylpolyoxyethylene; HLA, human leukocyte antigen; LNP, lipid nanoparticle; SD, standard deviation; TAMs, tumor-associated macrophages; ; chol, cholesterol; i.v., intravenously; siRNA, short interfering RNA.

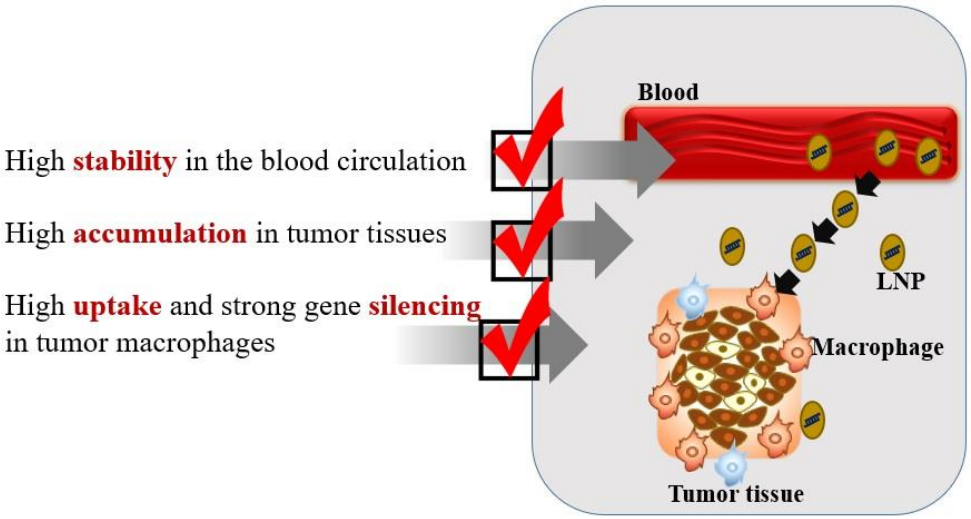

Fig. 3-8: The optimized CL4H6-LNP fulfilled all the requirements regarding Mφ-targeting. LNP, lipid nanoparticle; Mφ, macrophage.

Chapter 4: Obtaining anti-tumor therapeutic response by manipulating TAMs

4.1. Introduction

After confirming that the optimized siRNA-loaded CL4H6-LNP has high and selective uptake and strong silencing activity in TAMs, it was used to target TAMs and manipulate their function by silencing certain genes responsible for their M2 phenotype or pro-tumorous functions in OS-RC-2-bearing mice. This chapter describes the choice of targeted genes, the design of the anti-tumor experiment, and the final results summarized by success in obtaining an anti-tumor therapeutic response through gene silencing in TAMs which resulted in an increase of Mφ infiltration and M1 phenotype proportion in the TME, as well as reversing the pro-tumorous functions of M2 Mφ. The increase of M1 Mφ, which have an anti-tumorous function, combined with reversing the pro-tumorous functions of M2 Mφ enabled the reduction of tumor growth by inhibiting angiogenesis and tumor cell proliferation.

4.2. Results and discussion

4.2.1. The choice of targeted genes in TAMs

As explained in detail in (**Chapter 1, Section 1.2.2. and Table 1-3**), there are key differences between M1 (anti-tumorous) Mφ and M2 (pro-tumorous) Mφ at their genetic level. Both phenotypes express different transduction molecules, soluble mediators, transcript factors, and microRNAs (miRNAs) [153]. Therefore, there are many candidate genes to be silenced, especially in M2 Mφ, to reprogram them into M1 Mφ aiming to reverse their pro-tumorous functions and/or enhance their anti-tumorous functions. It was mentioned in **Chapter 1, Section 1.2.1.** some recent attempts by other researchers to reprogram Mφ from M2 to M1 by inhibiting certain genes such as Jmjd3 [128], STAT6 [129], STAT3 [130, 131], Dicer [132], superoxide (O(2-)) [133], IL4Rα [134], COX-2 [135], PI3Kγ [136], CSF1R [113], MARCO [137], HCK [138], NF-κB [139], and HDAC [140]. Other interesting candidate genes to be silenced are mechanistic target of rapamycin complex 2 (mTORC2) and interferon regulatory factor 4 (IRF4), which are involved in glucose utilization and support M2 activation [208], or suppressor of cytokine signaling (SOCS1), which down regulation could activate STAT1 and M1 polarization [209, 210]. However, we selected the

following targeted genes; STAT3 and hypoxia-inducible factor 1α (HIF-1α), since these two genes are important transcription factors that are highly expressed in M2 Mφ and are mediated in many pathways related to most, if not all, the pro-tumorous functions of TAMs [153].

- ***First targeted gene: STAT3***

STAT3, which is triggered by IL-10 and IL-6, is highly expressed in M2 Mφ, and it is involved in various pro-tumorous functions, such as tumor cell activation, angiogenesis, metastasis, and immune-suppression [69, 76, 211-213] (**Fig. 1-4, 1-5**) (**Fig. 4-1A**) Whereas STAT1, which is triggered by IFN-γ, is highly expressed in M1 Mφ and is involved in anti-tumorous functions. It was assumed that if STAT3 is down regulated in TAMs (M2 Mφ), the STAT1/STAT3 in Mφ could increase, facilitating the polarization into M1 phenotype and enhancing the anti-tumorous functions of TAMs (**Fig. 4-1B**). There are a few attempts carried out by other researchers to inhibit STAT3 in TAMs aiming to modify their function. For instance, some researchers use drugs or STAT3 inhibiters, such as sunitinib [130], sorafenib [131], oleanolic acid (OA) [214], and corosolic acid (CA) [215]. As mentioned previously in **Chapter 1**, Kortylewski *et al.* developed ON TLR9 agonist-STAT3 siRNA conjugates and succeeded in using it to improve the immunity of the TME by inducing silencing of STAT3, but this silencing was not limited to Mφ and induced silencing in other immune cells such as DCs and B cells [184]. There was another attempt to reprogram Mφ from M2 phenotype to M1 phenotype using siRNAs to silence STAT3 in TAMs in glioma-bearing animals [186]. However, in that study, a commercially-available transfection reagent was used to transfect siRNA into tumor locally and no systemic delivery system for siRNA was developed [186]. Furthermore, as stated in **Table 1-2**, there is an undergoing NIH clinical trial of STAT3 inhibition in Mφ using an antisense oligonucleotide for the treatment of metastatic hepatocellular carcinoma [152]. These research studies highlight the potentiality of STAT3 as a targeted gene in TAMs, which require further studies and investigations to realize this therapeutic modality, especially using Mφ-targeted and siRNA-loaded delivery systems.

- ***Second targeted gene: HIF-1α***

HIF-1α is also highly expressed in M2 Mφ [153, 216]. HIFs, essentially HIF-1, have been linked to the hypoxic conditions of the tumor and they are commonly overexpressed in various tumor types [217]. When oxygen levels drop during hypoxia, HIF-1α accumulates and translocates to the nucleus, where it forms the active transcription factor HIF-1 by dimerization with HIF-1β, and to

form a heterodimeric transcription factor [218]. This dimerization is regulated by an oxygen-dependent prolyl hydroxylase, and is involved with the induction of various hypoxia-related genes related to tumor aggressiveness, angiogenesis, metastasis [218-222] (**Fig. 4-2A**). It was also assumed that by down regulating HIF-1α in TAMs, we could blind TAMs of tumor hypoxia, and reduce its regulation of hypoxia-related genes, especially those related to angiogenesis and metastasis (**Fig. 4-2B**). Due to the significant role played by hypoxia and HIF-1 in the TME, they have been novel therapeutic targets for cancer treatment [221, 223]. Recent research studies aim whether to correct the acidic and hypoxic status of the tumor or apply HIF-1 inhibitors (*e.g.* small molecules or siRNA-loaded delivery systems) [218, 224, 225]. However, those studies aim to inhibit HIF-1 in the TME as a whole and not specifically in TAMs. In one of these studies, manganese dioxide NPs (MnO_2 NPs) have been used to target TAMs and reprogram them from M2 to M1 phenotype using mannose and hyaluronic acid (HA), respectively. The high reactivity of MnO_2 NPs toward hydrogen peroxide (H_2O_2) allowed the improvement of oxygenation, adjustment of the acidic pH in the tumor hypoxic core, and minimized tumor growth. However, although HIF-1α levels were decreased, they were not exclusively targeted and silenced in TAMs [226].

We decided to target two genes (STAT3 and HIF-1α) to maximize the chance and the efficiency of reprograming Mφ from M2 to M1. Although there is a reported attempt to inhibit both targeted genes in TAMs using the plant-derived flavonoid, Luteolin [227], to our knowledge, there are no current studies which aim to target both genes (STAT3 and HIF-1α) in TAMs using siRNA-loaded nanoparticles or other delivery systems.

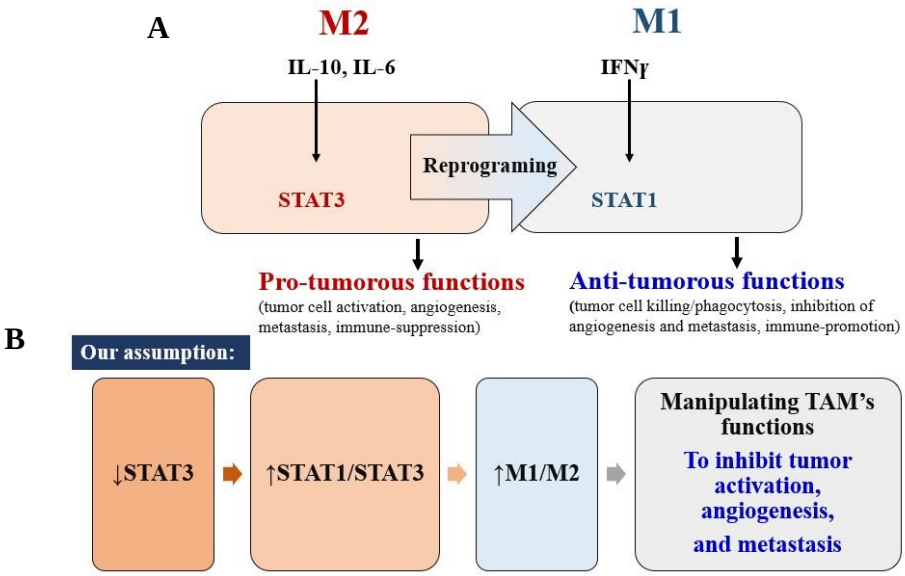

Fig. 4-1: Schematic illustration represents the expression of STAT3 in TAMs (M2 Mφ), its role in Mφ's pro-tumorous functions (A), and the possible anti-tumorous therapeutic scenario of its silencing (B). IFN, interferon; IL, interleukin; Mφ, macrophage; STAT, signal transducer and activator of transcription; TAMs, tumor-associated macrophages.

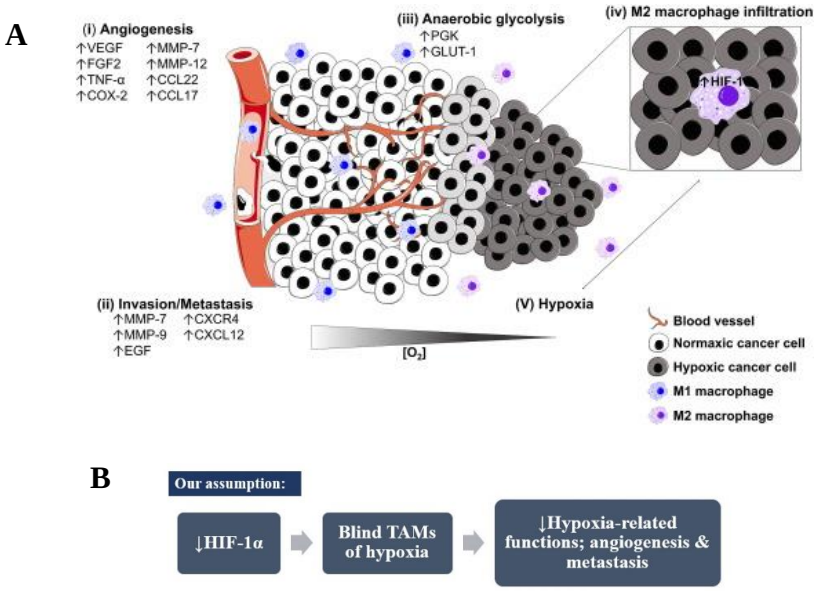

Fig. 4-2: Schematic illustration represents the expression of HIF-1 in TAMs (M2 Mφ) under the influence of tumor hypoxia, its role in Mφ's pro-tumorous functions (A) [218], and the possible anti-tumorous therapeutic scenario of HIF-1α silencing (B). CCL17, C-C motif chemokine ligand 17; CCL22, C-C motif chemokine ligand 22; COX-2, cyclooxygenase 2; CXCL12, C-X-C motif chemokine ligand 12; CXCR4, C-X-C motif chemokine receptor 4; EGF, epidermal growth factor; FGF2, fibroblast growth factor 2; HIF-1, hypoxia-inducible factor 1; GLUT-1, glucose transporter 1; MMP, matrix metalloproteinase; Mφ, macrophage; PGK, phosphoglycerate kinase 1; TAMs, tumor-associated macrophages; TNF-α, tumor necrosis factor α; VEGF, vascular endothelial growth factor [218].

4.2.2. Obtaining anti-tumor therapeutic response

To obtain an anti-tumor therapeutic response by reprograming TAMs and modulating their function in the tumor xenograft model that was previously described in **Chapter 3, Section 3.2.3.** and after the average tumor in OS-RC-2-bearing mice reached certain volume (≈ 60 mm^3), mice with extreme tumor volumes were excluded, and the rest were randomized into various groups and received different treatments, which were administered i.v. every 3 days and up to maximum three doses. The endpoint of the experiment was 2 days after the last dose. The treatment types were; phosphate-buffered saline (PBS (-)), the chemotherapeutic reagent Dox as "Dox-loaded liposomes", which was added as a positive control (at a dose of 3 mg Dox/kg) (**see physical characteristics in Table 6-7**), siRNA-free or empty CL4H6-LNPs, which were added as a negative control, and siRNA-loaded CL4H6-LNPs which have the following optimized composition: CL4H6:chol:DSG-PEG 2,000 (60/40/1 mol% of total lipids) and are encapsulating siSTAT3:siHIF-1α (1:1 ratio) (at a dose of 1 mg siRNA/kg) (**see physical characteristics in Table 6-6**). As shown in **Fig. 4-3A**, the optimized CL4H6-LNPs targeting TAMs and encapsulating siRNAs against STAT3 and HIF-1α genes induced a significant anti-tumor therapeutic response compared to the PBS (-)-treated group, this anti-tumor activity was comparable to or better than the positive control Dox-loaded liposomes, the activity was also dependent on siRNA since the siRNA-free or empty CL4H6- LNPs did not induce significant anti-tumor response. It is noteworthy to mention that although the anti-tumor experiment resulted in an encouraging outcome, it is difficult to conclude that the positive results were attributed to the silencing of targeted genes in TAMs and if their functions were altered. Therefore, at the endpoint day of the anti-tumor experiment, tumor tissues were collected, and alterations of gene expression were measured at the mRNA level using qRT-PCR.

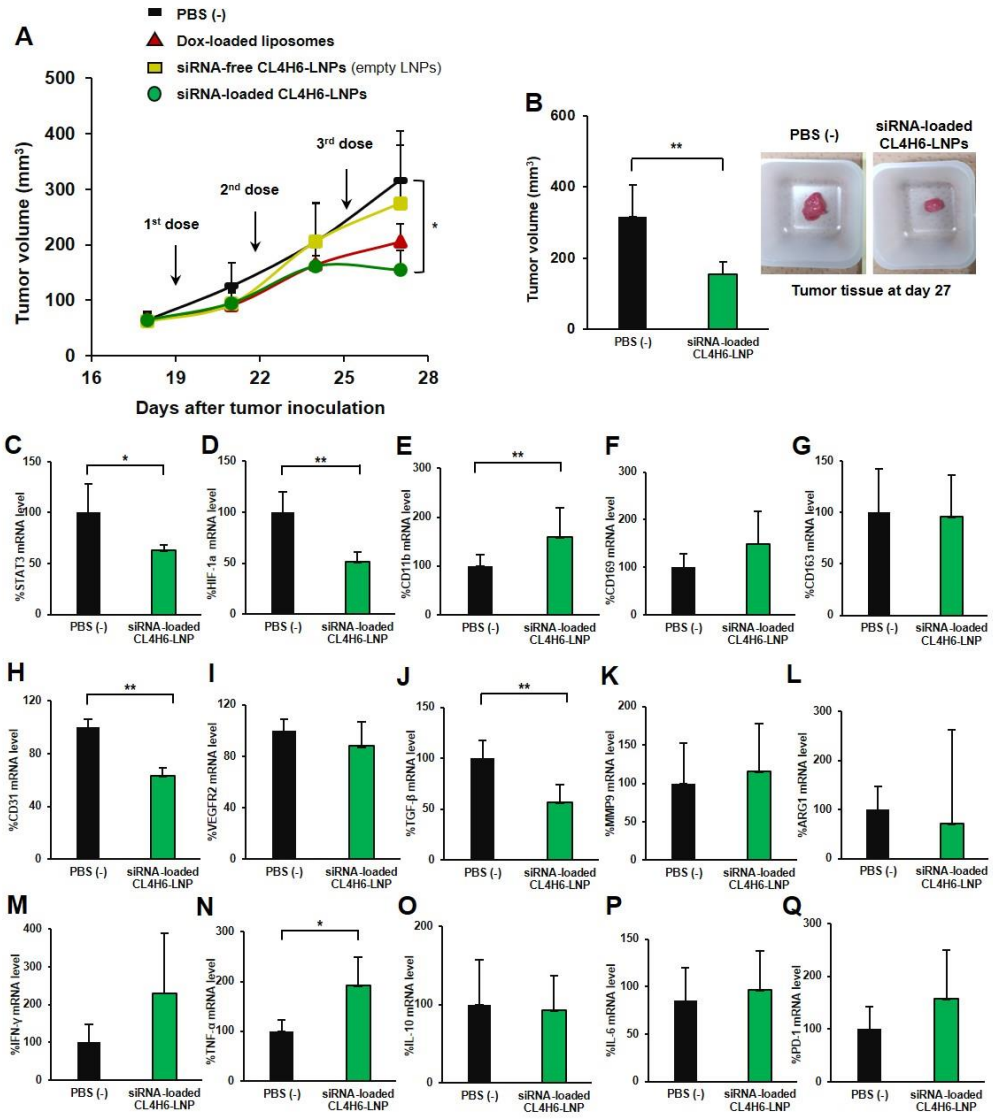

Fig. 4-3: Targeting TAMs for anti-tumor therapy. (A) Anti-tumor therapeutic response using siRNA-loaded CL4H6-LNPs. * $P < 0.05$ (Turkey-Kramer test). Means ± SD (n=5). (**B**) Anti-tumor therapeutic response using siRNA-loaded CL4H6-LNPs against PBS (-). ** $P < 0.01$ (two-tailed unpaired student's t-test against PBS (-)). Means ± SD (n=5). (**C-Q**) Exploring gene expression in TAMs and in the TME after the treatment with siRNA-loaded CL4H6-LNPs in the anti-tumor experiment, measured at the mRNA level by qRT-PCR. Reference gene for STAT3 and HIF-1α is CD11b. Reference gene for other genes is GUSB. * $P < 0.05$, ** $P < 0.01$ (two-tailed unpaired student's t-test against PBS (-)). Outliers were eliminated using Chauvenet's Criterion. Means ± SD (n=4-5). The OS-RC-2-bearing mice received different treatments i.v.. Dox-loaded liposomes were administered at a dose of 3 mg Dox/kg, and siRNA-loaded CL4H6-LNPs were administered at a dose of 1 mg siRNA/kg. The CL4H6-LNP composition: CL4H6:chol:DSG-PEG 2,000 (60/40/1 mol%). The siRNA used: siSTAT3:siHIF-1α (1:1 ratio). ARG1, arginase 1; Dox, doxorubicin; DSG-PEG 2,000, 1,2-distearoyl-*rac*-glycero-3-methylpolyoxyethylene; GUSB, glucuronidase beta; HIF-1α, hypoxia-inducible factor 1α; IFN-γ, interferon γ; IL, interleukin; LNP, lipid nanoparticle; MMP, matrix metalloproteinase; PBS (-), phosphate buffered saline; PD-1, programmed cell death 1; SD, standard deviation; STAT3, signal transducer and activator of transcription 3; TAMs, tumor-associated macrophages; TGF-β, transforming growth factor β; TME, tumor-microenvironment; TNF-α, tumor necrosis factor α; VEGFR2, vascular growth factor receptor 2; chol, cholesterol; i.v., intravenously; mRNA, messenger RNA; siRNA, short interfering RNA.

4.2.3. Mechanism of anti-tumor action of siRNA-loaded CL4H6-LNPs

At the endpoint of the anti-tumor experiment, tumor tissues were collected, RNA was extracted, and complementary DNA (cDNA) was prepared and used to evaluate gene expression at the mRNA level using qRT-PCR. This strategy could enable us to explore the alterations that occurred in the TME and to analyze the mechanism of action of siRNA-loaded CL4H6-LNPs which resulted in the anti-tumor therapeutic response. During analysis, although the siRNA-loaded CL4H6-LNP-treated group should be compared to siRNA-free CL4H6-LNP-treated group, it was instead compared to PBS (-)-treated group for the following reason; although the siRNA-free CL4H6-LNPs did not induce a significant anti-tumor response at the end of the experiment, they induced an anti-tumor response after the administration of the first dose, which is apparently not mediated by siRNA. Therefore, using them for comparison might not result in an accurate interpretation. If the time course of the experiment was extended, and if there was a more significant difference between siRNA-free and siRNA-loaded CL4H6-LNPs, in that case, using siRNA-free CL4H6-LNPs for comparison might be reliable. **Fig. 4-3B-Q** represents the alterations of various parameters in TAMs and the TME after the treatment of siRNA-loaded CL4H6-LNPs and compared to PBS (-)-treated group. It is also shown if the tendency to increase, decrease or no change of various parameters met our expectations or not. As shown in **Fig. 4-3B**, the treatment induced a significant anti-tumor response and decreased tumor size by 50% compared to PBS (-). The silencing of targeted genes in TAMs was also confirmed and STAT3 and HIF-1α were down-regulated at 37% and 48%, respectively (**Fig. 4-3C, D**). Although the same amount of siRNA against both genes was used, the small difference of their silencing could be attributed to different siRNA efficiency, difference expression of both genes, or the fact that HIF-1α is triggered not only by hypoxia but also by STAT3, therefore, silencing of STAT3 contributed to down-regulating HIF-1α as well [228]. The treatment resulted in a significant increase of macrophage ($CD11b^+$ cells) infiltration to TME by 59% (**Fig. 4-3E**), and -confirming to our assumption- increased the proportion of M1 Mφ ($CD169^+$ cells) by 50% (**Fig. 4-3F**). However, M2 Mφ ($CD163^+$ cells) proportion, which was expected to decrease, was not changed (**Fig. 4-3G**). As a result, M1/M2 ratio was increased by 50%. These results suggest that silencing of STAT3 and HIF-1α in TAMs resulted in polarizing them towards the M1 phenotype, which is supposed to have anti-tumorous functions. The treatment altered some parameters related to M2 functions. For instance, it decreased the expression of CD31 and VEGFR2, which are angiogenesis markers, by 37% and 12 %, respectively (**Fig. 4-3H, I**). The expression of transforming growth factor β (TGF-β), which is responsible for tumor cell activation, migration, and invasiveness [229-231] was decreased by 43% (**Fig. 4-3J**). Although the expression of matrix metalloproteinase 9 (MMP-9) (metastasis marker) was expected to be decreased, it increased by 16% (**Fig. 4-3K**). These results suggest that the anti-tumor response was mediated by reversing the M2-related pro-tumorous functions of TAMs, especially angiogenesis and tumor cell activation/invasiveness. As explained earlier in **Chapter 3, Section 3.2.3.**, this tumor model is carried in immune-deficient mice, and due to lack of proper immunity, and our intentional decision to exclude the immune-related functions, we did not have a specific expectation of how immune-related genes should be altered. However, we found that the treatment decreased the immune-suppressant arginase 1 (ARG1) by 29% (**Fig. 4-3L**), possibly because it is a downstream gene of STAT3 [69]. In addition, the immune-suppressants IL-6 and

PD-1 were increased. While the immune-suppressant IL-10 was not changed (**Fig. 4-3O-Q**). We further analyzed two genes (IFN-γ and tumor necrosis factor α (TNF-α)) related to M1 functions and found that these two immune-stimulators were increased by 130% and 91%, respectively (**Fig. 4-3M, N**). To sum up, these findings aiming to interpret the results and suggest a possible mechanism of anti-tumor action of TAMs-targeted and siRNA-loaded CL4H6-LNPs, we came up with a possible scenario summarized in **Fig. 4-4**. Before treatment, TAMs have an M2 phenotype (with pro-tumorous functions) and they express the M2 marker CD163, and after the administration of siRNA-loaded CL4H6-LNPs, although the surface marker (CD163) was not changed, their function was altered due to the silencing of the targeted genes: STAT3 and HIF-1α, which resulted in the inhibition of pro-tumorous functions of Mφ, mainly angiogenesis, measured by decrease of CD31 and VEGFR2 expression. The silencing of STAT3 also downregulated its downstream, the immune-suppressant ARG1. And as a result of inhibiting the angiogenesis and improving the neovascularization, Mφ ($CD11b^+$ cells) infiltration to the TME was enhanced, and this phenomenon coincides with previous reports [203, 232]. And as a result of Mφ infiltration and/or gene silencing of STAT3 which increased STAT1/STAT3 ratio and hence M1 polarization, the proportion of M1 Mφ ($CD169^+$ cells) in the TME was increased by 50%. The M1 Mφ could have been infiltrated from the bone marrow or from the spleen (in which they might be already carrying the LNPs), or they could be the reprogramed M2 Mφ that already existed in the TME and in which the targeted genes were silenced. And as a result of the final increase of M1/M2 ratio, which translates into enhancing the anti-tumorous and revering the pro-tumorous functions of TAMs, angiogenesis was also inhibited, and TGF-β was decreased, resulting in inhibiting tumor cell activation and invasiveness. Finally, tumor size was significantly reduced by 50% due to the inhibition of pro-tumorous functions of TAMs; angiogenesis and tumor cell activation. It is noteworthy to mention that due to lack of T cells in this model, we might be able to conclude that the anti-tumorous functions were merely due to manipulating TAMs, while excluding the positive or the negative influence from T cells. Furthermore, because murine-specific siRNAs were used, and because the LNPs were selectively taken up by TAMs (**Fig. 3-5**), we might be able to exclude the possibility that gene silencing in human tumor cells occurred.

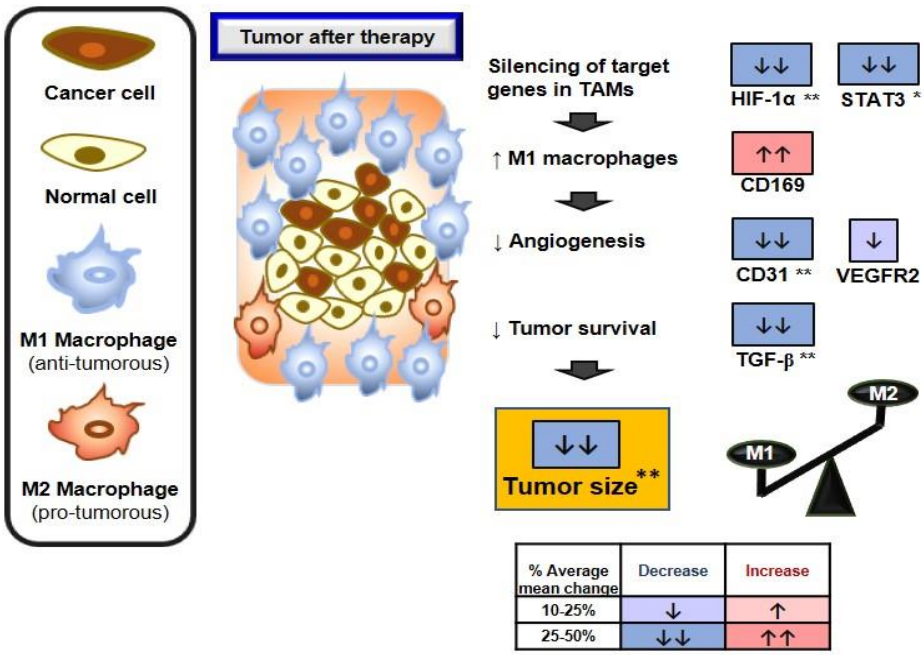

Fig. 4-4: Summary of our findings and a possible scenario of the mechanism of anti-tumor action of siRNA-loaded CL4H6-LNPs. Common criteria were used to evaluate the change of gene expression by calculating the percentage of average mean change compared to PBS (-)-treated group. The change of gene expression was divided into 2 categories at different levels (10-25% and 25-50%); increase of expression or decrease of expression. Reference gene for STAT3 and HIF-1α is CD11b. Reference gene for other genes is GUSB. * $P < 0.05$, ** $P < 0.01$ (two-tailed unpaired student's t-test against PBS (-)). Outliers were eliminated using Chauvenet's Criterion (n=4-5). (see **Fig. 4-3**). HIF-1α, hypoxia-inducible factor 1α; LNP, lipid nanoparticle; PBS (-), phosphate buffered saline; STAT3, signal transducer and activator of transcription 3; TAMs, tumor-associated macrophages; TGF-β, transforming growth factor β; VEGFR2, vascular endothelial growth factor receptor 2; siRNA, short interfering RNA.

4.3. Conclusion

We succeeded in proving our concept regarding targeting and manipulating TAMs to realize Mφ-based cancer immunotherapy. We used the optimized and TAMs-targeted CL4H6-LNPs to deliver siRNAs against STAT3 and HIF-1α genes, which are highly expressed in TAMs with M2 phenotype, in OS-RC-2-bearing mice. The treatment resulted in significant anti-tumor therapeutic response compared to PBS (-)-treated group. The positive outcome was mediated by increasing Mφ infiltration, M1 Mφ proportion, and the overall M1/M2 ratio in the TME, which enhanced the anti-tumorous functions of TAMs, and despite no change of M2 Mφ surface markers, their pro-tumorous functions were reversed. As a result, the tumor size was significantly reduced by 50% due to the inhibition of angiogenesis and tumor cell activation/invasiveness.

Chapter 5: Summary, applications, and future directions

5.1. Summary

In this research study, siRNA-loaded LNPs were successfully used and optimized to target TAMs. The LNPs which have the following composition: CL4H6 lipid:chol:DSG-PEG 2,000 (60/40/1 mol% of total lipids) obtained:

- Well tolerability by cells
- High stability in the blood circulation
- High accumulation in tumor tissues
- High and selective uptake by TAMs
- Strong gene silencing in TAMs

The optimized CL4H6-LNPs were successfully used to silence targeted genes (STAT3 and HIF-1α) in TAMs in OS-RC-2-bearing mice and obtained the following results:

- Increase of Mφ infiltration and M1 population in the TME
- Inhibition of the pro-tumorous functions of TAMs (in specific, angiogenesis and tumor cell activation/invasiveness)
- Significant anti-tumor therapeutic response

Only by targeting and manipulating TAMs, the TME was improved and a positive outcome was obtained.

5.2. Applications of this research

There are two main applications of this research:

1. Multi-target (integrated) cancer therapy

Although the siRNA-loaded CL4H6-LNPs were used to target and manipulate TAMs in a human tumor xenograft model in immune-deficient mice, they could be applied and manipulated to target not only Mφ, but also tumor cells, and other immune cells, such as T cells. Targeting those populations in another tumor model in immune-competent mice could enable us to maximize the therapeutic response by enhancing positive cell-cell interactions between various cell types in the

TME. This strategy could have promising clinical applications for the treatment of solid tumors as an alternative for CAR T cell therapy. As discussed earlier in **Chapter 1, Section 1.1.1.**, despite the clinical success of CAR T cell therapy [32, 45, 46]), they still have some challenges and limitations, such as systemic side effects and toxicity [47-50], resistance [51, 52], and difficult application for the treatment of solid tumors due to the complexity of their TME as well as the difficulty in selecting high affinity receptors to target specific antigens expressed by tumor cells- but not normal cells- to minimize off-target toxicity [53-56]. For example, CAR T cells engineered against Erb-B2 receptor tyrosine kinase 2 (ERBB2) to treat metastatic colorectal cancer resulted in multi-organ failure with acute pulmonary toxicity which lead to the recipient patient's death, due to off-target toxicity of CAR T cells on the lung epithelium [233]. And even if suitable antigens of solid tumors were identified and targeted, CAR T cells have poor accumulation to tumor tissues [57], limited survival within the host body [58, 59], and they are susceptible for suppression in the TME [60]. In contrast, Mφ have a more natural tendency to accumulate in solid tumors compared to T cells [76, 234, 235]. Furthermore, this strategy could be applied for the treatment of blood cancers as an alternative, or in combination with CAR T cell therapy, aiming to enhance CAR T cell therapy [236], or to overcome CAR T cell toxicity, especially CAR T cell-induced cytokine reactive syndrome (CRS), which was found to be mediated by M1 (anti-tumorous and pro-inflammatory) Mφ [237]. This study led me to introduce the following concept regarding Mφ-based therapeutics. In the case of solid tumors, reprograming Mφ from M2 to M1 might be an ideal approach for various types of tumors. However, in the case of blood cancers, and especially when combined with CAR T cell therapy, we might face what we call "Phenotype dilemma". Which means that although inhibiting M2 (pro-tumorous and anti-inflammatory) Mφ is required to cure the tumor, reprograming them to M1 is not ideal, since M1 (pro-tumorous and anti-inflammatory) Mφ are responsible for CAR T cell-induced CRS [237]. Therefore, we might have only two options; reprogram Mφ to M0 state with no specific functions or blocking/depleting them from the TME (**Fig. 5-1**). Such "Phenotype dilemma" might require a personalized Mφ-based therapeutic approach, *i.e.* a careful choice and selection of the desired Mφ phenotype that is customized to each cancer patient depending on their tumor type, Mφ role and phenotype, genetic makeup, and if they receive other therapeutic modalities.

2. Other *in vitro/ex vivo* applications

Since the siRNA-loaded CL4H6-LNPs induced superior transfection efficiency and more observable tolerability than the commercially available transfection reagent RNAiMAX in the isolated and *ex vivo* cultured BMDM (**Chapter 3, Section 3.2.1.**), they could be applied as an alternative reagent for transfection for commercial or scientific applications. Another interesting application is using the CL4H6-LNPs to deliver siRNA and genetically-engineer Mφ, *ex vivo*, after isolating them from the patient's blood. The genetically-engineered macrophages (GEMs) could be fused back to the same patient, in a similar approach to CAR T cell therapy, to induce an anti-tumor therapeutic response. The advantages of the this approach are overcoming delivery challenges due to limited EPR effect in humans [238], and minimizing systemic side effects/toxicities of delivery systems (**Fig. 5-2**).

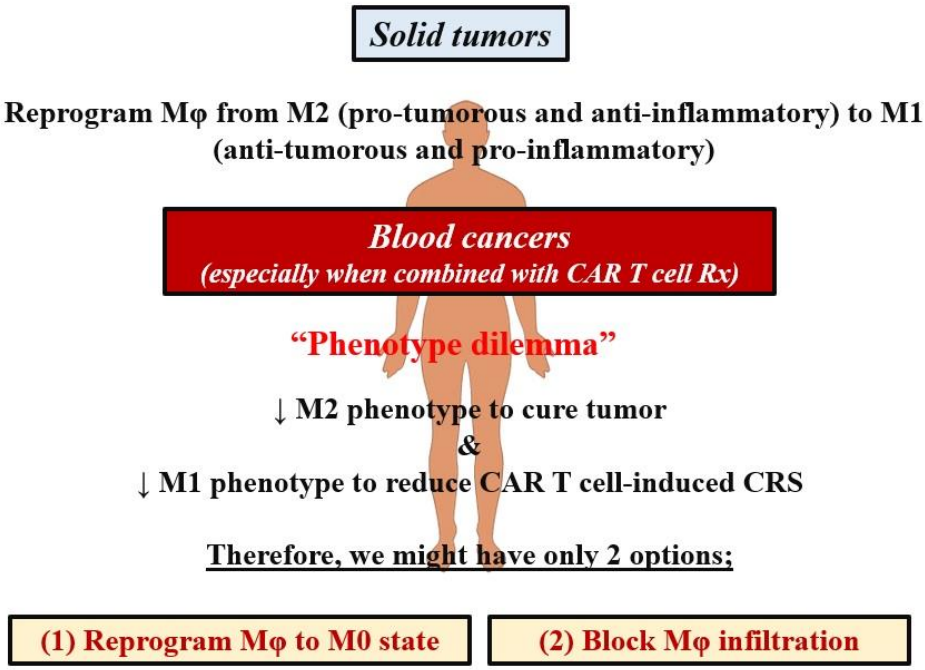

Fig. 5-1: Introducing the "Phenotype dilemma" concept which requires a personalized Mφ-based therapeutic approach. CAR T cell, chimeric antigen receptor T cell; CRS, cytokine release syndrome; Mφ, macrophage.

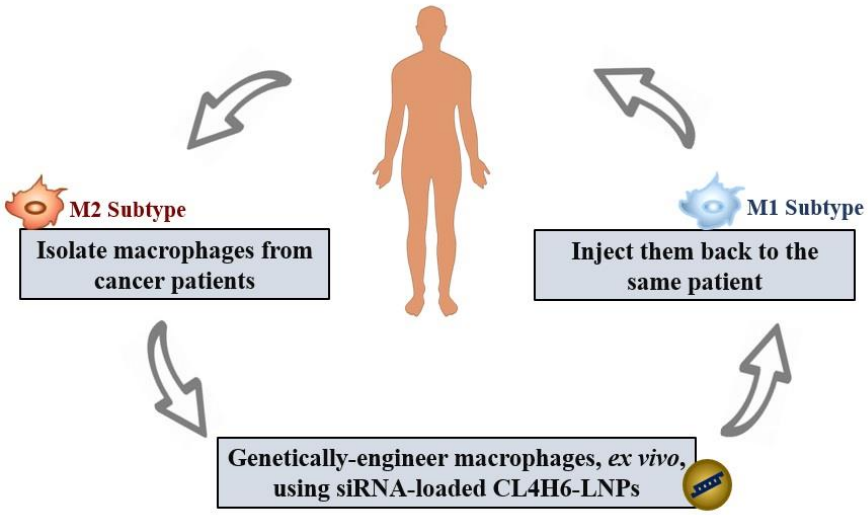

Fig. 5-2: Adoptive-transfer of GEMs as an interesting approach for cancer treatment using the siRNA-loaded CL4H6-LNPs optimized in this study. GEMs, genetically-engineered macrophages; LNP, lipid nanoparticle; siRNA, short interfering RNA.

5.3. Future directions

For future directions, the following question might be proposed; can we use the optimized siRNA-loaded CL4H6-LNPs to target Mφ in other tumor models -especially those in immune-competent mice- to explore the Mφ-T cell interaction and the influence of immune activity on the final therapeutic outcome?. The answer to this question is yes, the LNP could be used for that purpose due to the following facts:

1. In the anti-tumor experiment, and despite using immune-deficient mice, the LNPs altered gene expression of some immune markers in OS-RC-2-bearing mice. For instance, decrease of the immune-suppressants ARG1 and TGF-β, increase of the immune-stimulants TNF-α and IFN-γ, and increase of the immune-suppressant IL-6) (**Fig. 4-3**).

2. The LNPs also obtained high and selective uptake and induced gene silencing activity in TAMs in the syngeneic B16-F10 melanoma model in C57BL/6J immune-competent mice (data not shown).

These encouraging results provide the basis to build upon for further applications and scientific studies in the future.

Chapter 6: Material and methods

6.1. Material and equipment

Table 6-1: Material and equipment

Material (Catalogue number)	**Source**
ACK lysing buffer (Cat.# A1049201)	Gibco
Albumin bovine serum fraction V, ≥96% (BSA) (Cat.# A9647-100G)	SIGMA
Albumin, from bovine serum (BSA), Cohn Fraction V, pH7.0 (Cat.# 017-23294)	Wako
Amicon Ultra-15 Centrifugal Filter Units (Cat.# UFC910096)	Merck Millipore
Ammonium sulfate (Cat.# 019-03435)	Wako
APC anti-mouse CD45 antibody. Clone: 30-F11 (Cat.# 103111)	BioLegend
APC rat IgG2b,k. Clone: RTK4530 (Cat.# 400611)	BioLegend
Buffer Solution Standard (Phosphate pH Standard Equimolal Solution) pH6.86 (25 degrees C) (Cat.# 025-03195)	FUJIFILM Wako Pure Chemical Corporation
Buffer Solution Standard (Phthalate pH Standard Solution) pH4.01 (25 degrees C) (Cat.# 028-03185)	FUJIFILM Wako Pure Chemical Corporation
Buffer Solution Standard (Tetraborate pH Standard Solution) pH9.18 (25 degrees C) (Cat.# 028-03205)	FUJIFILM Wako Pure Chemical Corporation
t-Butyl alcohol (Cat.# 028-03386)	Wako
CELLBANKER, CB021 1 plus 100 mL	Takara bio
Cell culture plates (Cat.# 3513)	Costar

Cell strainer 100 µm (Cat.# 352360)	FALCON
Cell strainer (100 µm) (Cat.# 3-6649-03)	AS ONE
Cell strainer (40 µm) (Cat.# 352340)	FALCON
Chloroform (Cat.# 67-66-3)	NACALAI TESQUE
Chloroform (Cat.# 038-02606)	Wako
Cholesterol (Cat.# C8667-5G)	SIGMA
Citric acid monohydrate (Cat.# 035-03495)	Wako
Collagenase type1 280 U/mg (Cat.# 17100-017)	Gibco
Cosmonice Filter S (Solvents) 4mm 0.45 µm pore size (Cat.# 06541-24)	NACALAI TESQUE
D-Glucose solution 45% (Cat.# G8769)	SIGMA
DiD	Molecular Probes
DiI (Cat.# D-3899)	Molecular Probes
DiO	Molecular Probes
Disposable syringes and needles (23G, 25G, 26G, 27G)	Terumo
DMEM (Dulbecco's modified eagle's medium) (Cat.# D6046)	SIGMA
DMG-PEG 2,000 (GM-020) (Cat.# 160743-62-4)	NOF
DNase1 lyophilized powder, 25mg (Cat.# LS002138)	Worthington
Doxorubicin hydrochloride 100mg (Cat.# D4193)	TCI
D-PBS (-) (Cat.# 045-29795)	Wako
D-PBS (-) without Ca and Mg, liquid (Cat.# 14249-95)	NACALAI TESQUE

DSG-PEG 2,000 (GS-020) (Cat.# 308805-39-2)	NOF
DSPE-PEG 2,000 (Cat.# DSPE-020CN)	NOF
DSPC coatsome (Cat.# MC-8080)	NOF
Ethanol (ethyl alcohol) (Cat.# 057-00456)	Wako
Fetal bovine serum (FBS) (Cat.# 172012)	SIGMA
Filter-Tips, 200 µl (1024) (Cat.# 990332)	QIAGEN
Filter-Tips, 1000 µl (1024) (Cat.# 990352)	QIAGEN
FITC anti-mouse CD45 antibody. Clone: 30-F11 (Cat.# 103107)	BioLegend
FITC anti-mouse F4/80 antibody. Clone: BM8 (Cat.# 123108)	BioLegend
FITC anti-mouse Ly-6G antibody. Clone: 1A8 (Cat.# 127605)	BioLegend
FITC rat IgG2a,k. Clone: RTK2785 (Cat.# 400505)	BioLegend
HBSS (-) (Cat.# 17461-05)	NACALAI TESQUE
Heparin sodium (Cat.# 081-00136)	Wako
HEPES (Cat.# 342-01375)	Dojindo
HEPES 1M (Cat.# H0887)	SIGMA
HIF-1α silencer select pre-designed siRNA (Cat.# 4390771)	Ambion
Insulin syringe with a needle 29G× 1 /2(0.33×13mm) 0.5 mL (Cat.# ss-05M2913)	Terumo
Isopropyl alcohol (2-propanol) (Cat.# 166-04836)	Wako

LightCycler 480 Multiwell Plate 96, white (Cat.# 04729692001)	Roche
LightCycler 480 Sealing Foil (Cat.# 04729757001)	Roche
Lipofectamine reagent RNAiMAX, 1.5 mL (Cat.# 13778-151)	Invitrogen
2-ME 55 mM (Cat.# 21985023)	Gibco
Methanol (Cat.# 138-06473)	Wako
2NA EDTA 2NA (Cat.# 345-01865)	Dojindo
Nalgen Labtop cooler	SIGMA
Nunc EasYDish Dishes D × H 150×20 mm (Cat.# 150468)	ThermoFisher
Nunclon Delta treated dishes D×H 150×20 mm (Cat.# 168381)	ThermoFisher
On ice aluminum blocks (Cat.# ABR-24TR)	BIO-BIK
Opti-MEM (1X) “reduced serum medium” (Cat.# 31985-062)	Gibco
Pasteur pipettes	HIRSCHMANN
PE anti-human HLA-A,B,C antibody. Clone: W6/32 (Cat.# 311406)	BioLegend
PE anti-mouse/human CD11b antibody. Clone: M1/70 (Cat.# 101208)	BioLegend
PE anti-mouse F4/80 antibody. Clone: BM8 (Cat.# 123109)	BioLegend
Penicillin-streptomycin (10,000 U/mL) 100mL (Cat.# 15140-122)	Gibco
PE rat IgG2b,k. Clone: RTK4530 (Cat.# 400607)	BioLegend
PerCP anti-mouse/human CD11b antibody. Clone: M1/70 (Cat.# 101229)	BioLegend
pH-indicator stripes pH 5.0-10.0 (Cat.# 109533)	Merck Millipore
Pipette P-1000 (PIPETTMAN classic)	GILSON

Pipette P-2, P-20, P-200	RAININ
Plastic screw cap microtubes (Cat.# 2754-015)	IWAKI
Purified anti-mouse CD16/32 antibody. Clone: 93 (Cat.# 101302)	BioLegend
PrimeTime Gene Expression Master Mix 1×5mL (Cat.# 1055772)	IDT
Pyrex TE-32 Asahi glass tubes	IWAKI
RBC Lysis Buffer 10X (Cat.# 420301)	BioLegend
Recombinant mouse M-CSF 200 μg/mL (Cat.# 576404)	BioLegend
ReverTra Ace qPCR RT Master Mix with gDNA Remover (Cat.# FSQ-301)	TOYOBO
RNase-Free DNase Set (50) (Cat.# 79254)	QIAGEN
RNeasy Micro Kit (50) (Cat.# 74004)	QIAGEN
RPMI-1640 (Cat.# R8758)	SIGMA
Quant-iT RiboGreen RNA Assay Kit (Cat.# R11491)	Invitrogen
Safe-lock microcentrifuge tubes, 2 mL (Cat.# 0030120094)	Eppendorf
Screw cap tubes (Cat.# T330-6S)	Simport
siRNA (other than siHIF-1α and siSTAT3)	Hokkaido system science Applied Biosystems
Sodium azide (Cat.# 31233-42)	NACALAI TESQUE
Sodium dextran sulfate (Cat.# 194-13402)	Wako
Sodium dodecyl sulfate (SDS) (Cat.# 191-07145)	Wako
Sodium pyruvate solution X100 (Cat.# S8636-100ML)	SIGMA
S1 pipet filler, white	ThermoFisher

(Cat.# TS-9501)	
Stat 3 silencer select pre-designed siRNA	Ambion
(Cat.# 4390771)	
Sulfuric acid	Wako
(Cat.# 192-04696)	
Syringe filter 0.2 µm	Advantec
(Cat.# 02927601)	
THUNDERBIRD SYBR qPCR Mix	TOYOBO
(Cat.# QPS-201)	
Tissue culture dishes D×H 100×20 mm	FALCON
(Cat.# 353003)	
Tissue homogenizing CKMix - 2mL	Precellys 24
(Cat.# 03961-1-009)	
Triton X-100	SIGMA
(Cat.# 9002-93-1)	
Triton X-100/polyoxyethylene (10) octylphenyl ether	Wako
(Cat.# 168-11805)	
TRIzol reagent	Ambion
(Cat.# 15596018)	
Trypsin solution 2.5%	Gibco
(Cat.# 1738602)	
Tubes 1.5 mL, 5 mL	Watson
Tubes 15 mL, 50 mL	FALCON
Uncoated dish D×H 90×15 mm	AS ONE
(Cat.# 3-1491-01)	
UV-cuvette micro	BRAND
(Cat.# 759 200)	
Water for molecular biology	Merck Millipore
(Cat.# H20MB0106)	
Zirconium oxide beads (1.4 mm) bulk	Precellys 24
(Cat.# 03961-1-103)	

Equipment	Source
Biological safety cabinet	NK system
Bio-Labo clean bench (NS-13B)	Sanyo
Centrifuge machines:	
(MX-305)	TOMY
(himac CF7D2)	HITACHI
(Cubee)	Gene research
(Low speed refrigerated centrifuge AX-511)	TOMY
CO_2 incubators	Sanyo
Cool incubator (iCube) FL1-280	AS ONE
Digital caliper 500-444	Mitutoyo
Elix High-Throughput	Merck Millipore
Enspire 2300 Multilabel Reader	Perkin Elmer
FACSCalibur flow cytometer	BD Biosciences
FluorVivo 300 (small animal fluorescence imaging)	INDEC BioSystems
Gallios flow cytometer	Beckman Coulter
mHigh pressure stem sterilizer CBS-325	TOMY
Improved Neubauer's Counting Chamber (83-1112)	Erma
Infinite 200 microplate reader	Tecan
LightCycler 480 real-time PCR system	Roche
(96-or 384-well plate systems)	
Magnetic stirrer SA-501	Sansyo
Microscope (BH2)	Olympus
Microscope (IX70)	Olympus
Milli-Q Integral	Merck Millipore
Natural sterilizer (NDS-601D)	EYELA
pH meter (D71 LAQUA)	Horiba
Precellys 24 tissue homogenizer	Bertin technologies
QIAcube	QIAGEN
Shaking bath SB-13	As ONE
Shaking incubator SI-300C (1-5837-02)	As ONE
Sonicator 3000 (Ultrasonic cell disruptor)	Misonix Inc.
* Probe-type sonicator	
Thermal cycler (C1000 touch)	Bio rad
Ultrasonic cleaner (AU-25C) *Bath-type sonicator	Sansyo
UV/Vis spectrophotometer (DU730)	Beckman Coulter

Vortex-2 Genie	Scientific industries
Water bus HWA-50D	As ONE
Weighing semi microbalance (HR-202i)	A&D
Zetasizer nano ZS	Malvern

- ***Mice:***

- ICR, ♀, 4-10 wk (Source, Japan SLC, Inc.)
- BALB/cAjcl-nu/nu, ♂, 4 wk (Source, CLEA Japan, Inc.)

Table 6-2: siRNA sequences

siRNA	**sense strand (5‘- 3‘)**	**antisense strand (5‘- 3‘)**
siCD45	cuGGcuGAAuuucAGAGcAT*T	UGCUCUGAAAUUcAG CcAGT*T
siFVII	GGA**uc**A**ucuc**AAG**ucuu**ACT*T	G**u**AAGA**cuu**GAGA**u**G A**ucc**T*T
AF-647-siGL4	AF-647-ccgucgucuucgugaacaaTT	uugcucacgaauacgacggTT

2’-OMe modified nucleotides are depicted in lower case letters, 2’-fluoro modified nucleotides are in bold lower case letters, and phosphorothioate linkages are denoted by asterisks. AF, alexa fluor; CD, cluster of differentiation; FVII, coagulation factor VII; siRNA, short interfering RNA.

- ***Premixed probes and primers for probe-based qRT-PCR (Source, IDT):***

#1 Gene name: GAPDH (glyceraldehyde 3-phosphate dehydrogenase)

Assay name: Mm.PT.39a.1
REF #: 99665765
Product: PrimeTime Std qPCR Assay

Contains	nmoles	Sequence
Probe	2.5	5’/56-FAM/TGCAAATGG/ZEN/CAGCCCTGGTG/3IABkFQ/-3’
Primer 1	5.0	5’GTGGAGTCATACTGGAACATGTAG-3’
Primer 2	5.0	5’AATGGTGAAGGTCGGTGTG-3’

#2 Gene name: STAT3

Assay name: Mm.PT.58.11877007
REF #: 99665769
Product: PrimeTime Std qPCR Assay

Contains	nmoles	Sequence
Probe	2.5	5’/56-FAM/CGTGCCAAT/ZEN/TGTGATGCCTCCTTG/3IABkFQ/-3’
Primer 1	5.0	5’-AGTCTCGAAGGTGATCAGGT-3’
Primer 2	5.0	5’GTTCAAGCACCTGACCCTTAG-3’

#3/A Gene name: HIF-1α

Assay name: N010431.1.pt.Hif1a
REF #: 99665773
Product: PrimeTime Mini qPCR Assay

Contains	nmoles	Sequence
Probe	2.5	5'/56-FAM/ACTGCACGG/ZEN/GCCATATTCATGTCT/31ABkFQ/-3'
Primer 1	5.0	5'-GAACATCAAGTCAGCAACGTG-3'
Primer 2	5.0	5'-TTTGACGGATGAGGAATGGG-3'

#3/B Gene name: HIF-1α

Assay name: Mm.PT.58.11211292
REF #: 100050913
Product: PrimeTime Std qPCR Assay

Contains	nmoles	Sequence
Probe	2.5	5'/56-FAM/TCTAGACCA/ZEN/CCGGCATCCAGAAGT/31ABkFQ/-3'
Primer 1	5.0	5'-CCGTCATCTGTTAGCACCAT-3'
Primer 2	5.0	5'-GCTCACCATCAGTTATTTACGTG-3'

#4 Gene name: CD45

Assay name: Mm.PT.58.7583849
REF #: 99908500
Product: PrimeTime Std qPCR Assay

Contains	nmoles	Sequence
Probe	2.5	5'/56-FAM/TGGAGGCTG/ZEN/AATACCAGAGACTTCCT /31ABkFQ/-3'
Primer 1	5.0	5'-TTTCCAATGTGCTGTGTCCT-3'
Primer 2	5.0	5'-TGAAGAAGAGAGATCCACCCA-3'

Table 6-3: Primers for THUNDERBIRD SYBR-based qRT-PCR (Source, SIGMA)

Gene	**Forward (5'- 3')**	**Reverse (5'- 3')**
ARG1	CTCCAAGCCAAAGTCCTTAGAG	AGGAGCTGTCATTAGGGACATC
CD11b	AAGGCTGTTAACCAGACAGG	ATATTCACAGCCTCTGGAGG
CD31	TACAGTGGACACTACACCTG	GACTGGAGGAGAACTCTAAC
GAPDH	AGCAAGGACACTGAGCAAG	TAGGCCCCTCCTGTTATTATG
GUSB	GTGGTATGAACGGGAAGCAAT	AACTGCATAATAATGGGCACTGT

IFN-γ	ATGAACGCTACACACTGCATC	CCATCCTTTTGCCAGTTCCTC
IL-6	CTGCAAGAGACTTCCATCCAG	AGTGGTATAGACAGGTCTGTTGG
IL-10	GCTGGACAACATACTGCTAACC	ATTTCCGATAAGGCTTGGCAA
MMP9	CCCTCTGAATAAAGACGAC	TATAGTGGGACACATAGTGG
PD-1	ACCCTGGTCATTCACTTGGG	CATTTGCTCCCTCTGACACTG
TGF-β	CTCCCGTGGCTTCTAGTGG	GCCTTAGTTTGGACAGGATCTG
TNF-α	CAGGCGGTGCCTATGTCTC	CGATCACCCCGAAGTTCAGTAG

ARG1, arginase 1; CD, cluster of differentiation; GAPDH; glyceraldehyde 3-phosphate dehydrogenase; GUSB, glucuronidase beta; IFN-γ, interferon γ; IL, interleukin; MMP, matrix metalloproteinase; PD-1, programmed cell death 1; TGF-β, transforming growth factor β; TNF-α, tumor necrosis factor α.

Table 6-4: Pre-designed primers for THUNDERBIRD SYBR-based qRT-PCR (Source, IDT)

Gene	**forward (5‘- 3‘)**	**reverse (5‘- 3‘)**
CD163	GTCCTCCTCATTGTCTTCCTC	ATCCGCCTTTGAATCCATCTC
CD169	CTCCAGTTATGCTCCGTGTC	GCTCACTGTCCACTCGAC
VEGFR2	GGAATTGACAAGACAGCGACT	GGATCTTGAGTTCAGACATGAGG

CD; cluster of differentiation; VEGFR2, vascular growth factor receptor 2.

6.2. Methods

6.2.1. Preparation of the siRNA-loaded LNPs

The LNPs were prepared by alcohol dilution procedure (**Fig. 2-4**). The lipids, which include 1800 nmol of original lipids, such as CL4H6, 1200 nmol of cholesterol, and 30 nmol of PEG-lipid (DMG-PEG 2,000 or DSG-PEG 2,000), -which represent a molar ratio of 60/40/1, respectively- (*the molar ratio and lipid content can be altered during optimization*), were first dissolved in 400 µL of 90% (v/v) *t*-BuOH. When a fluorescent material (Dil or DiD) was incorporated into the LNPs, it was added at a concentration of 0.15-0.5 mol% of total lipids to the lipid solution. A 200 µL portion of an aqueous solution containing 80 µg siRNA was then added gradually to the lipid solution under vigorous mixing, producing a siRNA/lipid ratio of 0.042 (wt/wt). The siRNA-lipid solution was then gradually added to 2 mL of 20 mM citrate buffer (pH 4.0) under vigorous mixing to facilitate the precipitation and formation of the LNPs by electrostatic interactions between

positively-charged lipids and negatively-charged siRNAs. This yields a final *t*-BuOH concentration of 60% (v/v). Finally, ultrafiltration using amicon ultra centrifugal tubes (Merck Millipore) was performed to remove the *t*-BuOH, replace the external buffer with phosphate-buffered saline (PBS (-)) (pH 7.40), and concentrate the LNPs. The centrifuge conditions were (1,000×*g*, 21-23 min, r.t.).

6.2.2. Characterization of the siRNA-loaded LNPs

The size, PDI, and ζ-potential of LNPs were measured by DLS using a Zetasizer Nano ZS ZEN3600 instrument. The EE% of siRNA was determined using the RiboGreen assay. In which 100 µL of the siRNA-loaded LNP or pure siRNA solution (for standard curve) were diluted in another 100 µL of 10 mM HEPES buffer (pH 7.40) containing 20 µg/mL dextran sulfate and RiboGreen in the presence or absence of 0.1 w/v% Triton X-100 added to a 96-well plate (**Table 6-5**). Fluorescence was measured by Enspire 2300 multilabel reader. The siRNA concentration was calculated based on the siRNA standard curve. The siRNA EE% was calculated by comparing siRNA concentration in the presence and absence of Triton X-100. An example of typical physical characteristics of siRNA-loaded LNPs is shown in **Table 2-1.** In addition, **Table 6-6** shows the physical characteristics of siRNA-loaded CL4H6-LNPs used in the anti-tumor experiment.

$$\boldsymbol{siRNA\ EE}\ \% = \frac{\boldsymbol{Encapsulated\ siRNA - Unencapsulated\ siRNA}}{\boldsymbol{Total\ siRNA\ concentration}} \times \boldsymbol{100}$$

Table 6-5: Componenets of 100 µL HEPES solution for RiboGreen assay

Components	**Triton (+)**	**Triton (-)**
10 mM HEPES buffer (pH 7.40)	93.75µL	95.75µL
1 mg/mL Sodium dextran sulfate	4 µL	4 µL
10 wt/v % Triton X-100	2 µL	0 µL
RiboGreen	0.25 µL	0.25 µL

Fluorescnce conditions:

Excitation/Emission wavelength: 500/525 nm

Band width: 5 nm

Measurement time: 500 msec/well

Dynamic range: Autorange

Temperetaure: r.t.

The morphology of the LNPs was observed by transmission electron microscopy (TEM), in which a drop of an aqueous solution containing LNPs was adsorbed to carbon-coated copper grids (400 mesh) and the samples were stained with a 2% phosphotungstic acid solution (pH 7.0) for 20 sec. The sample was observed by a transmission electron microscope (JEM-1400Plus; JEOL Ltd., Tokyo, Japan) at an acceleration voltage of 100 kV. Digital images (3296 × 2472 pixels) were taken with a CCD camera (EM-14830RUBY2; JEOL Ltd., Tokyo, Japan).

Table 6-6: Physical characteristics of CL4H6-LNPs used in the anti-tumor experiment

	Size (nm)	**Number mean (nm)**	**PDI**	**ζ-potential (mV)**	**EE (%)**
siRNA-loaded LNP	131.32 ± 0.02	104.88 ± 0.11	0.06 ± 0	10.95 ± 1.49	94.93 ± 0.70
siRNA-free empty LNP	98.42 ± 2.23	74.30 ± 1.75	0.07 ± 0.02	21.70 ± 1.41	

LNP composition: CL4H6:chol:DSG-PEG 2,000 (60/40/1 mol% of total lipids). The siRNA used: siSTAT3:siHIF-1α (1:1 ratio). Means ± SD (n=2 after mixing many preparations). DSG-PEG 2,000, 1,2-distearoyl-*rac*-glycero-3-methylpolyoxyethylene; EE, encapsulation efficiency; HIF-1α, hypoxia-inducible factor 1 α; LNP, lipid nanoparticle; PDI, polydispersity index; SD, standard deviation; STAT3, signal transducer and activator of transcription 3; chol, cholesterol; siRNA, short interfering RNA.

6.2.3. Preparation of Dox-loaded liposomes

To prepare Dox-loaded liposomes, a remote loading approach was used, in which Dox was remotely loaded into prepared liposomes by transmembrane pH gradient [239]. Briefly, the lipids (1,2-distearoyl-*sn*-glycero-3-phosphocholine (DSPC)/chol) were dissolved in chloroform and mixed at 50:50 molar ratio, and after evaporating the organic solvent with N_2 gas, the resulting lipid film was hydrated with 300 mM ammonium sulphate buffer (pH 4.0) by stirring in a shaking bath for 15-30 min at 60°C, which is higher than the melting temperature of DSPC (*i.e.* 54.4°C) [240], and then sonicated using bath-type sonicator for 20 sec and probe-type sonicator for 10 min (12 W). Removing titanium was performed by 3-round centrifugation (15,000 rpm, 10 min, r.t.), and ultrafiltration using amicon (100K) was performed by 2-round centrifugation (2,000 *g*, 30 min, 25°C). Then, the resulted liposomes were diluted in PBS (-) (1 mL) and incubated with 10 mg/mL Dox (40 µl) (1,100 rpm, 30 min, 60°C). Then, ultrafiltration using amicon (100K) was performed by centrifugation (2,000 *g*, 30 min, 25°C), and the resulted Dox-loaded liposomes (1 mL, lipids: 2 mg, 6000 nmol) were incubated with 10 mM of *N*-(carbonyl-methoxypolyethyleneglycol 2,000)-

1,2-distearoyl-*sn*-glycero-3-phosphoethanolamine, sodium salt (DSPE-PEG 2,000) dissolved in ethanol (at 5 lipid molar ratio and 7.5% final volume of ethanol) (1,100 rpm, 30 min, 60°C). Finally, ultrafiltration using amicon (100K) was performed by 2-round centrifugation (2,000 *g*, 30 min, 25°C) and PEGylated Dox-loaded liposomes were suspended and diluted in PBS (-).

6.2.4. Characterization of Dox-loaded liposomes

Size, PDI, and ζ-potential were measured by DLS using a Zetasizer Nano ZS ZEN3600 instrument. The concentration and recovery ratio of Dox were measured after dissolving the liposomes with methanol to release the entrapped Dox (as reported previously [241]), and then, measuring the absorbance of Dox at 495 nm using DU730 UV/Vis spectrophotometer. Concentration and recovery ratio were calculated using 2 methods; the first method is using an equation derived from a standard curve of a sample with a known Dox concentration, and the second method is using Beer-lambert law using the following formula:

$$A=\epsilon lc$$

Where A is the measure of absorbance at 495 nm (no units), ϵ is absorption coefficient (*i.e.* 10840 mol/L), l is the path length (1 cm), and c is the concentration of Dox (mol/L).

The EE% of Dox was measured by comparing the absorbance of Dox at 495 nm (which reflects its concentration) before and after one-round centrifugation (2,000 *g*, 30 min, 25°C) and ultrafiltration using amicon (100K). EE% was calculated using the following formula:

$$EE\% = \frac{Encapsulated\ Dox\ (concentration\ after\ ultrafiltration)}{Total\ amound\ of\ Dox\ (concentration\ before\ ultrafiltration)} \times 100\%$$

It was also confirmed that the fluorescence of free-Dox in the permeate after one-round centrifugation is 0% using Enspire 2300 multilabel reader (Perkin Elmer). The physical characteristics of Dox-loaded liposomes used in the anti-tumor experiment are shown in **Table 6-7**.

Table 6-7: Physical characteristics of Dox-loaded liposomes used in the anti-tumor experiment

Size (nm)	Number mean (nm)	PDI	ζ-potential (mV)	EE (%)
133.27 ± 4.16	72.93 ± 13.67	0.23 ± 0.06	-22.48 ± 5.09	94.58 ± 3.86

Liposome composition: DSPC:chol:DSPE-PEG 2,000 (50/50/5 mol% of total lipids). Means ± SD (n=4 after mixing many preparations). DSPC: 1,2-distearoyl-*sn*-glycero-3-phosphocholine; DSPE-PEG 2,000, *N*-(carbonyl-methoxypolyethyleneglycol 2000)-1,2-distearoyl-*sn*-glycero-3-phosphoethanolamine, sodium salt; Dox, doxorubicin; EE, encapsulation efficiency; PDI, polydispersity index; SD, standard deviation; chol, cholesterol.

6.2.5. Isolation and culture of BMDM

After sacrificing and sterilizing mice ICR mice, their legs were cut, muscles removed, and bones (femur and tibia) were flushed in the clean bench to collect bone marrow-derived cells (BMDC), which then were passed through 40 µm cell strainer, centrifuged (180 *g* (1000 rpm), 3 min, r.t.), treated with ACK lysing buffer to lyse red blood cells, centrifuged again, and suspended in RPMI-1640 medium (which was supplemented in advance with heat inactivated fetal bovine serum (FBS) (10%), penicillin (100 IU/mL), and streptomycin (100 µg/mL), 1 mM sodium pyruvate, 10 mM 4-(2-hydroxyethyl)-1-piperazineethanesulfonic acid (HEPES), and 50 µM 2-mercaptoethnol (2-ME)). Then, cells were plated on uncoated dishes at a density of $5x10^5$ cells/mL in the above described RPMI-1640 medium containing 50 ng/mL recombinant mouse macrophage-colony stimulating factor (rmM-CSF), and cultured *ex vivo* under an atmosphere of 5% CO_2/air at 37°C for 7 days (old medium was replaced with a fresh one at day 4). At day 7, cells were collected, and their phenotype with the following criteria: ($CD45^+$, $CD11b^+$, $F4/80^+$, $Ly6G^-$ cells) was confirmed by measuring the expression of surface markers using flow cytometry, their morphology was observed using microscopy, or they were used for the transfection experiments. For measuring surface markers by flow cytometry, cells were suspended in fluorescence-activated cell sorting (FACS) buffer containing 0.5% bovine serum albumin (BSA) and 0.1% sodium azide. Then, cells were stained with anti-mouse CD16/32 antibody for 15 minutes (to block nonspecific binding), and antibodies (with their isotypes) for surface protein detection for another 30 minutes. The cells were washed with FACS buffer several times and then suspended in 0.5-1 mL for analyzing using FACSCalibur.

6.2.6. Cell culture

- *OS-RC-2 cells*

The OS-RC-2 (human RCC cells) were cultured in RPMI-1640 medium supplemented with heat inactivated FBS (10%), penicillin (100 IU/mL), and streptomycin (100 µg/mL) in 10-cm or 15-cm dishes at a density of ~5×10^5 or 10^6 cells/dish, respectively, and under an atmosphere of 5% CO_2/air at 37°C.

- *RAW 264.7 cells*

RAW 264.7 cells were cultured in Dulbecco's modified eagle medium (DMEM) supplemented with heat inactivated FBS (10%), penicillin (100 IU/mL), and streptomycin (100 µg/mL) in 10-cm dishes at a density of ~5×10^5 cells/dish, and under an atmosphere of 5% CO_2/air at 37°C.

Cell stocks were preserved in cell banker, dispensed in 1 mL screw-cap tubes at a density of 1×10^6 cells/tube and stored at -80°C.

6.2.7. Measuring gene silencing in Mφ, *in vitro*

- *In BMDM:*

At day 7 after isolating and culturing BMDM, *ex vivo*, as described in the previous section, cells were collected and seeded in 6-well plates at a density of 4×10^5 cells/well and transfected with siCD45 loaded in CL4H6-LNPs or in RNAiMAX at different siRNA concentrations. And after 24 hours of seeding and transfection, cells were lysed and homogenized using TRIzol reagent (according to the manufacturer's protocol) or RLT buffer (QIAGEN) (according to the manufacturer's protocol) to extract RNA by TRIzol reagent or by RNeasy micro kit (QIAGEN) using QIAcube, respectively. The reason behind using different RNA extraction methods is the difference in cell recovery after both treatments. The RNAiMAX resulted in noticeable cellular toxicity, therefore, the number of recovered cells after transfection was low and that required an RNA extraction method that is suitable for low starting number of cells, such as RNeasy micro kit. After RNA extraction, cDNA was prepared using ReverTra Ace qPCR RT Master Mix (according to the manufacturer's protocol), and mRNA expression was measured by probe-based qRT-PCR using premixed primers and probes, PrimeTime gene expression master mix, and LightCycler 480 96 system (according to the manufacturer's protocol).

- *In RAW 264.7 cells:*

RAW 264.7 cells were seeded in 6-well plates at a density of 1.5-2×10^5 cells/well 24 hours before being transfected with the siCD45-loaded LNPs. After 24 hours of transfection, cells were lysed and homogenized, and RNA was extracted using TRIzol reagent. Then RNA was converted to cDNA using ReverTra Ace qPCR RT Master Mix (according to the manufacturer's protocol). Finally, gene expression at the mRNA level was quantified using THUNDERBIRD SYBR-based qRT-PCR (according to the manufacturer's protocol).

6.2.8. Measuring blood circulation and stability

ICR mice were injected i.v. with siRNA-loaded CL4H6-LNPs, in which lipids were labeled with DiI (0.15 mol% of total lipids), and siRNAs were labeled with alexa fluor (AF)-647 (100% of siRNAs used were labeled). The injection volume was fixed (200 µL) to minimize variables, this volume was customized to obtain a dose of 1 mg siRNA/kg in mice which had an average weight of 20 g. After different time points (1 min, 1.5 h, 3 h, 6 h, 9 h, and 24 h), blood was collected from the tail vein, lysed using 1% sodium dodecyl sulfate (SDS), and the fluorescence of both lipids and siRNAs was measured using Tecan infinite M200 microplate reader with icontrol software. DiI excitation/emission wavelength 549/565 nm, AF-647 excitation/emission wavelength 649/679 nm.

6.2.9. Tumor inoculation and establishment

BALB/cAjcl-nu/nu mice were injected s.c. in the dorsum with OS-RC-2 cells at a volume of 1×10^6 cells suspended in 80 µL PBS (-).

Tumor volume was measured by digital calipers using this formula:

A (mm) × B^2 (mm)×0.52= volume (mm^3)

A: longest diameter (length)

B: shortest diameter (width)

6.2.10. Observation and quantification of biodistribution

When the tumor in OS-RC-2-bearing mice reached a volume of 50-100 mm^3, mice were i.v. injected with siRNA-loaded CL4H6-LNPs, in which lipids were labeled with DiD (0.5 mol% of total lipids). The injection volume was fixed (250 µL) to minimize variables, this volume was customized to obtain a dose of 1 mg siCD45/kg in mice which had an average weight of 25 g. After

24 h of injection, mice were sacrificed and their body organs (liver, spleen, lungs, kidneys, and tumor tissue) were collected and the fluorescence of DiD-lipid was observed using FluorVivo 300 small animal fluorescence imaging. For quantifying the fluorescence intensity in each organ, ImageJ software was used as follows; after selecting the region of interest (ROI) in each image, its corrected fluorescence was measured using the following formula:

Corrected fluorescence = Integrated Density – (Area of ROI × Mean gray value of background reading) The corrected fluorescence of the treated samples were then normalized to the corrected fluorescence of PBS (-)-treated samples and then divided by the area of the ROI.

6.2.11. Preparation of tumor single cell suspension for flow cytometry

Tumor tissues were collected from mice using sharp scissors, and then minced in a solution containing the following ingredients for digestion (for each mouse);

280 U/mg Collagenase type I	20 mg
10 mg/mL DNase I	20 μL
Heat-inactivated FBS	0.2 mL
500 mM $CaCl_2$	20 μL
Hank's balanced salt solution (HBSS)	up to 2 mL

Then, samples were incubated in shaking incubator (1,000 rpm, 30 to 60 min, 37℃). After complete digestion, debris was removed using 100 μM cell strainer, and cells were washed using HBSS several times with the following centrifuge conditions (400 *g*, 4 min, 4℃). RBC lysis buffer was also used to remove blood cell contamination. Next, cells were suspended in FACS buffer (containing 0.5% BSA and 0.1% sodium azide) at a concentration of 1×10^6 cells/1 mL/tube or less, depends on cell recovery. Finally, cells were stained with anti-mouse CD16/32 antibody for 15 minutes (to block nonspecific binding), and single or multiple anti-mouse conjugated antibodies for surface protein detection for another 30 minutes. The cells were washed with FACS buffer several times and then suspended in 0.5-1 mL for analyzing using FACSCalibur or Gallios.

6.2.12. Measuring the LNP's uptake by different tumor populations

When the tumor in OS-RC-2-bearing mice reached a volume of 50-100 mm^3, mice were i.v. injected with siRNA-loaded CL4H6-LNPs, in which lipids were labeled with DiD (0.15 mol% of

total lipids). The injection dose was 1 mg siFVII 2'-fluoro /kg. After 2 h or 24 h of injection, mice were sacrificed, tumor single cell suspension was prepared as described in the previous section, and the uptake of DiD-lipid was measured in various tumor populations by FACSCalibur. This was the criteria of defining and gating different cell populations: non-leukocytes (which might include tumor cells and ECs) ($CD45^-$ cells), TAMs ($CD45^+$, $CD11b^+$, $F4/80^+$ cells), neutrophils ($CD45^+$, $CD11b^+$, $F4/80^-$ cells), leukocytes other than TAMs or neutrophils, which might include DCs ($CD45^+$, $CD11b^-$ cells) (**Fig. 3-5B-E**).

6.2.13. Measuring gene silencing activity in TAMs

When the tumor in OS-RC-2-bearing mice reached a volume of 100-200 mm^3, mice were injected with siRNA-loaded CL4H6-LNPs i.v. at two doses of 2 mg siRNA/kg against CD45 as a model target gene. After 2 days of the last injection (to give some time for silencing at the protein level), mice were sacrificed, tumor single cell suspension was prepared as described in the previous section, and silencing efficiency in TAMs was evaluated by measuring the expression of CD45 surface protein using Gallios. In that experiment, TAMs were defined as $F4/80^+$, human leukocyte antigen (HLA)-A,B,C^- cells (**Fig. 3-7B**). A negative control, siRNA-free or empty LNP was also added.

6.2.14. Design of the anti-tumor experiment

When the tumor in OS-RC-2-bearing mice reached a volume of ≈ 60 mm^3 on average, mice with extreme tumor volumes were excluded, and the rest were randomized into various groups and received different treatments, which were administered i.v. every 3 days and up to maximum three doses. The endpoint of the experiment was 2 days after the last dose. The treatment types were; PBS (-), Dox-loaded liposomes, which was added as a positive control (at a dose of 3 mg Dox/kg), siRNA-free or empty CL4H6-LNPs, which were added as a negative control, and siRNA-loaded CL4H6-LNPs which have the following optimized composition: CL4H6:chol:DSG-PEG 2,000 (60/40/1 mol% of total lipids) and are encapsulating siSTAT3:siHIF-1α (1:1 ratio) (at a dose of 1 mg siRNA/kg). Tumor volume was measured by digital calipers using the formula d escribed in (**Section 6.2.9**.). At the endpoint day of the experiment, mice were sacrificed, tumor tissues were harvested, lysed and homogenized, and RNA was extracted using TRIzol reagent. Then RNA was converted to cDNA using ReverTra Ace qPCR RT Master Mix (according to the manufacturer's protocol). Finally, gene expression at the mRNA level was quantified using THUNDERBIRD

SYBR-based qRT-PCR (according to the manufacturer's protocol) for some genes, and using probe-based qRT-PCR using premixed primers and probes, PrimeTime gene expression master mix, and LightCycler 480 96 system (according to the manufacturer's protocol) for others. in the experiment, body weight of mice was also constantly measured to evaluate the effect of treatment on body weight loss.

The quality of PCR primers was checked, and all primers used in this study obtained the following hallmarks of an optimized qPCR assay:

1- A linear standard curve (R^2>0.980)

2- Consistency across replicates

3- High amplification efficiency (90-105%)

References:

1. *What Is Cancer* 2015 [cited 2019 May 27]; Available from: https://www.cancer.gov/about-cancer/understanding/what-is-cancer.
2. *Cancer Fact Sheets*. 2019, The International Agency for Research on Cancer (IARC) Cancer today.
3. *Cancer Statistics*. 2018 April 27 [cited 2019 May 27]; Available from: https://www.cancer.gov/about-cancer/understanding/statistics.
4. *Global Oncology Trends 2018*. QuintilesIMS Institute.
5. *SEER Cancer Statistics Review (CSR) 1975-2016*. Surveillance Research Program: National Cancer Institute.
6. *CANCER DEATH RATE, AGE-STANDARDIZED (INDEX)*. [cited 2019 May 27]; Available from: https://ourworldindata.org/grapher/cancer-deaths-rate-and-age-standardized-rate-index?time=1990..2016.
7. *FDA Approved Drugs for Oncology*. [cited 2019 May 27]; Available from: https://www.centerwatch.com/drug-information/fda-approved-drugs/therapeutic-area/12/oncology.
8. Riley, R.S., et al., *Delivery technologies for cancer immunotherapy.* Nature Reviews Drug Discovery, 2019. **18**(3): p. 175-196.
9. Orimo, A., et al., *Stromal fibroblasts present in invasive human breast carcinomas promote tumor growth and angiogenesis through elevated SDF-1/CXCL12 secretion.* Cell, 2005. **121**(3): p. 335-48.
10. Kalluri, R. and M. Zeisberg, *Fibroblasts in cancer.* Nat Rev Cancer, 2006. **6**(5): p. 392-401.
11. Dunn, G.P., L.J. Old, and R.D. Schreiber, *The three Es of cancer immunoediting.* Annu Rev Immunol, 2004. **22**: p. 329-60.
12. Gabrilovich, D.I., S. Ostrand-Rosenberg, and V. Bronte, *Coordinated regulation of myeloid cells by tumours.* Nature Reviews Immunology, 2012. **12**: p. 253.
13. O'Sullivan, T., et al., *Cancer immunoediting by the innate immune system in the absence of adaptive immunity.* J Exp Med, 2012. **209**(10): p. 1869-82.
14. Jin, R.J., et al., *NE-10 neuroendocrine cancer promotes the LNCaP xenograft growth in castrated mice.* Cancer Res, 2004. **64**(15): p. 5489-95.
15. Leiblich, A., et al., *Human prostate cancer cells express neuroendocrine cell markers PGP 9.5 and chromogranin A.* Prostate, 2007. **67**(16): p. 1761-9.
16. Ayala, G.E., et al., *Cancer-related axonogenesis and neurogenesis in prostate cancer.* Clin Cancer Res, 2008. **14**(23): p. 7593-603.
17. Roberts, D.L., C. Dive, and A.G. Renehan, *Biological mechanisms linking obesity and cancer risk: new perspectives.* Annu Rev Med, 2010. **61**: p. 301-16.
18. Gilbert, C.A. and J.M. Slingerland, *Cytokines, obesity, and cancer: new insights on mechanisms linking obesity to cancer risk and progression.* Annu Rev Med, 2013. **64**: p. 45-57.
19. Donohoe, C.L., et al., *The role of obesity in gastrointestinal cancer: evidence and opinion.* Therap Adv Gastroenterol, 2014. **7**(1): p. 38-50.
20. Hanahan, D. and J. Folkman, *Patterns and emerging mechanisms of the angiogenic switch during tumorigenesis.* Cell, 1996. **86**(3): p. 353-64.
21. Koshikawa, N., et al., *Constitutive upregulation of hypoxia-inducible factor-1alpha mRNA occurring in highly metastatic lung carcinoma cells leads to vascular endothelial growth factor overexpression upon hypoxic exposure.* Oncogene, 2003. **22**(43): p. 6717-24.
22. Cheng, L., et al., *Glioblastoma Stem Cells Generate Vascular Pericytes to Support Vessel Function and Tumor Growth.* Cell, 2013. **153**(1): p. 139-152.

23. Guillaumond, F., et al., *Strengthened glycolysis under hypoxia supports tumor symbiosis and hexosamine biosynthesis in pancreatic adenocarcinoma.* Proc Natl Acad Sci U S A, 2013. **110**(10): p. 3919-24.
24. Birbrair, A., et al., *Type-2 pericytes participate in normal and tumoral angiogenesis.* Am J Physiol Cell Physiol, 2014. **307**(1): p. C25-38.
25. Chen, F., et al., *New horizons in tumor microenvironment biology: challenges and opportunities.* BMC Med, 2015. **13**: p. 45.
26. Wang, M., et al., *Role of tumor microenvironment in tumorigenesis.* J Cancer, 2017. **8**(5): p. 761-773.
27. Coley, W.B., *The Treatment of Inoperable Sarcoma by Bacterial Toxins (the Mixed Toxins of the Streptococcus erysipelas and the Bacillus prodigiosus).* Proc R Soc Med, 1910. **3**(Surg Sect): p. 1-48.
28. Ehrlich, P. and S.H.H. Dale, *The Collected Papers: In Four Volumes, Including a Complete Bibliography*. 1960: Pergamon Press.
29. Burnet, F.M., *Immunological surveillance in neoplasia.* Transplant Rev, 1971. **7**: p. 3-25.
30. Dunn, G.P., et al., *Cancer immunoediting: from immunosurveillance to tumor escape.* Nat Immunol, 2002. **3**(11): p. 991-8.
31. Friedman, C.F., T.A. Proverbs-Singh, and M.A. Postow, *Treatment of the Immune-Related Adverse Effects of Immune Checkpoint Inhibitors: A Review.* JAMA Oncol, 2016. **2**(10): p. 1346-1353.
32. Ellis, P.M., E.T. Vella, and Y.C. Ung, *Immune Checkpoint Inhibitors for Patients With Advanced Non-Small-Cell Lung Cancer: A Systematic Review.* Clin Lung Cancer, 2017. **18**(5): p. 444-459.e1.
33. Lee, S. and K. Margolin, *Cytokines in cancer immunotherapy.* Cancers, 2011. **3**(4): p. 3856-3893.
34. Stone, J.D., et al., *T cell receptor engineering.* Methods Enzymol, 2012. **503**: p. 189-222.
35. Liu, L., et al., *Inclusion of Strep-tag II in design of antigen receptors for T-cell immunotherapy.* Nat Biotechnol, 2016. **34**(4): p. 430-4.
36. Tolcher, A.W., et al., *Phase Ib Study of Utomilumab (PF-05082566), a 4-1BB/CD137 Agonist, in Combination with Pembrolizumab (MK-3475) in Patients with Advanced Solid Tumors.* Clin Cancer Res, 2017. **23**(18): p. 5349-5357.
37. Segal, N.H., et al., *Results from an Integrated Safety Analysis of Urelumab, an Agonist Anti-CD137 Monoclonal Antibody.* Clin Cancer Res, 2017. **23**(8): p. 1929-1936.
38. Buchan, S.L., A. Rogel, and A. Al-Shamkhani, *The immunobiology of CD27 and OX40 and their potential as targets for cancer immunotherapy.* Blood, 2018. **131**(1): p. 39-48.
39. Guo, C., et al., *Therapeutic cancer vaccines: past, present, and future.* Adv Cancer Res, 2013. **119**: p. 421-75.
40. Chiang, C.L., G. Coukos, and L.E. Kandalaft, *Whole Tumor Antigen Vaccines: Where Are We?* Vaccines (Basel), 2015. **3**(2): p. 344-72.
41. Pardi, N., et al., *mRNA vaccines - a new era in vaccinology.* Nat Rev Drug Discov, 2018. **17**(4): p. 261-279.
42. Liu, M.A., *DNA vaccines: an historical perspective and view to the future.* Immunol Rev, 2011. **239**(1): p. 62-84.
43. Li, L., S.P. Goedegebuure, and W.E. Gillanders, *Preclinical and clinical development of neoantigen vaccines.* Ann Oncol, 2017. **28**(suppl_12): p. xii11-xii17.
44. Lauss, M., et al., *Mutational and putative neoantigen load predict clinical benefit of adoptive T cell therapy in melanoma.* Nat Commun, 2017. **8**(1): p. 1738.
45. Fesnak, A.D., C.H. June, and B.L. Levine, *Engineered T cells: the promise and challenges of cancer immunotherapy.* Nat Rev Cancer, 2016. **16**(9): p. 566-81.

46. Porter, D., et al., *Chimeric antigen receptor T cells persist and induce sustained remissions in relapsed refractory chronic lymphocytic leukemia. Sci. Transl. Med. 7 (303), 303ra139–303ra139 (2015)*. 2015.
47. Friedman, C.F., T.A. Proverbs-Singh, and M.A. Postow, *Treatment of the Immune-Related Adverse Effects of Immune Checkpoint Inhibitors: A ReviewImmune-Related Adverse Effects of Immune Checkpoint InhibitorsImmune-Related Adverse Effects of Immune Checkpoint Inhibitors.* JAMA Oncology, 2016. **2**(10): p. 1346-1353.
48. Fitzgerald, J.C., et al., *Cytokine Release Syndrome After Chimeric Antigen Receptor T Cell Therapy for Acute Lymphoblastic Leukemia.* Crit Care Med, 2017. **45**(2): p. e124-e131.
49. van den Berg, J.H., et al., *Case Report of a Fatal Serious Adverse Event Upon Administration of T Cells Transduced With a MART-1-specific T-cell Receptor.* Mol Ther, 2015. **23**(9): p. 1541-50.
50. Zheng, P.P., J.M. Kros, and J. Li, *Approved CAR T cell therapies: ice bucket challenges on glaring safety risks and long-term impacts.* Drug Discov Today, 2018. **23**(6): p. 1175-1182.
51. Restifo, N.P., M.J. Smyth, and A. Snyder, *Acquired resistance to immunotherapy and future challenges.* Nat Rev Cancer, 2016. **16**(2): p. 121-6.
52. O'rourke, D.M., et al., *A single dose of peripherally infused EGFRvIII-directed CAR T cells mediates antigen loss and induces adaptive resistance in patients with recurrent glioblastoma.* Science translational medicine, 2017. **9**(399): p. eaaa0984.
53. Klebanoff, C.A., S.A. Rosenberg, and N.P. Restifo, *Prospects for gene-engineered T cell immunotherapy for solid cancers.* Nat Med, 2016. **22**(1): p. 26-36.
54. Hege, K.M., et al., *Safety, tumor trafficking and immunogenicity of chimeric antigen receptor (CAR)-T cells specific for TAG-72 in colorectal cancer.* Journal for immunotherapy of cancer, 2017. **5**(1): p. 22.
55. Migliorini, D., et al., *CAR T-Cell Therapies in Glioblastoma: A First Look.* Clin Cancer Res, 2018. **24**(3): p. 535-540.
56. Knochelmann, H.M., et al., *CAR T Cells in Solid Tumors: Blueprints for Building Effective Therapies.* Frontiers in immunology, 2018. **9**: p. 1740-1740.
57. Pule, M.A., et al., *Virus-specific T cells engineered to coexpress tumor-specific receptors: persistence and antitumor activity in individuals with neuroblastoma.* Nat Med, 2008. **14**(11): p. 1264-70.
58. Thistlethwaite, F.C., et al., *The clinical efficacy of first-generation carcinoembryonic antigen (CEACAM5)-specific CAR T cells is limited by poor persistence and transient pre-conditioning-dependent respiratory toxicity.* Cancer Immunol Immunother, 2017. **66**(11): p. 1425-1436.
59. Hege, K.M., et al., *Safety, tumor trafficking and immunogenicity of chimeric antigen receptor (CAR)-T cells specific for TAG-72 in colorectal cancer.* J Immunother Cancer, 2017. **5**: p. 22.
60. Scarfo, I. and M.V. Maus, *Current approaches to increase CAR T cell potency in solid tumors: targeting the tumor microenvironment.* J Immunother Cancer, 2017. **5**: p. 28.
61. Mechnikov, I.i.I.i., *Immunity in infective diseases.* Reviews of infectious diseases, 1988. **10**(1): p. 223-227.
62. van Furth, R. and Z.A. Cohn, *THE ORIGIN AND KINETICS OF MONONUCLEAR PHAGOCYTES.* The Journal of Experimental Medicine, 1968. **128**(3): p. 415-435.
63. Kain, V. and G.V. Halade, *Big eater macrophages dominate inflammation resolution following myocardial infarction.* Journal of Molecular and Cellular Cardiology, 2015. **87**: p. 225-227.
64. *Macrophage*. [cited 2019 May 28]; Available from: https://en.wikipedia.org/wiki/Macrophage#cite_note-5.
65. Krombach, F., et al., *Cell size of alveolar macrophages: an interspecies comparison.* Environ Health Perspect, 1997. **105 Suppl 5**: p. 1261-3.

66. Wynn, T.A., A. Chawla, and J.W. Pollard, *Macrophage biology in development, homeostasis and disease.* Nature, 2013. **496**(7446): p. 445-55.
67. Davies, L.C., et al., *Tissue-resident macrophages.* Nature immunology, 2013. **14**(10): p. 986.
68. Ginhoux, F. and S. Jung, *Monocytes and macrophages: developmental pathways and tissue homeostasis.* Nature Reviews Immunology, 2014. **14**: p. 392.
69. Sica, A. and A. Mantovani, *Macrophage plasticity and polarization: in vivo veritas.* The Journal of clinical investigation, 2012. **122**(3): p. 787-795.
70. Shapouri-Moghaddam, A., et al., *Macrophage plasticity, polarization, and function in health and disease.* J Cell Physiol, 2018. **233**(9): p. 6425-6440.
71. Ngambenjawong, C., H.H. Gustafson, and S.H. Pun, *Progress in tumor-associated macrophage (TAM)-targeted therapeutics.* Advanced Drug Delivery Reviews, 2017. **114**: p. 206-221.
72. Mantovani, A., *Macrophages, Neutrophils, and Cancer: A Double Edged Sword.* New Journal of Science, 2014. **2014**: p. 14.
73. Jiang, Z., J.X. Jiang, and G.X. Zhang, *Macrophages: a double-edged sword in experimental autoimmune encephalomyelitis.* Immunol Lett, 2014. **160**(1): p. 17-22.
74. Gordon, S., *Alternative activation of macrophages.* Nature Reviews Immunology, 2003. **3**(1): p. 23-35.
75. Mills, C., *M1 and M2 macrophages: oracles of health and disease.* Critical Reviews™ in Immunology, 2012. **32**(6).
76. Komohara, Y., et al., *Tumor-associated macrophages: Potential therapeutic targets for anti-cancer therapy.* Advanced Drug Delivery Reviews, 2016. **99**: p. 180-185.
77. Ngambenjawong, C., H.H. Gustafson, and S.H. Pun, *Progress in tumor-associated macrophage (TAM)-targeted therapeutics.* Adv Drug Deliv Rev, 2017. **114**: p. 206-221.
78. Mills, C.D., et al., *M-1/M-2 Macrophages and the Th1/Th2 Paradigm.* The Journal of Immunology, 2000. **164**(12): p. 6166-6173.
79. Mantovani, A., et al., *The chemokine system in diverse forms of macrophage activation and polarization.* Trends Immunol, 2004. **25**(12): p. 677-86.
80. Biswas, S.K. and A. Mantovani, *Macrophage plasticity and interaction with lymphocyte subsets: cancer as a paradigm.* Nature Immunology, 2010. **11**: p. 889.
81. Rőszer, T., *Understanding the Mysterious M2 Macrophage through Activation Markers and Effector Mechanisms.* Mediators of inflammation, 2015. **2015**: p. 816460-816460.
82. Sica, A., et al., *Tumour-associated macrophages are a distinct M2 polarised population promoting tumour progression: Potential targets of anti-cancer therapy.* European Journal of Cancer, 2006. **42**(6): p. 717-727.
83. Sica, A., et al. *Macrophage polarization in tumour progression*. in *Seminars in cancer biology*. 2008. Elsevier.
84. Qian, B.-Z. and J.W. Pollard, *Macrophage diversity enhances tumor progression and metastasis.* Cell, 2010. **141**(1): p. 39-51.
85. DeNardo, D.G., et al., *Leukocyte complexity predicts breast cancer survival and functionally regulates response to chemotherapy.* Cancer discovery, 2011. **1**(1): p. 54-67.
86. Jinushi, M. and Y. Komohara, *Tumor-associated macrophages as an emerging target against tumors: Creating a new path from bench to bedside.* Biochim Biophys Acta, 2015. **1855**(2): p. 123-30.
87. Petty, A.J. and Y. Yang, *Tumor-associated macrophages: implications in cancer immunotherapy.* Immunotherapy, 2017. **9**(3): p. 289-302.
88. Poh, A.R. and M. Ernst, *Targeting Macrophages in Cancer: From Bench to Bedside.* Frontiers in oncology, 2018. **8**: p. 49-49.

89. Wei, C., et al., *M2 macrophages confer resistance to 5-fluorouracil in colorectal cancer through the activation of CCL22/PI3K/AKT signaling.* Onco Targets Ther, 2019. **12**: p. 3051-3063.
90. Dong, N., et al., *M2 macrophages mediate sorafenib resistance by secreting HGF in a feed-forward manner in hepatocellular carcinoma.* Br J Cancer, 2019.
91. Wei, Y., et al., *The local immune landscape determines tumor PD-L1 heterogeneity and sensitivity to therapy.* J Clin Invest, 2019. **130**.
92. Dalton, H.J., et al., *Macrophages Facilitate Resistance to Anti-VEGF Therapy by Altered VEGFR Expression.* Clin Cancer Res, 2017. **23**(22): p. 7034-7046.
93. Cassetta, L. and J.W. Pollard, *Targeting macrophages: therapeutic approaches in cancer.* Nature Reviews Drug Discovery, 2018. **17**: p. 887.
94. *A Study of Trabectedin (YONDELIS) in Patients With Locally Advanced or Metastatic Liposarcoma or Leiomyosarcoma*. https://ClinicalTrials.gov/show/NCT01692678.
95. *Study With Trabectedin in BRCA1 and BRCA2 Mutation Carrier and BRCAness Phenotype Ovarian Cancer*. https://ClinicalTrials.gov/show/NCT01772979.
96. *Combination Therapy of Gemcitabine and Trabectedin in L-sarcomas*. https://ClinicalTrials.gov/show/NCT01426633.
97. Zeisberger, S., et al., *Clodronate-liposome-mediated depletion of tumour-associated macrophages: a new and highly effective antiangiogenic therapy approach.* British journal of cancer, 2006. **95**(3): p. 272.
98. Torres Andon, F. and M.J. Alonso, *Nanomedicine and cancer immunotherapy–targeting immunosuppressive cells.* Journal of drug targeting, 2015. **23**(7-8): p. 656-671.
99. Zhan, X., et al., *Targeted depletion of tumour-associated macrophages by an alendronate–glucomannan conjugate for cancer immunotherapy.* Biomaterials, 2014. **35**(38): p. 10046-10057.
100. Zhu, S., et al., *Targeting of tumor-associated macrophages made possible by PEG-sheddable, mannose-modified nanoparticles.* Molecular pharmaceutics, 2013. **10**(9): p. 3525-3530.
101. Niu, M., et al., *Biodistribution and in vivo activities of tumor-associated macrophage-targeting nanoparticles incorporated with doxorubicin.* Molecular pharmaceutics, 2014. **11**(12): p. 4425-4436.
102. Yan, Z., et al., *LyP-1-conjugated PEGylated liposomes: a carrier system for targeted therapy of lymphatic metastatic tumor.* Journal of controlled release, 2012. **157**(1): p. 118-125.
103. Hattori, Y., et al., *Evaluation of antitumor effect of zoledronic acid entrapped in folate-linked liposome for targeting to tumor-associated macrophages.* Journal of liposome research, 2015. **25**(2): p. 131-140.
104. Turk, M.J., D.J. Waters, and P.S. Low, *Folate-conjugated liposomes preferentially target macrophages associated with ovarian carcinoma.* Cancer letters, 2004. **213**(2): p. 165-172.
105. Roth, F., et al., *Aptamer-mediated blockade of IL4Rα triggers apoptosis of MDSCs and limits tumor progression.* Cancer research, 2012. **72**(6): p. 1373-1383.
106. Kelly, C., C. Jefferies, and S.-A. Cryan, *Targeted liposomal drug delivery to monocytes and macrophages.* Journal of drug delivery, 2011. **2011**.
107. Andon, F.T., et al., *Targeting tumor associated macrophages: The new challenge for nanomedicine.* Semin Immunol, 2017. **34**: p. 103-113.
108. Zhang, J., L. Patel, and K.J. Pienta, *CC chemokine ligand 2 (CCL2) promotes prostate cancer tumorigenesis and metastasis.* Cytokine Growth Factor Rev, 2010. **21**(1): p. 41-8.
109. Qian, B.Z., et al., *CCL2 recruits inflammatory monocytes to facilitate breast-tumour metastasis.* Nature, 2011. **475**(7355): p. 222-5.
110. Huang, E.H., et al., *A CXCR4 antagonist CTCE-9908 inhibits primary tumor growth and metastasis of breast cancer.* J Surg Res, 2009. **155**(2): p. 231-6.

111. Wong, D., et al., *Targeting CXCR4 with CTCE-9908 inhibits prostate tumor metastasis.* BMC Urol, 2014. **14**: p. 12.
112. Aharinejad, S., et al., *Colony-stimulating factor-1 blockade by antisense oligonucleotides and small interfering RNAs suppresses growth of human mammary tumor xenografts in mice.* Cancer Res, 2004. **64**(15): p. 5378-84.
113. Pyonteck, S.M., et al., *CSF-1R inhibition alters macrophage polarization and blocks glioma progression.* Nat Med, 2013. **19**(10): p. 1264-72.
114. Ahn, G.O., et al., *Inhibition of Mac-1 (CD11b/CD18) enhances tumor response to radiation by reducing myeloid cell recruitment.* Proc Natl Acad Sci U S A, 2010. **107**(18): p. 8363-8.
115. Bonapace, L., et al., *Cessation of CCL2 inhibition accelerates breast cancer metastasis by promoting angiogenesis.* Nature, 2014. **515**(7525): p. 130-3.
116. *S0916, MLN1202 in Treating Patients With Bone Metastases*. https://ClinicalTrials.gov/show/NCT01015560.
117. *FOLFIRINOX Plus PF-04136309 in Patients With Borderline Resectable and Locally Advanced Pancreatic Adenocarcinoma*. https://ClinicalTrials.gov/show/NCT01413022.
118. Stafford, J.H., et al., *Colony stimulating factor 1 receptor inhibition delays recurrence of glioblastoma after radiation by altering myeloid cell recruitment and polarization.* Neuro Oncol, 2016. **18**(6): p. 797-806.
119. *First Study of the Safety of CNTO 888 in Patients With Solid Tumors*. https://ClinicalTrials.gov/show/NCT00537368.
120. Pienta, K.J., et al., *Phase 2 study of carlumab (CNTO 888), a human monoclonal antibody against CC-chemokine ligand 2 (CCL2), in metastatic castration-resistant prostate cancer.* Invest New Drugs, 2013. **31**(3): p. 760-8.
121. Ries, C.H., et al., *Targeting tumor-associated macrophages with anti-CSF-1R antibody reveals a strategy for cancer therapy.* Cancer cell, 2014. **25**(6): p. 846-859.
122. Mok, S., et al., *Inhibition of CSF-1 receptor improves the antitumor efficacy of adoptive cell transfer immunotherapy.* Cancer research, 2014. **74**(1): p. 153-161.
123. *A Study of IMC-CS4 in Subjects With Advanced Solid Tumors*. https://ClinicalTrials.gov/show/NCT01346358.
124. *A Study of AMG 820 in Subjects With Advanced Solid Tumors*. https://ClinicalTrials.gov/show/NCT01444404.
125. *Phase 1 Study of PLX7486 as Single Agent in Patients With Advanced Solid Tumors*. https://ClinicalTrials.gov/show/NCT01804530.
126. *Safety Study of PLX108-01 in Patients With Solid Tumors*. https://ClinicalTrials.gov/show/NCT01004861.
127. Leuschner, F., et al., *Therapeutic siRNA silencing in inflammatory monocytes in mice.* Nature biotechnology, 2011. **29**(11): p. 1005.
128. Satoh, T., et al., *The Jmjd3-Irf4 axis regulates M2 macrophage polarization and host responses against helminth infection.* Nat Immunol, 2010. **11**(10): p. 936-44.
129. Sinha, P., V.K. Clements, and S. Ostrand-Rosenberg, *Reduction of myeloid-derived suppressor cells and induction of M1 macrophages facilitate the rejection of established metastatic disease.* J Immunol, 2005. **174**(2): p. 636-45.
130. Xin, H., et al., *Sunitinib inhibition of Stat3 induces renal cell carcinoma tumor cell apoptosis and reduces immunosuppressive cells.* Cancer Res, 2009. **69**(6): p. 2506-13.
131. Edwards, J.P. and L.A. Emens, *The multikinase inhibitor sorafenib reverses the suppression of IL-12 and enhancement of IL-10 by PGE(2) in murine macrophages.* Int Immunopharmacol, 2010. **10**(10): p. 1220-8.

132. Baer, C., et al., *Suppression of microRNA activity amplifies IFN-gamma-induced macrophage activation and promotes anti-tumour immunity.* Nat Cell Biol, 2016. **18**(7): p. 790-802.
133. Zhang, Y., et al., *ROS play a critical role in the differentiation of alternatively activated macrophages and the occurrence of tumor-associated macrophages.* Cell Res, 2013. **23**(7): p. 898-914.
134. Linde, N., et al., *Vascular endothelial growth factor-induced skin carcinogenesis depends on recruitment and alternative activation of macrophages.* J Pathol, 2012. **227**(1): p. 17-28.
135. Na, Y.R., et al., *Cyclooxygenase-2 inhibition blocks M2 macrophage differentiation and suppresses metastasis in murine breast cancer model.* PLoS One, 2013. **8**(5): p. e63451.
136. Kaneda, M.M., et al., *Macrophage PI3Kgamma Drives Pancreatic Ductal Adenocarcinoma Progression.* Cancer Discov, 2016. **6**(8): p. 870-85.
137. Georgoudaki, A.M., et al., *Reprogramming Tumor-Associated Macrophages by Antibody Targeting Inhibits Cancer Progression and Metastasis.* Cell Rep, 2016. **15**(9): p. 2000-11.
138. Poh, A.R., et al., *Inhibition of Hematopoietic Cell Kinase Activity Suppresses Myeloid Cell-Mediated Colon Cancer Progression.* Cancer Cell, 2017. **31**(4): p. 563-575.e5.
139. Hagemann, T., et al., *"Re-educating" tumor-associated macrophages by targeting NF-kappaB.* The Journal of experimental medicine, 2008. **205**(6): p. 1261-1268.
140. Lobera, M., et al., *Selective class IIa histone deacetylase inhibition via a nonchelating zinc-binding group.* Nat Chem Biol, 2013. **9**(5): p. 319-25.
141. De Palma, M., et al., *Tumor-targeted interferon-alpha delivery by Tie2-expressing monocytes inhibits tumor growth and metastasis.* Cancer Cell, 2008. **14**(4): p. 299-311.
142. Beatty, G.L., et al., *CD40 agonists alter tumor stroma and show efficacy against pancreatic carcinoma in mice and humans.* Science, 2011. **331**(6024): p. 1612-6.
143. Rolny, C., et al., *HRG inhibits tumor growth and metastasis by inducing macrophage polarization and vessel normalization through downregulation of PlGF.* Cancer Cell, 2011. **19**(1): p. 31-44.
144. Kaczanowska, S., A.M. Joseph, and E. Davila, *TLR agonists: our best frenemy in cancer immunotherapy.* Journal of leukocyte biology, 2013. **93**(6): p. 847-863.
145. Chao, M.P., et al., *Anti-CD47 antibody synergizes with rituximab to promote phagocytosis and eradicate non-Hodgkin lymphoma.* Cell, 2010. **142**(5): p. 699-713.
146. Russ, A., et al., *Blocking "don't eat me" signal of CD47-SIRPα in hematological malignancies, an in-depth review.* Blood Reviews, 2018. **32**(6): p. 480-489.
147. Mawby, W.J., et al., *Isolation and characterization of CD47 glycoprotein: a multispanning membrane protein which is the same as integrin-associated protein (IAP) and the ovarian tumour marker OA3.* Biochemical Journal, 1994. **304**(2): p. 525-530.
148. Tsai, R.K. and D.E. Discher, *Inhibition of "self" engulfment through deactivation of myosin-II at the phagocytic synapse between human cells.* The Journal of cell biology, 2008. **180**(5): p. 989-1003.
149. *Feasibility of the Combination of Chemotherapy (Carbo/Caelyx or Carbo/Doxorubicin) With Tocilizumab (mAb IL-6R) and Peg-Intron in Patients With Recurrent Ovarian Cancer*. https://ClinicalTrials.gov/show/NCT01637532.
150. *Combination Immunotherapy of GM.CD40L Vaccine With CCL21 in Lung Cancer*. https://ClinicalTrials.gov/show/NCT01433172.
151. *Tremelimumab and CP-870,893 in Patients With Metastatic Melanoma*. https://ClinicalTrials.gov/show/NCT01103635.
152. *A Phase I/Ib Study of AZD9150 (ISIS-STAT3Rx) in Patients With Advanced/Metastatic Hepatocellular Carcinoma*. https://ClinicalTrials.gov/show/NCT01839604.
153. Szebeni, G.J., et al., *Inflammation and Cancer: Extra- and Intracellular Determinants of Tumor-Associated Macrophages as Tumor Promoters.* Mediators Inflamm, 2017. **2017**: p. 9294018.

154. Wacheck, V., *[Oligonucleotide therapeutics - an emerging novel class of compounds].* Wien Med Wochenschr, 2006. **156**(17-18): p. 481-7.
155. Askari, F.K. and W.M. McDonnell, *Antisense-Oligonucleotide Therapy.* New England Journal of Medicine, 1996. **334**(5): p. 316-318.
156. Mello, C.C. and D. Conte, Jr., *Revealing the world of RNA interference.* Nature, 2004. **431**(7006): p. 338-42.
157. Nimjee, S.M., et al., *Aptamers as Therapeutics.* Annu Rev Pharmacol Toxicol, 2017. **57**: p. 61-79.
158. Elbashir, S.M., et al., *Duplexes of 21-nucleotide RNAs mediate RNA interference in cultured mammalian cells.* Nature, 2001. **411**(6836): p. 494-8.
159. Fire, A., et al., *Potent and specific genetic interference by double-stranded RNA in Caenorhabditis elegans.* Nature, 1998. **391**(6669): p. 806-11.
160. Burnett, J.C. and J.J. Rossi, *RNA-based therapeutics: current progress and future prospects.* Chemistry & biology, 2012. **19**(1): p. 60-71.
161. Petrocca, F. and J. Lieberman, *Promise and challenge of RNA interference-based therapy for cancer.* J Clin Oncol, 2011. **29**(6): p. 747-54.
162. Martinez, J., et al., *Single-stranded antisense siRNAs guide target RNA cleavage in RNAi.* Cell, 2002. **110**(5): p. 563-74.
163. Rand, T.A., et al., *Argonaute2 cleaves the anti-guide strand of siRNA during RISC activation.* Cell, 2005. **123**(4): p. 621-9.
164. Eguchi, A., et al., *Efficient siRNA delivery into primary cells by a peptide transduction domain-dsRNA binding domain fusion protein.* Nat Biotechnol, 2009. **27**(6): p. 567-71.
165. Layzer, J.M., et al., *In vivo activity of nuclease-resistant siRNAs.* Rna, 2004. **10**(5): p. 766-71.
166. Tiwari, G., et al., *Drug delivery systems: An updated review.* International journal of pharmaceutical investigation, 2012. **2**(1): p. 2-11.
167. Park, K., *Controlled drug delivery systems: past forward and future back.* Journal of controlled release : official journal of the Controlled Release Society, 2014. **190**: p. 3-8.
168. *Terminology for nanomaterials. Publicly available specification 136*. 2007 [cited 2019 June 3]; Available from: http://shop.bsigroup.com/upload/Shop/Download/Nano/PAS136.pdf.
169. Kim, B.Y., J.T. Rutka, and W.C. Chan, *Nanomedicine.* N Engl J Med, 2010. **363**(25): p. 2434-43.
170. Bulbake, U., et al., *Liposomal Formulations in Clinical Use: An Updated Review.* Pharmaceutics, 2017. **9**(2): p. 12.
171. Zhao, Y. and L. Huang, *Lipid nanoparticles for gene delivery.* Adv Genet, 2014. **88**: p. 13-36.
172. Chauhan, A.S., *Dendrimers for Drug Delivery.* Molecules, 2018. **23**(4).
173. Rode, A., S. Sharma, and D.K. Mishra, *Carbon Nanotubes: Classification, Method of Preparation and Pharmaceutical Application.* Curr Drug Deliv, 2018. **15**(5): p. 620-629.
174. Sivaram, A.J., et al., *Nanogels for delivery, imaging and therapy.* Wiley Interdiscip Rev Nanomed Nanobiotechnol, 2015. **7**(4): p. 509-33.
175. Hu, J., et al., *Long Circulating Polymeric Nanoparticles for Gene/Drug Delivery.* Curr Drug Metab, 2018. **19**(9): p. 723-738.
176. Croy, S.R. and G.S. Kwon, *Polymeric micelles for drug delivery.* Curr Pharm Des, 2006. **12**(36): p. 4669-84.
177. Cabuzu, D., et al., *Biomedical applications of gold nanoparticles.* Curr Top Med Chem, 2015. **15**(16): p. 1605-13.
178. Chen, F., et al., *Multifunctional nanomedicine with silica: Role of silica in nanoparticles for theranostic, imaging, and drug monitoring.* J Colloid Interface Sci, 2018. **521**: p. 261-279.
179. Ban, Y., et al., *Targeting autocrine CCL5–CCR5 axis reprograms immunosuppressive myeloid cells and reinvigorates antitumor immunity.* Cancer research, 2017. **77**(11): p. 2857-2868.

180. Qian, Y., et al., *Molecular-Targeted Immunotherapeutic Strategy for Melanoma via Dual-Targeting Nanoparticles Delivering Small Interfering RNA to Tumor-Associated Macrophages.* ACS Nano, 2017. **11**(9): p. 9536-9549.
181. Ortega, R.A., et al., *Biocompatible mannosylated endosomal-escape nanoparticles enhance selective delivery of short nucleotide sequences to tumor associated macrophages.* Nanoscale, 2015. **7**(2): p. 500-510.
182. Ortega, R.A., et al., *Manipulating the NF-κB pathway in macrophages using mannosylated, siRNA-delivering nanoparticles can induce immunostimulatory and tumor cytotoxic functions.* International journal of nanomedicine, 2016. **11**: p. 2163.
183. Conde, J., et al., *Dual targeted immunotherapy via in vivo delivery of biohybrid RNAi‐peptide nanoparticles to tumor‐associated macrophages and cancer cells.* Advanced functional materials, 2015. **25**(27): p. 4183-4194.
184. Kortylewski, M., et al., *In vivo delivery of siRNA to immune cells by conjugation to a TLR9 agonist enhances antitumor immune responses.* Nat Biotechnol, 2009. **27**(10): p. 925-32.
185. Binnemars-Postma, K., et al., *Targeting the Stat6 pathway in tumor-associated macrophages reduces tumor growth and metastatic niche formation in breast cancer.* Faseb j, 2018. **32**(2): p. 969-978.
186. Zhang, L., et al., *Stat3 inhibition activates tumor macrophages and abrogates glioma growth in mice.* Glia, 2009. **57**(13): p. 1458-67.
187. Sato, Y., et al., *A pH-sensitive cationic lipid facilitates the delivery of liposomal siRNA and gene silencing activity in vitro and in vivo.* J Control Release, 2012. **163**(3): p. 267-76.
188. Sato, Y., et al., *[Development of an efficient short interference RNA (siRNA) delivery system with a new pH-sensitive cationic lipid].* Yakugaku Zasshi, 2012. **132**(12): p. 1355-63.
189. Hatakeyama, H., et al., *The systemic administration of an anti-miRNA oligonucleotide encapsulated pH-sensitive liposome results in reduced level of hepatic microRNA-122 in mice.* J Control Release, 2014. **173**: p. 43-50.
190. Hatakeyama, H., H. Akita, and H. Harashima, *A multifunctional envelope type nano device (MEND) for gene delivery to tumours based on the EPR effect: a strategy for overcoming the PEG dilemma.* Adv Drug Deliv Rev, 2011. **63**(3): p. 152-60.
191. Sato, Y., et al., *Understanding structure-activity relationships of pH-sensitive cationic lipids facilitates the rational identification of promising lipid nanoparticles for delivering siRNAs in vivo.* J Control Release, 2019. **295**: p. 140-152.
192. Sato, Y., et al., *Relationship Between the Physicochemical Properties of Lipid Nanoparticles and the Quality of siRNA Delivery to Liver Cells.* Mol Ther, 2016. **24**(4): p. 788-95.
193. Jayaraman, M., et al., *Maximizing the potency of siRNA lipid nanoparticles for hepatic gene silencing in vivo.* Angew Chem Int Ed Engl, 2012. **51**(34): p. 8529-33.
194. Hoy, S.M., *Patisiran: First global approval.* Drugs, 2018. **78**(15): p. 1625-1631.
195. Mui, B.L., et al., *Influence of Polyethylene Glycol Lipid Desorption Rates on Pharmacokinetics and Pharmacodynamics of siRNA Lipid Nanoparticles.* Mol Ther Nucleic Acids, 2013. **2**: p. e139.
196. Sato, Y., et al., *Elucidation of the physicochemical properties and potency of siRNA-loaded small-sized lipid nanoparticles for siRNA delivery.* J Control Release, 2016. **229**: p. 48-57.
197. Cabral, H., et al., *Accumulation of sub-100 nm polymeric micelles in poorly permeable tumours depends on size.* Nat Nanotechnol, 2011. **6**(12): p. 815-23.
198. Huo, S., et al., *Superior penetration and retention behavior of 50 nm gold nanoparticles in tumors.* Cancer Res, 2013. **73**(1): p. 319-30.
199. Tang, L., et al., *Investigating the optimal size of anticancer nanomedicine.* Proc Natl Acad Sci U S A, 2014. **111**(43): p. 15344-9.

200. Perry, J.L., et al., *Mediating Passive Tumor Accumulation through Particle Size, Tumor Type, and Location.* Nano letters, 2017. **17**(5): p. 2879-2886.
201. Santoni, M., et al., *Emerging role of tumor-associated macrophages as therapeutic targets in patients with metastatic renal cell carcinoma.* Cancer Immunol Immunother, 2013. **62**(12): p. 1757-68.
202. Yang, Z., et al., *Infiltrating macrophages increase RCC epithelial mesenchymal transition (EMT) and stem cell-like populations via AKT and mTOR signaling.* Oncotarget, 2016. **7**(28): p. 44478-44491.
203. Sakurai, Y., et al., *Remodeling of the Extracellular Matrix by Endothelial Cell-Targeting siRNA Improves the EPR-Based Delivery of 100 nm Particles.* Molecular therapy : the journal of the American Society of Gene Therapy, 2016. **24**(12): p. 2090-2099.
204. Akinc, A., et al., *Targeted delivery of RNAi therapeutics with endogenous and exogenous ligand-based mechanisms.* Mol Ther, 2010. **18**(7): p. 1357-64.
205. Matsumura, Y. and H. Maeda, *A new concept for macromolecular therapeutics in cancer chemotherapy: mechanism of tumoritropic accumulation of proteins and the antitumor agent smancs.* Cancer research, 1986. **46**(12 Part 1): p. 6387-6392.
206. Dreher, M.R., et al., *Tumor vascular permeability, accumulation, and penetration of macromolecular drug carriers.* Journal of the National Cancer Institute, 2006. **98**(5): p. 335-344.
207. Allen, T.M. and P.R. Cullis, *Liposomal drug delivery systems: from concept to clinical applications.* Adv Drug Deliv Rev, 2013. **65**(1): p. 36-48.
208. Huang, S.C., et al., *Metabolic Reprogramming Mediated by the mTORC2-IRF4 Signaling Axis Is Essential for Macrophage Alternative Activation.* Immunity, 2016. **45**(4): p. 817-830.
209. Hashimoto, M., et al., *Silencing of SOCS1 in macrophages suppresses tumor development by enhancing antitumor inflammation.* Cancer Sci, 2009. **100**(4): p. 730-6.
210. Liang, Y.B., et al., *Downregulated SOCS1 expression activates the JAK1/STAT1 pathway and promotes polarization of macrophages into M1 type.* Mol Med Rep, 2017. **16**(5): p. 6405-6411.
211. Wilson, H.M., *SOCS Proteins in Macrophage Polarization and Function.* Front Immunol, 2014. **5**: p. 357.
212. Goswami, K.K., et al., *Tumor promoting role of anti-tumor macrophages in tumor microenvironment.* Cell Immunol, 2017. **316**: p. 1-10.
213. Wang, Y., et al., *The role of STAT3 in leading the crosstalk between human cancers and the immune system.* Cancer Lett, 2018. **415**: p. 117-128.
214. Fujiwara, Y., et al., *Oleanolic acid inhibits macrophage differentiation into the M2 phenotype and glioblastoma cell proliferation by suppressing the activation of STAT3.* Oncol Rep, 2011. **26**(6): p. 1533-7.
215. Andersen, M.N., et al., *STAT3 inhibition specifically in human monocytes and macrophages by CD163-targeted corosolic acid-containing liposomes.* Cancer Immunol Immunother, 2019. **68**(3): p. 489-502.
216. Casazza, A., et al., *Tumor stroma: a complexity dictated by the hypoxic tumor microenvironment.* Oncogene, 2014. **33**(14): p. 1743.
217. Dhani, N., et al. *The clinical significance of hypoxia in human cancers*. in *Seminars in nuclear medicine*. 2015. Elsevier.
218. Silva, V.L. and W.T. Al-Jamal, *Exploiting the cancer niche: Tumor-associated macrophages and hypoxia as promising synergistic targets for nano-based therapy.* Journal of Controlled Release, 2017. **253**: p. 82-96.
219. Lewis, C. and C. Murdoch, *Macrophage responses to hypoxia: implications for tumor progression and anti-cancer therapies.* The American journal of pathology, 2005. **167**(3): p. 627-635.

220. Doedens, A.L., et al., *Macrophage expression of hypoxia-inducible factor-1 alpha suppresses T-cell function and promotes tumor progression.* Cancer Res, 2010. **70**(19): p. 7465-75.
221. Zeng, W., et al., *Hypoxia and hypoxia inducible factors in tumor metabolism.* Cancer letters, 2015. **356**(2): p. 263-267.
222. Yang, L. and Y. Zhang, *Tumor-associated macrophages: from basic research to clinical application.* Journal of hematology & oncology, 2017. **10**(1): p. 58-58.
223. Chouaib, S., et al., *Hypoxia promotes tumor growth in linking angiogenesis to immune escape.* Frontiers in immunology, 2012. **3**: p. 21.
224. Bartholomeusz, G., et al., *In vivo therapeutic silencing of hypoxia-inducible factor 1 alpha (HIF-1α) using single-walled carbon nanotubes noncovalently coated with siRNA.* Nano Research, 2009. **2**(4): p. 279-291.
225. Liu, X.-Q., et al., *Therapeutic Delivery of siRNA Silencing HIF-1 Alpha with Micellar Nanoparticles Inhibits Hypoxic Tumor Growth.* Molecular Pharmaceutics, 2012. **9**(10): p. 2863-2874.
226. Song, M., et al., *Bioconjugated manganese dioxide nanoparticles enhance chemotherapy response by priming tumor-associated macrophages toward M1-like phenotype and attenuating tumor hypoxia.* ACS nano, 2015. **10**(1): p. 633-647.
227. Fang, B., et al., *Luteolin inhibits angiogenesis of the M2like TAMs via the downregulation of hypoxia inducible factor1alpha and the STAT3 signalling pathway under hypoxia.* Mol Med Rep, 2018. **18**(3): p. 2914-2922.
228. Xu, Q., et al., *Targeting Stat3 blocks both HIF-1 and VEGF expression induced by multiple oncogenic growth signaling pathways.* Oncogene, 2005. **24**(36): p. 5552-60.
229. Liu, Z., et al., *TGF-β1 secreted by M2 phenotype macrophages enhances the stemness and migration of glioma cells via the SMAD2/3 signalling pathway.* International journal of molecular medicine, 2018. **42**(6): p. 3395-3403.
230. Hambardzumyan, D., D.H. Gutmann, and H. Kettenmann, *The role of microglia and macrophages in glioma maintenance and progression.* Nature neuroscience, 2016. **19**(1): p. 20-27.
231. Caja, L., et al., *TGF-beta and the Tissue Microenvironment: Relevance in Fibrosis and Cancer.* Int J Mol Sci, 2018. **19**(5).
232. Huang, Y., et al., *Vascular normalizing doses of antiangiogenic treatment reprogram the immunosuppressive tumor microenvironment and enhance immunotherapy.* Proceedings of the National Academy of Sciences, 2012. **109**(43): p. 17561-17566.
233. Morgan, R.A., et al., *Case report of a serious adverse event following the administration of T cells transduced with a chimeric antigen receptor recognizing ERBB2.* Mol Ther, 2010. **18**(4): p. 843-51.
234. Panni, R.Z., D.C. Linehan, and D.G. DeNardo, *Targeting tumor-infiltrating macrophages to combat cancer.* Immunotherapy, 2013. **5**(10): p. 1075-1087.
235. Lee, H.W., et al., *Recruitment of monocytes/macrophages in different tumor microenvironments.* Biochim Biophys Acta, 2013. **1835**(2): p. 170-9.
236. Sterner, R.M., et al., *GM-CSF inhibition reduces cytokine release syndrome and neuroinflammation but enhances CAR-T cell function in xenografts.* Blood, 2019. **133**(7): p. 697-709.
237. Giavridis, T., et al., *CAR T cell-induced cytokine release syndrome is mediated by macrophages and abated by IL-1 blockade.* Nat Med, 2018. **24**(6): p. 731-738.
238. Danhier, F., *To exploit the tumor microenvironment: Since the EPR effect fails in the clinic, what is the future of nanomedicine?* J Control Release, 2016. **244**(Pt A): p. 108-121.
239. Mayer, L.D., et al., *Characterization of liposomal systems containing doxorubicin entrapped in response to pH gradients.* Biochim Biophys Acta, 1990. **1025**(2): p. 143-51.

240. Fidorra, M., T. Heimburg, and H.M. Seeger, *Melting of individual lipid components in binary lipid mixtures studied by FTIR spectroscopy, DSC and Monte Carlo simulations.* Biochim Biophys Acta, 2009. **1788**(3): p. 600-7.
241. Kibria, G., et al., *Anti-tumor effect via passive anti-angiogenesis of PEGylated liposomes encapsulating doxorubicin in drug resistant tumors.* Int J Pharm, 2016. **509**(1-2): p. 178-187.

Acknowledgment

"I say unto you: one must still have chaos in oneself to be able to give birth to a dancing star" From Fredrich Nietzsche's Thus Spoken Zarathustra, Towards the Ubermensch

I started this dissertation with the above quote because it perfectly describes the hardship of the journey in pursuing a doctoral degree, and the obstacles and the challenges that one needs to overcome to make a significant scientific contribution and to write a doctoral dissertation "a dancing star" that should not only shine the road for the doctoral candidate but for all humanity as well.

I feel honored to be selected by the Japanese government, **the Ministry of Education, Culture, Sports, Science and Technology (*Monbukagakusho* (MEXT))** to pursue my higher education (Master's and Ph.D.) under the MEXT scholarship in Japan. Studying and living in Japan was an extraordinary experience that enriched my cultural and scientific knowledge and opened my mind for unlimited possibilities and new ways of thinking. I am proud to be accepted by **Prof. Hideyoshi Harashima** to be part of the **(Laboratory for Molecular Design of Pharmaceutics/Yakusetsu)** at the Faculty of Pharmaceutical Sciences at Hokkaido University, and to give me the opportunity to follow my passion of studying three interesting fields during the doctoral course; nanotechnology (drug delivery), gene therapy, and cancer immunotherapy. **Prof. Harashima** has been a great teacher and mentor. I am very grateful for his continuous support, guidance, patience, wisdom, and insightful advice that helped me grow as a person and as a scientist. I enjoyed all our monthly discussions and felt very lucky to learn from his deep knowledge and valuable experience. I am also very proud and lucky to be mentored by **Assistant Prof. Dr. Yusuke Sato**, who kindly, patiently and generously tutored and supported me during each step of the scientific journey. From doing and designing experiments, to writing papers, to presenting at seminars and scientific conferences and much more. I have been and always be very grateful for him as a great teacher. This thesis is the fruit of my teachers' effort.

I would like to thank members of the Laboratory for Molecular Design of Pharmaceutics and the Laboratory of Innovative Nanomedicine for their kindness and support. Especially, **Associate Prof. Dr. Yuma Yamada, Assistant Prof. Dr. Takashi Nakamura, Assistant Prof. Dr. Ikramy Khalil** for their insightful scientific advice during discussions and seminars. I would like also to

thank great teachers who left our lab, **Prof. Hidetaka Akita, Dr. Yu Sakurai, and Dr. Kazuki Kajimoto.** I would like also to thank secretaries **Ms. Eiko Abe** and **Ms. Eriko Kano** for their kind effort and time in supporting all international students.

I am very honored and grateful for **Prof. Mikako Ogawa** (Laboratory for Bioanalysis and Molecular Imaging) for agreeing to chair my dissertation panel and for evaluating this doctoral work with insightful advice and great discussion.

My heartful gratitude also goes to **Sato group members** for their kindness and support -those who graduated and those who still in the lab-; **Dr. Lewis Lee, Dr. West Paraiso, Dr. Sarochin Santiwarangkool, Dr. Sa'ed Abbasi, Mr. Yusuke Note, Mr. Hideki Matsui, Mr. Kazuki Hashiba, Mr. Ahmed AlBaloul, Ms. Risa Sato, Ms. Nana Okabe, Mr. Hiroaki Sasaki, Mr. Yoshiyuki Kinami, Mr. Yuichi Suzuki.**

I am also very thankful for members of other groups for sharing much of their knowledge and experience -those who graduated and those who still in the lab-, especially; **Mr. Hideyuki Masuda, Mr. Ritsuto Endo, Mr. Satrialdi, Ms. Laila Berger, Mr. Mahmoud Younis, Ms. Kato Tsuki, Ms. Miki Kawai, Mr. Mahmoud Mansour, Ms. Sion Elisabeth, Mr. Seigo Kimura, Ms. Kyoko Kawakami, Mr. Ryo Hiradate.**

Personally, my heartful gratitude and thanks go to my friends and family, especially to **my mother "Nadia"** and **my sister "Sally"** for bringing joy to my life.

I hope this doctoral dissertation can add value to the scientific research in general and to cancer research in specific. I believe that the future of cancer therapy belongs to macrophage-based immunotherapy, and this research could pave the way for scientific and clinical application related to this promising field.

Nour A. K. Shobaki

Sapporo, Japan

Summer 2019